Multi-patch Discontinuous Galerkin Isogeometric Analysis for Porous Media Flow

Kenny David
EEMCS
Delft University of Technology

A thesis submitted for the degree of
Master of Science in Applied Mathematics
January 2017

Multi-patch Discontinuos Galerkin Isogeometric Analysis for Porous Media Flow

by
Kenny David
EEMCS

in partial fulfillment of the requirements for the degree of

Master of Science
in Applied Mathematics

at the Delft University of Technology,
to be defended publicly on Thursday January 26, 2017 at 11:00 AM.

Supervisor:	**Dr. Matthias Möller,**	**TU Delft**
Thesis committee:	**Prof. dr. ir. K. Vuik,**	**TU Delft**
	Dr. P. Wilders,	**TU Delft**

An electronic version of this thesis is available at
http://repository.tudelft.nl/.

Abstract

The role of reservoir simulations in oil and gas industry is vital. It is understandable since a reservoir simulation will give figures of oil and gas production for short and long period of time. Those profiles will determine the amount of investments and future planning of an oil and gas field. Lately, this necessity is even emerging due to the fact that finding an economically feasible oil and gas field is nearly impossible. The remaining options are either optimizing developed fields or exploiting unconventional oil and gas fields. Whichever option is picked, it is a problem of massive capital expenditure. Thus it is a clear message that the desire to have a reliable reservoir simulation is undisputed.

At the beginning of its development, reservoir simulation calculations were based on the Two Point Flux Approximation (TPFA) method [7, 14, 48]. However, as the anisotropy of the reservoir began to be a main issue in the industry, while TPFA is not able to represent the full permeability tensor [19, 36, 39], an idea to utilize Finite Element Analysis (FEA) for reservoir simulation arose immediately.

Isogeometric Analysis (IGA) is a finite element based analysis. This discretization technique has gained considerable attention since its birth. It is not only because it allows integration between design and analysis, but also because of its unique features such as refinements, multi-patch concepts, and its ability to blend gradually higher-order basis functions with higher continuity to basis functions that are locally less continuous or even discontinuous. IGA and FEA share common principles up to the weak formulation. Nonetheless, IGA uses B-splines as its test functions.

In this thesis, we examine and evaluate IGA in dealing with reservoir anisotropy. For this pilot project, we restrict ourselves to the applications of IGA for 2D, incompressible, and single phase Darcy's equation. We also consider the Discontinuous Galerkin (DG) application in IGA, and as a consequence, we consider multi-patch technique.

It is found that up to a certain level of anisotropy, IGA could handle the anistropy problem seamlessly. However, in a very severe case, IGA could not handle the anisotropy problem. These poor results of IGA also occur in FEA. Nonetheless, FEA requires greatly more degrees of freedom to achieve the same level of accuracy of IGA.

Acknowledgements

"*Seek your happiness in the Lord, and He will give you your heart's desire.*"
— Psalm 37:4

First of all, I would like to thank my Lord for all bless and mercy. I also would like to thank my family, my wife Isyana Ginarsi Kalembang, and my son Kaleb Barani Sitompul. Thank you for all your prayers and thoughts.

I would like to show my deep gratitude to my supervisor, Dr. Matthias Möller. Thank you for your guidance and your patience. I also would like to acknowledge the Indonesian governments for the financial support through Indonesia Endowment Fund for Education scholarship program. Last, but not the least, I would like to salute all my comrades from Applied Math master program, Mario, Baruch, Mircea, Zoe, Shobhit, and Nam. We did it, guys!

Contents

Chapter 1

Introduction

> "*Drill for oil? You mean drill into the ground to try and find oil? You're crazy.*"
> — Drillers whom Edwin L. Drake tried to enlist in his project to drill for oil in 1859 [30].

Edwin L. Drake (1819 - 1880) has changed the world since his success to drill the first American oil well in 1859. Indeed, Drake was not the first man who drilled an oil well [26]. However, his success triggered modern oil and gas business.

Despite all controversies of petroleum industries, e.g. environmental issues and world's politics, the role of oil and gas as the primary energy sources is not arguable. With the contribution of 39.9% and 15.1% of world's energy supply, oil and gas are the key players of energy today [5]. In fact, this situation will remain unchanged in the near future. World Oil Outlook 2015 emphasizes that oil will continue to be central to the global energy mix over the next 25 years, helping to satisfy the world's growing energy needs [10].

From the industries point of view, it is not an easy task to fulfill energy demands in the coming years. Finding a new economically feasible conventional oil and gas field is almost like expecting a pig to fly. Therefore, ready or not, the industries must set their business on the unconventional oil and gas fields [46]. For instances, coal seam gas or naturally fractured reservoirs. Those new kind of natural energy sources give more difficulties to be taken care of than the conventional ones do, i.e. dual porosity, and dual porosity and permeability system of reservoirs for the case of coal seam gas and naturally fractured reservoirs. Indeed, the necessity of a more reliable tool for production forecast, i.e. reservoir simulation, is undisputed.

Two Point Flux Approximation in reservoir simulation

The history of reservoir simulation begun in the 1930's. At that time the calculations were very simple, consisted mostly of analytical methods, zero-dimensional material balances, and 1-D Buckley-Leverett calculations. The situation was changing in the early 1960's thanks to the development of computers. The simple calculations were transformed into relatively sophisticated computer programs [14]. Initially, the simulators deployed Finite Volume Method (FVM) technique, to be specific Two Point

Figure 1.1: Outcrop photograph of distributary channel sand body overlying a coal bed as an illustration of reservoir heterogeneity in middle Miocene Mahakam Delta deposits [13].

Flux Approximation (TPFA), to solve Darcy's law numerically [7, 14, 48]. TPFA is a cell centered approximation. This technique is leading to 5-point and 7-point stencil for 2-D and 3-D problems, respectively. Continuity of flux and pressure is readily incorporated into the standard discretization by approximating the interface coefficients with a harmonic average of neighboring grid block permeabilities [19]. This method was proven to be robust, considering computation stability and satisfaction of the conservation principles which are inherent to the FVM by construction. Nonetheless, a problem arises when reservoir heterogeneity, i.e. anisotropy, is considered. The full permeability tensor or grid distortion can not be handled by TPFA [19, 36, 39].

Finite Element Method in reservoir simulation

An idea to exploit the Finite Element Method (FEM) in reservoir simulation arose immediately in the late 1960's. Some research groups, such as Gulf Research & Development Company and Intercomp Resource Development and Engineering Ltd., implemented FEM in reservoir simulation and showed the robustness of this technique [44, 50, 49]. Later, the research has been extended to several new FEM-based techniques such as Mixed FEM (MFEM) [20, 16], or Control Volume FEM (CVFEM) [23, 24].

MFEM is a reformulation of Darcy's equation, which is a second order system of equations, into a first order system. This technique solves the two unknowns, which

are pressure and velocity fields, simultaneously [36]. The motivations of this technique are to ensure local mass conservation and to provide a flux approximation as part of the formulation [39]. The spirit of conservation is also driving the development of the CVFEM. This method was introduced by Baliga and Patankar at the beginning of the 1980's for convection and diffusion problems [8, 9]. For reservoir modeling purpose the method works as follows. First, the calculation domain is divided into three-node triangular elements, and then polygonal control volumes are constructed by joining the centroids of the elements to the midpoints of the corresponding sides. The pressure is discretized in a finite element manner, while a control volume approach allows upstream weighting of the phase mobilities [23].

A recent development of FEM in reservoir simulation was proposed by Eymard et al. in the 2010's [21, 22]. This technique is called Vertex Approximate Gradient (VAG). VAG is very much the same as Galerkin FEM (GFEM), the main difference is firstly the introduction of cell centered unknowns in addition to the vertex unknowns, and secondly the interpolation to obtain the unknowns at the face centers [27].

Multi Point Flux Approximation in reservoir simulation

An advancement of the concept of FVM was proposed by Aavatsmark et al [3, 4], and Edwards and Rogers [19] in the late 1990's. It is an improvement of TPFA. Instead of having a 5-point and a 7-point stencil for 2-D and 3-D problems, this technique is leading to 9-point and 27-point stencil for 2D and 3D problems, respectively. This method is so-called Multi Point Flux Approximation (MPFA).

The first MPFA is called O-method later this approach is developed into several techniques, such as L-method [51], U-method [2], and Z-method [41]. The MPFA method uses the surface midpoints to ensure the linear variation and the continuity of pressure and flux. An interaction region is created in each grid node, involving four and eight neighboring cells for the case of 2D and 3D, respectively. By having such construction, this technique leads to 9-point and 27-point stencil for 2D and 3D problems, respectively. Therefore, the contributions of surrounding grids will be exposed more than the TPFA does. Hence the reservoir anisotropy problem is taken care.

Comparisons between FEM and MPFA

Several studies try to expose and to compare FEM and its extensions with MPFA, for instance in [36] and [39], which show that each method has its superiorities. An interesting comparison is given by Hćgland et al. in [27] between VAG and MPFA (O- and L-method) for 3D general grids problem. To mimic reservoir conditions, this research applies compression and perturbation to the grids. It is reported that for the case of *compressed unperturbed* and *compressed perturbed grids*, VAG is superior over MPFA. Even for the case *compressed perturbed grids* both MPFA methods fail to converge. These results do make sense since it is well known that FEM has more flexibility than FVM in modeling any geometric shape. In FVM we are dealing with fluxes that are calculated at the mid-point between the discrete nodes in the

domain. It would not be a problem for regular mesh, but for an irregular mesh, those calculations could lead to an excruciating amount of fluxes [1]. It is not the case in FEM. In FEM we are dealing with the weak formulation and integrate the equation in a discretized domain. Therefore, for FEM irregular geometry would not be an obstacle compared with FVM.

Isogeometric Analysis as a new numerical approximation approach in reservoir modeling

Realizing the advantages of FEM in handling anisotropy and geometric problems in reservoir simulation triggers the idea to apply Isogeometric Analysis (IGA) in such field. IGA is actually a finite element based analysis. The main difference between IGA and Finite Element Analysis (FEA) is the application of B-splines as basis functions. The idea of applying B-splines as basis functions is driven by the desire to integrate Computer Aided Design (CAD) with FEA, and to have a strategy to replace the concept of a huge number of little cells (the finite elements) by ensembling of larger patches covering the entire domain [15].

IGA immediately gains attention from its birth. It is not only because it allows the integration between CAD and FEA, but also because of its ability to represent geometries more accurately than FEA. IGA also allows us to blend gradually higher-order basis functions, with higher continuity, to locally less continuous or even discontinuous basis functions. It has been proved that IGA is superior over FEA for extensive analysis [15]. However, its superiority has not been entirely exposed for the purpose of reservoir simulation.

1.1 Scope of the thesis

Applications of IGA in reservoir simulations would be a very broad topic to be covered in one master thesis. We, therefore, restrict ourselves to reservoir anisotropy problem for 2D and single phase assumption in this pilot project. For the purpose of this research, we will also consider multi-patch and Discontinuous Galerkin (DG) applications.

Initially, we would not like to compare the IGA to any proven method. This thesis would only go deeper into exposing IGA in handling reservoir anisotropy. However, as the research was progressing, the necessity to compare IGA with FEM was unavoidable. Therefore, we also consider the FEA in handling reservoir anisotropy in this thesis.

It is important to mention that not all materials related to the topic will be discussed in this thesis. We will present only those that we consider essential for the purpose of this work. Readers may refer to cited references for further explanations.

1.2 State of the art

IGA initially was developed by Hughes et al. in 2005 [29]. The method has been originally developed in the field of mechanical problems, then extended to linear and nonlinear structures, laminar and turbulent flows, and fluid-structure interaction [15]. Nowadays, there are several groups all over the world that are working on the topics connected to IGA. The Johann Radon Institute for Computational and Applied Mathematics (RICAM) with its G+SMO project [32] or the Center for Numerical Porous Media of King Abdullah University of Science and Technology (KAUST) with its PetIGA project [38]. Having said that, based on the author's best knowledge, there are not many published attempts to apply IGA in reservoir modeling specifically. One paper by Lynd et al. [35] was published during the completion of this thesis. Nonetheless, the research is still limited to the application of IGA for reservoir simulation in general. It is not deep digging a particular application.

In this study, we consider the application of discontinuity in the basis functions. Therefore, DG method is being analyzed, and as a consequence, we will consider the multi-patch application. Research in DG methods for multi-patch problem has been showed by Brunero in [12], and Langer et al. in [34] and in [33].

1.3 Software Packages

For the purpose of this research we are using **G+SMO** for IGA implementations in 2D, and **deal.II** for FEM implementations also in 2D. Both are open source object-oriented, templated C++ libraries. deal.II was initially developed in Universität Heidelberg, Germany, but later it is developed by a worldwide group of developers [11].

Chapter 2

Modeling Equation

The purpose of this chapter is to present the governing equations of flow and transport in porous media, and the partial differential equation (PDE) that is used in this thesis. Readers would immediately understand the context of anisotropy in reservoirs through this chapter.

2.1 Darcy's law

Darcy's law is known as the fundamental law of the fluid flow in porous medium. The law describes that a volumetric flow density (u_α) for a given phase (α) is given by [28]:

$$u_\alpha = -\lambda_\alpha \nabla p_\alpha \tag{2.1}$$

The equation implies that the movement of a phase α depends on the pressure (p) difference, and the velocity is defined by the medium and the phase conductivities. Nevertheless, the lowest phase pressure does not necessarily mean the actual direction of the flow, since λ_α is a hydraulic conductivity tensor. It is defined as:

$$\lambda_\alpha = \frac{K_r^\alpha}{\mu_\alpha} \tag{2.2}$$

where K_r^α and μ_α are relative permeability tensor and viscosity of phase α [28].

$$K_r^\alpha = \begin{pmatrix} K^\alpha_{r(xx)} & K^\alpha_{r(xy)} & K^\alpha_{r(xz)} \\ K^\alpha_{r(yx)} & K^\alpha_{r(yy)} & K^\alpha_{r(yz)} \\ K^\alpha_{r(zx)} & K^\alpha_{r(zy)} & K^\alpha_{r(zz)} \end{pmatrix} \tag{2.3}$$

To ensure physical consistent conductivity, the tensor of permeability must always be symmetric and positive definite [18]. This tensor is the one which represents anisotropy of reservoirs.

Taking into account the gravity (g) and the reservoir height, $h(x, y, z)$, from a reference plane, equation (2.1) yields:

$$u_\alpha = -\lambda_\alpha(\nabla p_\alpha + \gamma_\alpha \nabla h) \tag{2.4}$$

where γ_α is the specific gravity and ρ_α is the density of phase α.

$$\gamma_\alpha = g\rho_\alpha \tag{2.5}$$

For practical reason the vector of physical dimensions with entries (x, y) and (x, y, z) for 2D and 3D case is denoted by $\mathbf{x}$.

We are going to use conservation principle for the remaining derivations. Therefore, it is important to visit conservation law.

2.2 Conservation law

The principle of conservation is a cornerstone of mathematical modeling of physical phenomena. Consider a quantity u contained in a fixed control volume Ω. The change of u inside Ω is caused by a boundary flux F over Γ and the possible amount Q of u being generated within Ω. In integral form, the conservation of u reads [28]:

$$\int_\Omega \frac{\partial u}{\partial t}\, dV + \int_\Gamma F \cdot \mathbf{n}\, dS = \int_\Omega Q\, dV \tag{2.6}$$

Using Gauss's divergence theorem yields:

$$\begin{aligned} \int_\Omega \frac{\partial u}{\partial t}\, dV + \int_\Omega \nabla \cdot F\, dV &= \int_\Omega Q\, dV \\ \Leftrightarrow \int_\Omega (\frac{\partial u}{\partial t} + \nabla \cdot F - Q)\, dV &= 0 \end{aligned} \tag{2.7}$$

Since equation (2.7) holds for an arbitrary control volume Ω, then it is equivalent to

$$\frac{\partial u}{\partial t} + \nabla \cdot F = Q \tag{2.8}$$

Here, the conserved quantity u is mass per unit volume, that is:

$$u = \phi\rho_\alpha S_\alpha \tag{2.9}$$

where ϕ is the effective porosity,

$$\phi = \frac{V_p}{V} \tag{2.10}$$

V_p is the connected pore volume, and S_α is the phase saturation,

$$S_\alpha = \frac{V_\alpha}{V_p} \tag{2.11}$$

Furthermore, since the flux is equal to mass density times the velocity, that is:

$$F = \rho_\alpha u_\alpha \tag{2.12}$$

substitute equation (2.4) into (2.12), then it holds:

$$F = -\rho_\alpha \lambda_\alpha (\nabla p_\alpha + \gamma_\alpha \nabla h) \tag{2.13}$$

Finally, substitute equation (2.9) and (2.13) into (2.8) then the conservation law reads:

$$\frac{\partial(\phi\rho_\alpha S_\alpha)}{\partial t} - \nabla \cdot (\rho_\alpha \lambda_\alpha (\nabla p_\alpha + \gamma_\alpha \nabla h)) = Q \tag{2.14}$$

2.3 Model construction

Equation (2.14) can be extended for any purpose of fluid flow in a porous medium. However, for this thesis, we only consider single phase and incompressible fluid, and also constant porosity. Therefore, equation (2.14) is simplified as follows:

Single phase assumption

We only consider a single phase fluid, it means $S_\alpha = 1$, therefore, we can neglect the phase subscript. Equation (2.14) yields:

$$\frac{\partial(\phi\rho)}{\partial t} - \nabla \cdot (\rho\lambda(\nabla p + \gamma\nabla h)) = Q \tag{2.15}$$

The remaining unknowns are the phase pressure (p) and the density (ρ), however those two terms are defined by the fluid compressibility.

Incompressible fluid and constant medium matrix assumption

Now, let us define $\Phi = p + \rho g h$, and the following equality holds

$$\begin{aligned} \nabla\Phi &= \nabla p + g\rho\nabla h + gh\nabla\rho \\ &= \nabla p + g\rho\nabla h \\ &= \nabla p + \gamma\nabla h \end{aligned} \tag{2.16}$$

Moreover, under the assumption that the fluid is incompressible, it means ρ is constant, and we substitute equation (2.16) into (2.15). Thus, it holds:

$$\frac{\partial\phi}{\partial t} - \nabla \cdot \lambda\nabla\Phi = \frac{Q}{\rho} \tag{2.17}$$

We define $\tilde{Q} = \frac{Q}{\rho}$, and since the porosity is also assumed to be constant. Therefore, equation (2.17) reads:

$$-\nabla \cdot \lambda\nabla\Phi = \tilde{Q} \tag{2.18}$$

Finally, considering common boundary conditions for Darcy's equation in $\mathbb{R}^d$, $d \in \{1, 2\}$, the equation reads:

$$\begin{aligned} -\nabla \cdot (\lambda\nabla\Phi) &= \tilde{Q} && \text{in } \Omega \\ \Phi &= \Phi_D && \text{on } \Gamma^D \\ \lambda\nabla\Phi \cdot n &= F_N && \text{on } \Gamma^N \end{aligned} \tag{2.19}$$

We will refer to the last equation as the Darcy's equation. Furthermore, under the assumption that the relative permeability tensor (2.3) is symmetric and positive definite, the Darcy's equation is an elliptic PDE [52].

Chapter 3

Finite Element Method

This chapter is meant to give an introduction to IGA by visiting the origin analysis, i.e. FEA, since IGA shares many common principles with FEA. This section covers the weak formulations, functional settings, and analysis for FEA that also hold for IGA. In this section, we are also presenting all tools to verify the quality of the numerical approximations. A benchmark problem for 1D is presented in this section, and we will refer to this problem for the application of IGA in 1D in the later chapter.

3.1 Galerkin FEM

The main idea of FEM is to have numerical approximations of a PDE by applying the variational principle. This method was invented by Walther Ritz (1878 - 1909) to make a systematic approach for solving variational problems which were proposed by Euler (1707 - 1783). Later, this method was developed by Galerkin (1871 - 1945) which is so called Galerkin FEM (GFEM) [25]. The latter approach gains the most attention in the FEM world.

Galerkin method is actually a direct generalization of Ritz method [52]. Instead of having a minimization problem, this method directly deals with the weak formulation. In this thesis, we refer to Galerkin FEM as FEM.

Now, let us recall Darcy's equation that has already been described in equation (2.19). It will be easier to understand the mathematical settings of the PDE if we rewrite the equation properly. For this purpose we are referring to [12] and [42] with some adaptations in the notations. Let $\Omega \subset \mathbb{R}^d$, $d \in \{1, 2\}$, be a bounded Lipschitz domain. Let $\tilde{Q} \in L^2(\Omega)$, $\Phi_D \in H^{\frac{1}{2}}(\Gamma_D)$, and $F_N \in L^2(\Gamma_N)$ be given functions. Thus the problem reads as follows:

Find $\Phi : \bar{\Omega} \to \mathbb{R}$ such that

$$\begin{aligned} -\nabla \cdot (\lambda \nabla \Phi) &= \tilde{Q} && \text{in } \Omega \\ \Phi &= \Phi_D && \text{on } \Gamma^D \\ \lambda \nabla \Phi \cdot n &= F_N && \text{on } \Gamma^N \end{aligned}$$

where $\lambda \in (L^\infty(\Omega))^{d \times d}$ and n is the unit outward normal vector in $\partial\Omega$. The boundary $\partial\Omega$ consists of two disjoints parts, Γ_D on which Dirichlet conditions are imposed,

and Γ_N on which Neumann conditions conditions are imposed: $\Gamma_D \cup \Gamma_N = \partial\Omega$, $\Gamma_D \cap \Gamma_N = \emptyset$, and *meas* $\Gamma_D > 0$.

3.2 Weak formulation

The Darcy's equation (2.19) will be converted into a weak formulation by the following steps. We employ the standard Sobolev space notations. Let us denote the trial space by S and the test space by V. We take the function $\Phi \in S$ and a test function $v \in V$ and multiply the equation (2.19) by the test function v. It is important to take care of the boundary conditions at this point. The trial space S and the test space V are the Hilbert spaces with some additional restrictions caused by Dirichlet boundary conditions, to be precise:

$$\begin{aligned} -\int_\Omega (\nabla \cdot \lambda \nabla \Phi)\ v\ d\Omega &= \int_\Omega \tilde{Q}\ v\ d\Omega \\ \int_\Omega \lambda \nabla \Phi \cdot \nabla v\ d\Omega - \int_\Gamma v \lambda \nabla \Phi \cdot n\ d\Gamma &= \int_\Omega \tilde{Q}\ v\ d\Omega \\ \int_\Omega \lambda \nabla \Phi \cdot \nabla v\ d\Omega &= \int_\Omega \tilde{Q}\ v\ d\Omega + \int_{\Gamma_N} F_N\ v\ d\mathbf{s} \end{aligned} \tag{3.1}$$

The weak formulation of the equation (2.19) reads:

$$\text{find } \Phi \in S \text{ such that for all } v \in V,\ a(\Phi, v) = f(v) \tag{3.2}$$

where:

$$a(\Phi, v) = \int_\Omega \lambda \nabla \Phi \cdot \nabla v\ d\Omega \tag{3.3}$$

$$f(v) = \int_\Omega \tilde{Q}\ v\ d\Omega + \int_{\Gamma_N} F_N\ v\ d\mathbf{s} \tag{3.4}$$

Moreover, we construct $S^h \subset S$ and $V^h \subset V$ which are finite-dimensional subspaces of S and V. We assume: $S^h = V^h$. Thus the discrete weak formulation reads:

$$\text{find } \Phi^h \in V^h \text{ such that for all } v^h \in V^h,\ a(\Phi^h, v^h) = f(v^h) \tag{3.5}$$

where:

$$a(\Phi^h, v^h) = \int_\Omega \lambda \nabla \Phi^h \cdot \nabla v^h\ d\Omega \tag{3.6}$$

$$f(v^h) = \int_\Omega \tilde{Q}\ v^h\ d\Omega + \int_{\Gamma_N} F_N\ v^h\ d\mathbf{s} \tag{3.7}$$

Due to Lax-Milgram's theorem, equation (3.5) has a unique solution [12, 42].

3.3 1D benchmark problem

To see how the FEM works we will consider (2.19) with $\lambda(\mathbf{x}) = \mathbb{I}$. Thus, it is easy to realize that we end up with a Poisson's equation. Let us consider a 1D Poisson's problem given as:

$$\begin{aligned} -\frac{d^2\Phi}{dx^2} &= \tilde{Q}(x), \text{ in } \Omega = (0,1) \\ \Phi(0) &= 0 \\ \Phi(1) &= 0 \end{aligned} \tag{3.8}$$

with $\tilde{Q}(x) = \pi^2 \sin(\pi x)$. We will refer this problem as our 1D benchmark problem. Moreover, it is easy to check that is the analytical solution to the above problem as:

$$\Phi_{ex}(x) = \sin(\pi x) \tag{3.9}$$

From (3.5) - (3.7) the discrete weak formulation of equation (3.8) reads:

$$\text{find } \Phi^h \in V^h \text{ such that for all } v^h \in V^h,\ a(u^h, v^h) = f(v^h) \tag{3.10}$$

where:

$$a(\Phi^h, v^h) = \int_0^1 \frac{d\Phi^h}{dx}\frac{dv^h}{dx}\, dx \tag{3.11}$$

$$f(v^h) = \int_0^1 \tilde{Q}\ v^h\ dx \tag{3.12}$$

We define $\Phi^h = \sum_1^n \Phi_i \varphi_i$ where n is the number of degrees of freedom (DOF) and φ_i is the i-th basis function of the considered trial space. Furthermore, realizing that it is enough to use basis function of V^h as test functions v, the discrete weak formulation can be rewritten in form of linear system, that is:

$$A\mathbf{\Phi} = \mathbf{b} \tag{3.13}$$

where the entries of matrix A are defined as $a_{ij} = a(\varphi_i, \varphi_j)$, entries of vector $\mathbf{b}$ as $b_i = f(\varphi_i)$ and $\mathbf{\Phi}$ is the vector of unknown solution coefficients Φ_i.

3.4 Results

We consider quadratic Lagrange basis functions as depicted in Figure 3.1 and 3.2 for the 1D benchmark problem. The type of basis functions is optional. It depends on the desired accuracy. If we want a higher order accuracy, it is necessary to use higher order polynomials. In $\mathbb{R}^1$, a quadratic interpolation polynomial over an element with vertices x_1 and x_3 and midpoint x_2 can be written as [52]:

$$\Phi(x) = \varphi_1(x)\Phi_1 + \varphi_2(x)\Phi_2 + \varphi_3(x)\Phi_3 \tag{3.14}$$

with $\varphi_i(x)$ the quadratic Lagrangian polynomials defined by:

$$\varphi_1(x) = \frac{(x-x_2)(x-x_3)}{(x_1-x_2)(x_1-x_3)} \tag{3.15}$$

$$\varphi_2(x) = \frac{(x-x_3)(x-x_1)}{(x_2-x_3)(x_2-x_1)} \tag{3.16}$$

$$\varphi_3(x) = \frac{(x-x_1)(x-x_2)}{(x_3-x_1)(x_3-x_2)} \tag{3.17}$$

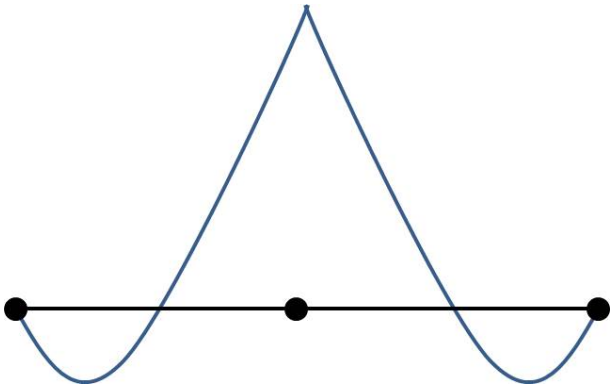

Figure 3.1: Basis function for a vertex

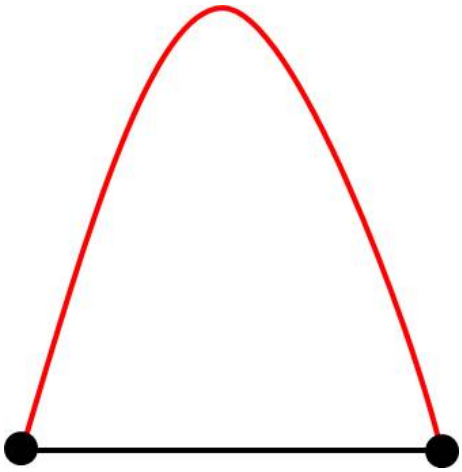

Figure 3.2: Midpoint basis function

To assess the quality of the numerical approximations, we compare the approximations with the exact solution in terms of L2 norm. The comparison is defined as:

$$\|\Phi_{ex} - \Phi^h\|_2 = \Big(\int_0^1 (\Phi_{ex}(\mathbf{x}) - \Phi^h(\mathbf{x}))^2 d\mathbf{x} \Big)^{\frac{1}{2}} \tag{3.18}$$

The error of the numerical approximations for various size of element (h) and number of degrees of freedom is shown in Table 3.1, and it is depicted in Figure 3.3.

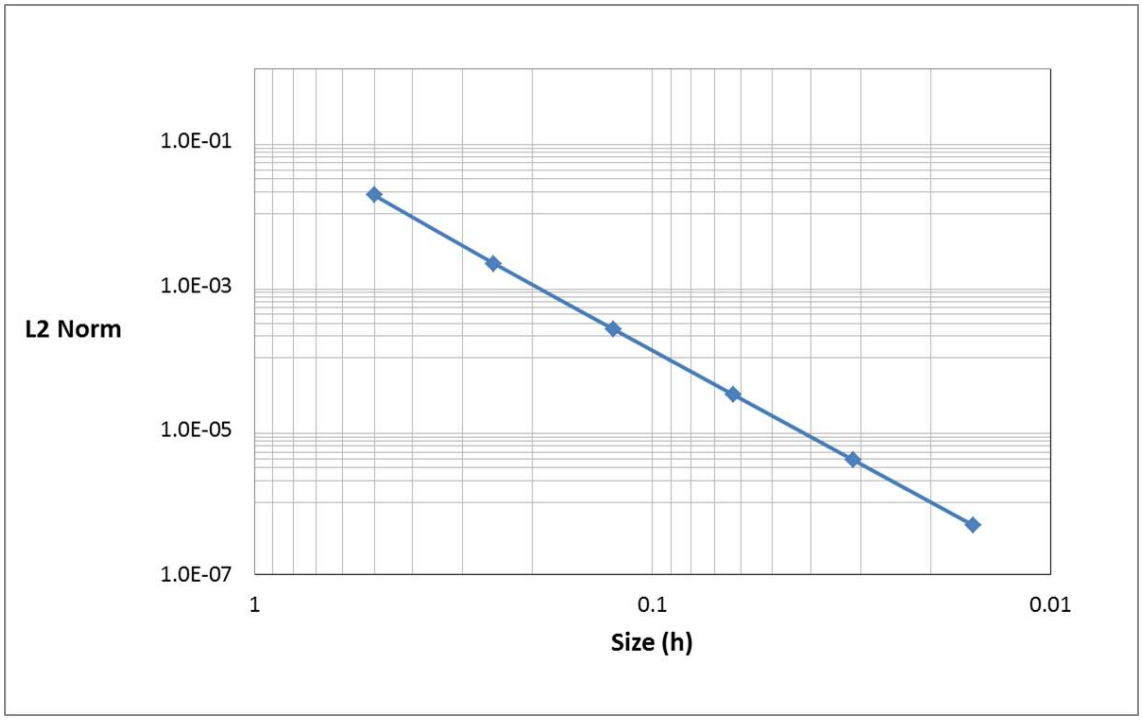

Figure 3.3: The plot of numerical approximation error in L2 norm for the 1D benchmark problem.

h	$\#\ DOF$	*Error in L2 norm*
$\frac{1}{2}$	3	1.79113E-02
$\frac{1}{4}$	5	2.03298E-03
$\frac{1}{8}$	9	2.48187E-04
$\frac{1}{16}$	17	3.08414E-05
$\frac{1}{32}$	33	3.84952E-06
$\frac{1}{64}$	65	4.81013E-07

Table 3.1: The numerical approximation error in L2 norm for various size of element and number of degrees of freedom.

Furthermore, we can verify the error by considering the fact that it holds [45]:

$$\|\Phi_{ex} - \Phi^h\|_2 \leq Ah^{p+1} \tag{3.19}$$

where p is the **polynomial order** of the set of basis functions. Indeed, relying the results that are shown in Table 3.1 and Figure 3.3 for verifications would be difficult.

Therefore, we would like to introduce what is so-called **convergence rates**. By considering (3.19), it holds:

$$\log_2 \frac{\|\Phi_{ex} - \Phi^h\|_2}{\|\Phi_{ex} - \Phi^{h/2}\|_2} \approx p + 1 \tag{3.20}$$

Thus, we can easily implement (3.20) to obtain Table 3.2.

h	$\#\ DOF$	$Convergence\ rates$
$\frac{1}{4}$	5	3.13920
$\frac{1}{8}$	9	3.03410
$\frac{1}{16}$	17	3.00849
$\frac{1}{32}$	33	3.00212
$\frac{1}{64}$	65	3.00053

Table 3.2: The numerical approximation convergence rates for the 1D benchmark problem, $p = 2$.

Considering the convergence rates that are shown in Table 3.2, we know for sure the implemented FEM code is valid since the L2 norm converges at the right rate.

Chapter 4

Isogeometric Analysis

IGA and FEA share common principles up to the weak formulation. Nonetheless, IGA uses B-splines as its test functions. It is understandable since IGA, in the beginning, was meant to integrate FEA and Computer Aided Design (CAD). To allow such integration, they have to share something in common. CAD is using B-splines or Non Uniform Rational B-Splines (NURBS) to represent geometries. Therefore, IGA is also using B-splines as its basis functions.

The integration has some benefits, in comparison with FEA, such as a better domain representation, and a simpler connection from design to mesh generation and refinement. Having said that, it also comes with prices. First, the frame of work adjustments. Indeed, we are talking about the environment in B-splines now. Consequently, we have to know the principles inherited in B-splines. Second, the cost of computation. It is suggested that an efficient code implementation is essential for IGA implementations [31].

4.1 B-Splines

The B-spline parameter space is local to patches rather than elements, in comparison with FEA. In FEA, the parameter space is mapped into a single element in the physical space. Therefore, each element has its own mapping. Meanwhile, the B-spline mapping takes a patch of multiple elements in the parameter space into the physical space. Each element in the physical space is the image of a corresponding element in the parameter space, but the mapping itself is global to the whole patch, rather than to the elements themselves.

Patches play the role of subdomains within which element types are assumed to be uniform. A single patch might comprise many elements.

4.2 Knot vectors

The initial step to construct B-splines is to define **knot vectors**. A knot vector in one dimension is a non-decreasing set of coordinates in the parameter space [15], written as $\Xi = \{\xi_1, \xi_2, ..., \xi_{n+p+1}\}$, where $\xi_i \in \mathbb{R}$ is the i-th knot. We denote n as the number

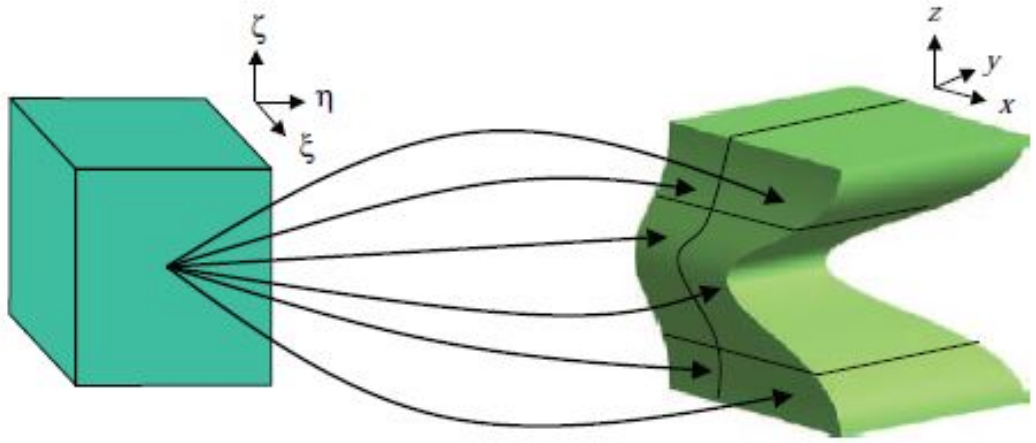

Figure 4.1: In FEA, the parameter space is local to individual elements. Each element has its own mapping from the reference element [15].

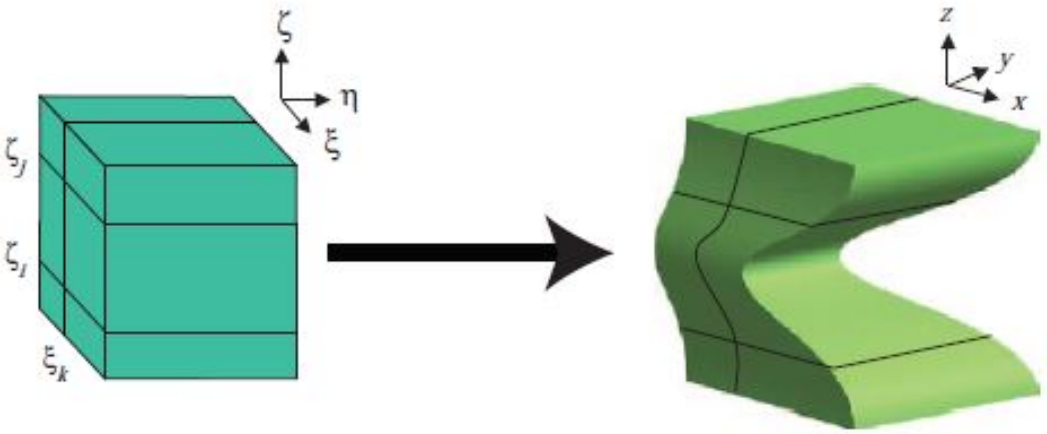

Figure 4.2: The B-spline parameter space is local to the entire patch. Internal knots partition the patch into elements. A single B-spline map takes the patch from the parameter space to the physical space [15].

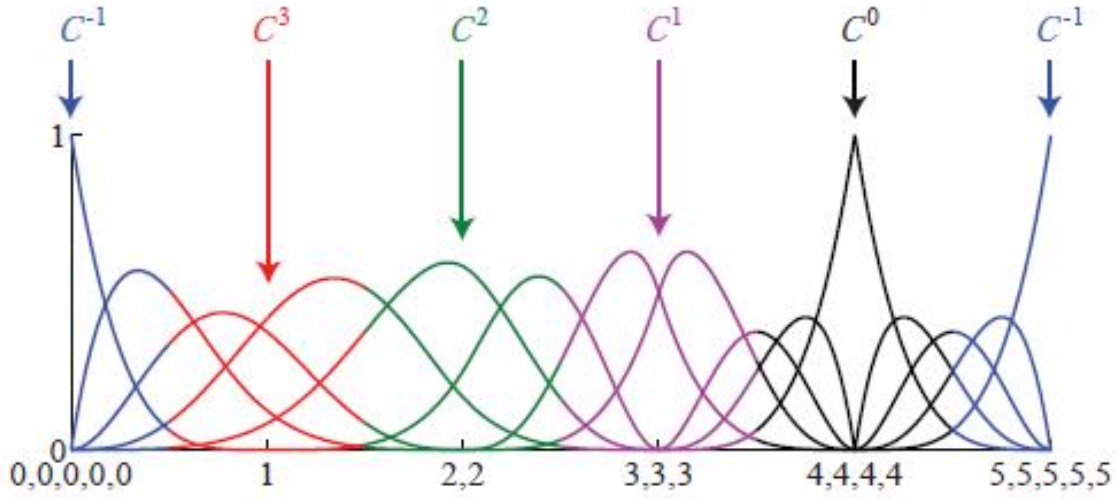

Figure 4.3: Quartic ($p = 4$) basis functions for an open, non-uniform knot vector, $\Xi = \{0, 0, 0, 0, 0, 1, 2, 2, 3, 3, 3, 4, 4, 4, 4, 5, 5, 5, 5, 5\}$. The continuity across an interior element boundary is a direct result of the polynomial order and the multiplicity of the corresponding knot value [15].

of basis functions. A knot vector is called **uniform** if the knots are equally spaced in the parameter space and **non-uniform** if they are not. It is called **open** if its first and last knot values appear $p + 1$ times.

4.3 Basis functions

The B-spline basis functions are defined recursively starting with piecewise constants ($p = 0$), we refer to Cox-de Boor recursion formula [17] for the construction. That is:

$$N_{i,0} = \begin{cases} 1, & \text{if } \xi_i \leq \xi < \xi_{i+1} \\ 0, & \text{otherwise} \end{cases} \tag{4.1}$$

and for $p = 1, 2, 3, ...$, they are defined by:

$$N_{i,p}(\xi) = \frac{\xi - \xi_i}{\xi_{i+p} - \xi_i} N_{i,p-1}(\xi) + \frac{\xi_{i+p+1} - \xi}{\xi_{i+p+1} - \xi_{i+1}} N_{i+1,p-1}(\xi) \tag{4.2}$$

Applying a non-uniform knot vector gives richer behaviors than a simple uniform does. In general, basis functions of order p have $p - m_i$ continuous derivatives across knot ξ_i, where m_i is the number of multiplicity at knot value i-th. If the multiplicity is $p + 1$, then the basis functions become discontinuous and the patch boundary is formed.

There are several important features of the basis functions that are pointed by Hughes et al. [15]. First, the basis function constructs a partition of unity, that is:

$$\sum_{i=1}^{n} N_{i,p}(\xi) = 1, \ \forall \xi \in [\xi_1, \xi_{n+p+1}] \tag{4.3}$$

Second, there is nonnegative value for the basis function over the entire domain, to be precise:

$$N_{i,p}(\xi) \neq 0, \ \forall \xi \in (\xi_i, \xi_{n+p+1}) \tag{4.4}$$

Third, every p^{th} order function has $p-1$ continuous derivatives across the knots. Finally, for every B-spline function of order p there is always $p+1$ **knot spans**, distance between knots, as the support.

The derivatives of B-splines are represented in terms of B-spline lower order bases, indeed as it comes directly from the recursive definition given in equation (4.1) and (4.2). Thus, the derivative of the i-th basis function of order p is given by [15]:

$$\frac{d}{d\xi} N_{i,p} = \frac{p}{\xi_{i+p} - \xi_i} N_{i,p-1}(\xi) - \frac{p}{\xi_{i+p+1} - \xi_{i+1}} N_{i+1,p-1}(\xi) \tag{4.5}$$

4.4 B-spline geometries

By taking a linear combination of B-spline basis functions, the B-spline curves in $\mathbb{R}^d$ are constructed. **Control points** are defined as vector-valued coefficients of the basis functions. Let us consider a basis consisting of n basis functions given as $N_{i,p}, i = 1, 2, ..., n$ and corresponding control points $\mathbf{B_i} \in \mathbb{R}, i = 1, 2, ..., n$, thus a piecewise-polynomial **B-spline curve** is given as:

$$C(\xi) = \sum_{i=1}^{n} N_{i,p}(\xi) \mathbf{B_i} \tag{4.6}$$

The linear interpolation of the control points is called the **control polygon**.

Furthermore, a tensor product for a given **control net** $\mathbf{B_{i,j}}, i = 1, 2, ..., n, j = 1, 2, ..., m$ for polynomial orders p and q, and knot vectors $\Xi = \{\xi_1, \xi_2, ..., \xi_{n+p+1}\}$ and $\mathscr{H} = \{\eta_1, \eta_2, ..., \eta_{m+q+1}\}$, is called **B-spline surface**. It is defined as:

$$S(\xi, \eta) = \sum_{i=1}^{n} \sum_{j=1}^{m} N_{i,p}(\xi) M_{j,q}(\eta) \mathbf{B_{i,j}} \tag{4.7}$$

It is important to point out that many properties of a B-spline surface are the results of its tensor product nature. Multivariate B-splines basis functions are nonnegative, have local support, and form a partition of unity [15]. To be precise:

$$\sum_{i=1}^{n} \sum_{j=1}^{m} N_{i,p}(\xi) M_{j,q}(\eta) = \left(\sum_{i=1}^{n} N_{i,p}(\xi) \right) \left(\sum_{j=1}^{m} M_{j,q}(\eta) \right) = 1 \tag{4.8}$$

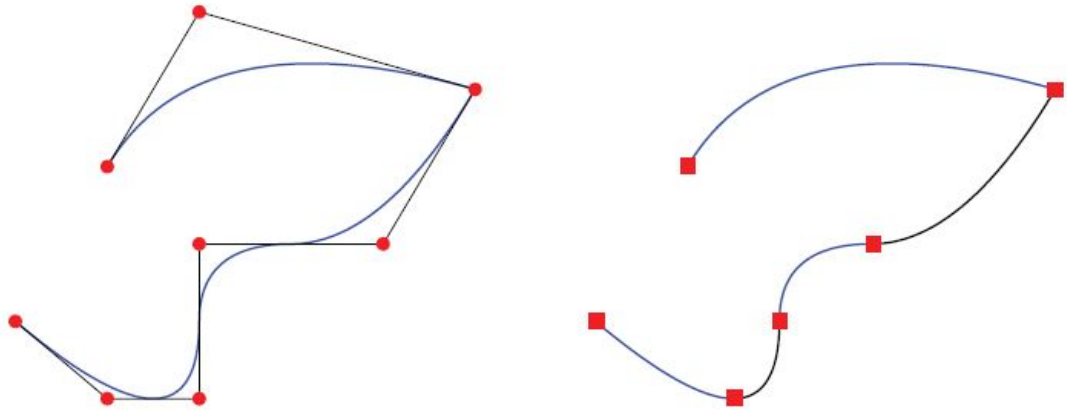

(a) Curve and control points

(b) Curve and mesh denoted by knot locations

Figure 4.4: B-spline, piecewise quadratic curve in $\mathbb{R}^2$ [15].

4.5 B-spline refinements

One interesting property of B-splines is their ability to enrich the basis without changing the shape of the geometry. This is possible through refinements. The refinements in B-spline can be done at the knot vectors and/or the degree of polynomial basis functions. There are three types of refinements, those are: **knot insertions**, **order elevation**, and **k-refinement**.

4.5.1 Knot insertions

The first mechanism is performed by adding m knots into an existing knot vector $\Xi = \{\xi_1, \xi_2, ..., \xi_{n+p+1}\}$, thus the extended knot vector $\bar{\Xi} = \{\bar{\xi}_1 = \xi_1, \bar{\xi}_2, ..., \bar{\xi}_{n+m+p+1} = \xi_{n+p+1}\}$. Indeed, $\Xi \subset \bar{\Xi}$. The new $n+m$ basis functions are defined by (4.1) and (4.2). Moreover, the new $n+m$ control points, $\bar{\mathscr{B}} = \{\bar{\mathbf{B}}_1, \bar{\mathbf{B}}_2, ..., \bar{\mathbf{B}}_{n+m}\}^T$, are defined by taking linear combinations of the initial control points, $\mathscr{B} = \{\mathbf{B}_1, \mathbf{B}_2, ..., \mathbf{B}_n\}^T$, to be precise [15]:

$$\bar{\mathscr{B}} = T^p \mathscr{B} \tag{4.9}$$

where

$$T^0_{i,j} = \begin{cases} 1, & \bar{\xi}_i \in [\xi_j, \xi_{j+1}) \\ 0, & \text{otherwise} \end{cases} \tag{4.10}$$

and for $q = 0, 1, 2, ..., p-1$

$$T^{q+1}_{ij} = \frac{\bar{\xi}_{i+q} - \xi_j}{\xi_{j+q} - \xi_j} T^q_{ij} + \frac{\xi_{j+q+1} - \bar{\xi}_{i+q}}{\xi_{j+q+1} - \xi_{j+1}} T^q_{ij+1} \tag{4.11}$$

4.5.2 Order elevation

The second mechanism of refinement is more complicated than the first one. The process involves raising the polynomial order of the basis functions. It should be noted that to keep the $p - m_i$ continuous derivatives across the element, for every t increment of order elevation there will also be t increment for every knot value. In other words, to increase the order by 1 for a given knot vector of order p with o number of unique knot values, there will be additional o knot values, and as a consequence, there will be $o - 1$ new degrees of freedom.

The procedure works as follows: first, we replicate existing knots until their multiplicity is equal to the polynomial order, then effectively subdividing the curve into many Bèzier curves by knot insertion. Second, we elevate the order of the polynomial on each of these individual segments. Lastly, we remove excess knots and combine the segments into one, order-elevated, B-spline curve. Several efficient algorithms exist which combine the steps so as to minimize the computational cost of the process [29]. We may refer to [43] for a thorough treatment.

4.5.3 k-refinement

It is important to note that the order elevation and knot insertion are non-commutative. For instance a new knot value $\bar{\xi}$ is inserted to curve of order p, then the C^{p-1} continuity is also obtained at $\bar{\xi}$. Suppose that this curve is increased by the order elevation to q, then the C^{p-1} continuity at $\bar{\xi}$ is still preserved. Changing the order of refinements, it is obtained C^{q-1} at $\bar{\xi}$. The latter operation it is so called the k-refinement.

4.6 Non-uniform rational B-splines

Although in this thesis we restrict ourselves to the application of B-splines, it is worth to mention that there are some geometries that can not be represented exactly with the use of B-splines such as circles and ellipses. Non-uniform rational B-splines (NURBS) allows us to represent a much wider class of objects than B-splines do.

A NURBS entity in $\mathbb{R}^d$ is obtained by the projective transformation of a B-spline entity in $\mathbb{R}^{d+1}$ [29]. To have a better idea how it works we refer to Figure 4.5.

We denote $\mathbf{C}^w(\xi)$ as B-spline curve, in the context of NURBS it is called **projective curve**, and $\mathbf{B}_i^w(\xi)$ as projective control points. The NURBS curve is denoted by $\mathbf{C}(\xi)$ and the control points by $\mathbf{B}_i$. With a given projective B-spline curve and its associated projective control points at hand, the control points for the NURBS curve are obtained by the following relations [15]:

$$(\mathbf{B}_i)_j = \frac{(\mathbf{B}_i^w)_j}{w_i},\ j = 1, ..., d \tag{4.12}$$

$$w_i = (\mathbf{B}_i^w)_{d+1} \tag{4.13}$$

where $(\mathbf{B}_i)_j$ is the j-th component of vector $\mathbf{B}_i$ and w_i corresponds to i-th **weight**.

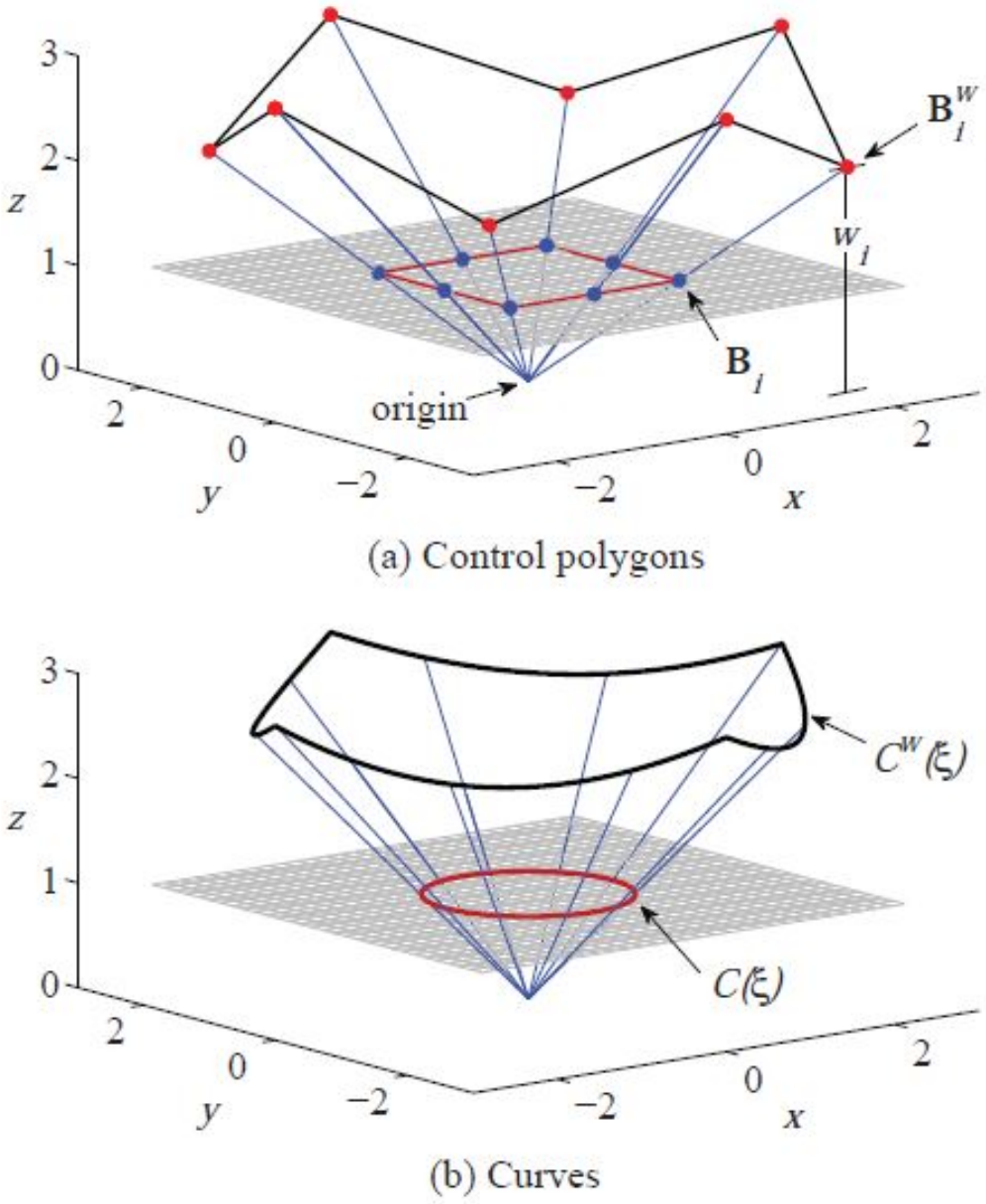

Figure 4.5: A circle in $\mathbb{R}^2$ constructed by the projective transformation of a piecewise quadratic B-spline in $\mathbb{R}^3$ [15].

The **weighting function** is defined as [15]:

$$W(\xi) = \sum_{i=1}^{n} N_{i,p}(\xi) w_i \tag{4.14}$$

where $N_{i,p}(\xi)$ is the standard B-spline basis function. The NURBS basis function is defined as [15]:

$$R_i^p(\xi) = \frac{N_{i,p}(\xi) w_i}{W(\xi)} \tag{4.15}$$

Then the NURBS curve can be obtained as [15]:

$$(\mathbf{C}(\xi))_j = \frac{(\mathbf{C}^w(\xi))_j (\xi)_j}{W(\xi)}, \ j = 1, ..., d \tag{4.16}$$

since $\mathbf{C}^w(\xi)$ and $W(\xi)$ are both piecewise polynomial functions, the curve $\mathbf{C}(\xi)$ is a piecewise **rational function**. The practice expression of (4.16) can be obtained using (4.15) in conjunction with the control points of (4.13), that is [15]:

$$(\mathbf{C}(\xi))_j = \sum_{i=1}^{n} R_i^p(\xi) \mathbf{B}_i \tag{4.17}$$

Furthermore, we can obtain **NURBS surfaces** using the rational basis functions that is [15]:

$$R_{i,j}^{p,q}(\xi, \eta) = \frac{N_{i,p}(\xi) M_{j,q}(\eta) w_{i,j}}{\sum_{\hat{i}=1}^{n} \sum_{\hat{j}=1}^{m} N_{\hat{i},p}(\xi) M_{\hat{j},q}(\eta) w_{\hat{i},\hat{j}}} \tag{4.18}$$

Chapter 5

B-splines as basis for analysis

The purpose of this chapter is to show implementations of IGA. We will revisit the 1D benchmark problem that is given in (3.8). Then, we will continue with the 2D benchmark problems. It should be noted, that up to the 1D problem the implementation of both analyses, FEA and IGA, are encoded in MATLAB. For further implementations, the **G+SMO** open-source C++ library is being used due to the efficiency of the computation. Readers who are interested in G+SMO are advised to read [32].

5.1 IGA 1D benchmark problem

Let us reconsider the 1D benchmark problem given in (3.8). The discrete weak formulations for the benchmark problem are already obtained in equations (3.10) - (3.12). Analogue with the FEA counterpart, we define $\Phi^h = \sum_1^n \Phi_i \varphi_i$ where n is the number of degrees of freedom (DOF) and φ_i is the i-th DOF of the considered trial space. Furthermore, we grant an open and uniform knot vector for $p \in \{1, 2, 3, 4\}$, and we assess the quality of the numerical approximations through the L2 norm given in the equation (3.18) and the convergence rates given in the equation (3.20).

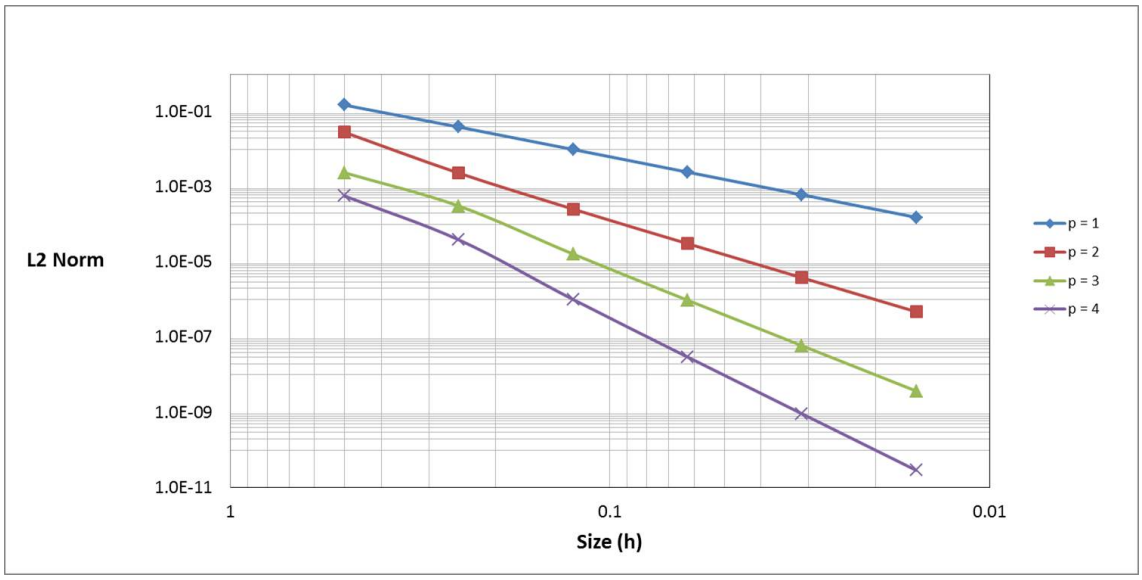

Figure 5.1: The plot of numerical approximation error in L2 norm for the 1D benchmark problem, $p \in \{1, 2, 3, 4\}$.

h	*Error in L2 norm*			
	$p = 1$	$p = 2$	$p = 3$	$p = 4$
$\frac{1}{2}$	1.50877E-01	2.84145E-02	2.38869E-03	5.72595E-04
$\frac{1}{4}$	3.92843E-02	2.33277E-03	3.11035E-04	3.91649E-05
$\frac{1}{8}$	9.92092E-03	2.57384E-04	1.63705E-05	1.01254E-06
$\frac{1}{16}$	2.48650E-03	3.11276E-05	9.72452E-07	3.00295E-08
$\frac{1}{32}$	6.22018E-04	3.85845E-06	5.99884E-08	9.29504E-10
$\frac{1}{64}$	1.55529E-04	4.81292E-07	3.73697E-09	2.90365E-11

Table 5.1: The error of numerical approximations in L2 norm for the 1D benchmark problem, $p \in \{1, 2, 3, 4\}$.

h	*Convergence rates*			
	$p=1$	$p=2$	$p=3$	$p=4$
$\frac{1}{4}$	1.94135	3.60651	2.94107	3.86988
$\frac{1}{8}$	1.98541	3.18005	4.24791	5.27351
$\frac{1}{16}$	1.99636	3.04765	4.07333	5.07545
$\frac{1}{32}$	1.99909	3.01210	4.01887	5.01378
$\frac{1}{64}$	1.99977	3.00304	4.00474	5.00052

Table 5.2: The numerical approximation convergence rates for the 1D benchmark problem, $p \in \{1, 2, 3, 4\}$.

Table 5.1 shows the error of the numerical approximations for various element sizes (h), and order of polynomial(p). Those results are depicted in Figure 5.1. As it is expected, the order of error is $\mathscr{O}(h^{p+1})$ [45] which is confirmed by Table 5.2.

5.2 IGA 2D benchmark problem

Now, we will define our 2D benchmark problem that is:

$$\begin{aligned} -\Delta\Phi(\mathbf{x}) &= \tilde{Q}(\mathbf{x}), \text{ in } \Omega = (0,1)\times(0,1), \\ \Phi(\mathbf{x}) &= 0, \text{ on } \partial\Omega \end{aligned} \tag{5.1}$$

with $\tilde{Q}(\mathbf{x}) = -2\pi^2 \sin(\pi x)\sin(\pi y)$. It is easy to check that the analytical solution of the given problem is:

$$\Phi_{ex}(\mathbf{x}) = \sin(\pi x)\sin(\pi y) \tag{5.2}$$

This analytical solution is special in this thesis, since we will always refer to this analytical solution (5.2) for the remaining chapters.

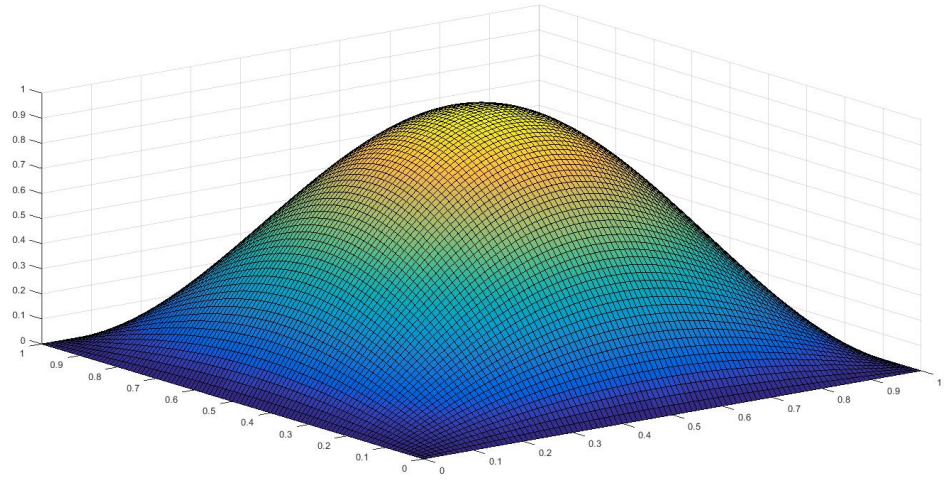

Figure 5.2: The analytical solution for the 2D benchmark problem.

Using the given discrete weak formulations in equations (3.5) - (3.7), we can easily proceed to the linear system of equation. However, it should be noted that the DOF are resulting from the tensor product construction of B-spline basis functions in direction ξ and η. We might refer to [37] for the practice of matrix and vector assembly.

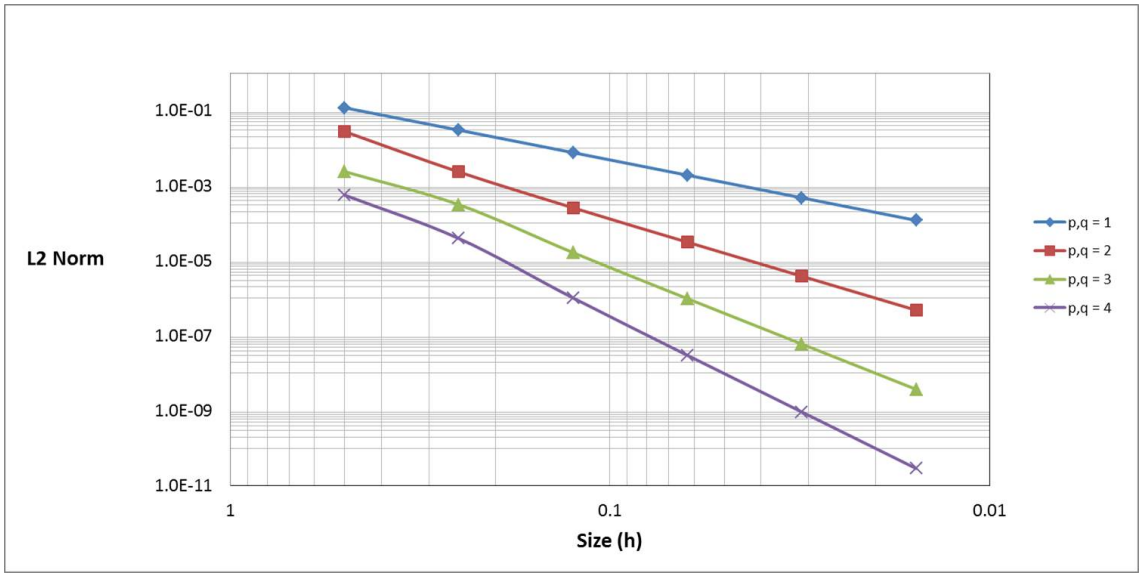

Figure 5.3: The plot of numerical approximation error in L2 norm for the 2D benchmark problem, $p = q \in \{1, 2, 3, 4\}$.

h	*Error in L2 norm*			
	$p, q = 1$	$p, q = 2$	$p, q = 3$	$p, q = 4$
$\frac{1}{2}$	1.19146E-01	2.76355E-02	2.36990E-03	5.61179E-04
$\frac{1}{4}$	3.01896E-02	2.31365E-03	3.10615E-04	3.90479E-05
$\frac{1}{8}$	7.58781E-03	2.56829E-04	1.63693E-05	1.01212E-06
$\frac{1}{16}$	1.89974E-03	3.11107E-05	9.72450E-07	3.00280E-08
$\frac{1}{32}$	4.75114E-04	3.85793E-06	5.99884E-08	9.29497E-10
$\frac{1}{64}$	1.18790E-04	4.81276E-07	3.73697E-09	2.90365E-11

Table 5.3: The numerical approximation error in L2 norm for the 2D benchmark problem. $p = q \in \{1, 2, 3, 4\}$.

h	*Convergence rates*			
	$p, q = 1$	$p, q = 2$	$p, q = 3$	$p, q = 4$
$\frac{1}{4}$	1.98061	3.57828	2.93163	3.84514
$\frac{1}{8}$	1.99230	3.17129	4.24606	5.26979
$\frac{1}{16}$	1.99788	3.04533	4.07322	5.07493
$\frac{1}{32}$	1.99946	3.01151	4.01887	5.01371
$\frac{1}{64}$	1.99986	3.00289	4.00474	5.00051

Table 5.4: The numerical approximation convergence rates for the 2D benchmark problem, $p = q \in \{1, 2, 3, 4\}$.

We consider an open-uniform knot vector for ξ and η, and fix the same order of polynomial for both directions, i.e. $p = q \in \{1, 2, 3, 4\}$. We also define the same element size for both directions.

Table 5.3 shows the quality of the numerical approximations in L2 norm for various size of element (h) and order of polynomial (p and q). The error of the numerical approximations is depicted in Figure 5.3. As it is expected, that the order of the error is $\mathcal{O}(h^{p+1})$ [45]. The convergence rates in Table 5.4 are at the optimum rate, and they confirm the results.

5.3 IGA Darcy's equation 1

We have seen the implementations of IGA for the two benchmark problems, which are Poisson's equations, in the previous sections. It is clear from the demonstrations that the implemented code has been validated for a particular benchmark problem.

The numerical approximation error converges at the right rate. Now, we will consider our main problem, that is the Darcy's equation, where λ is not necessarily equal to $\mathbb{I}$. Let us consider:

$$\lambda(\mathbf{x}) = \begin{pmatrix} 4 & x+y \\ x+y & 4 \end{pmatrix} \tag{5.3}$$

We set the exact solution that is already given on (5.2), then we do reverse calculation to obtain the source function, $\tilde{Q}(\mathbf{x})$, as follows:

$$\tilde{Q}(\mathbf{x}) = 8\pi^2 \sin(\pi x)\sin(\pi y) - 2\pi^2(x+y)\cos(\pi x)\cos(\pi y) - \pi \sin(\pi x + \pi y) \tag{5.4}$$

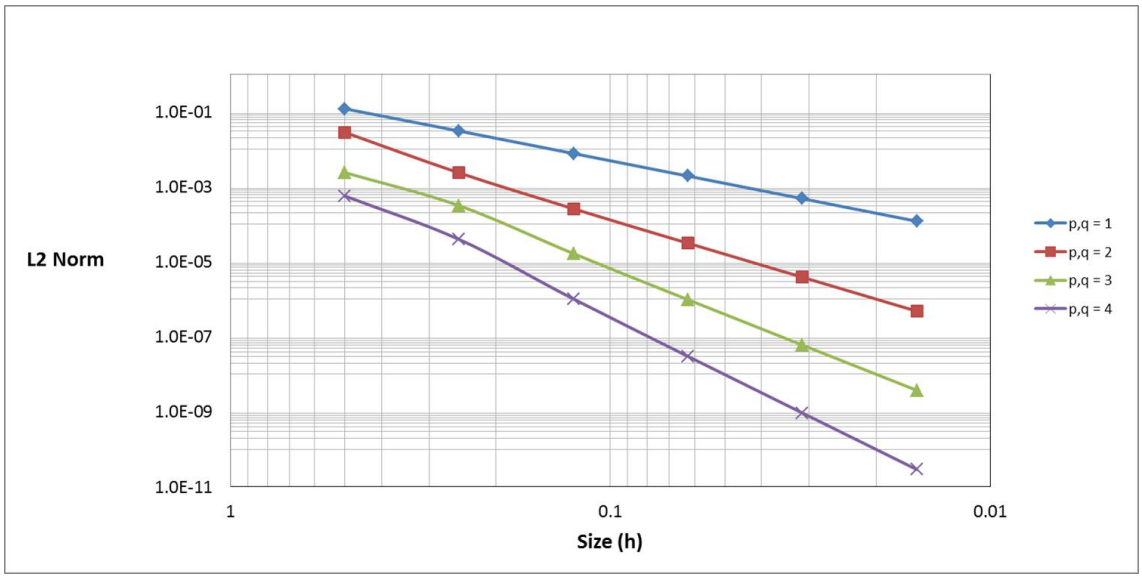

Figure 5.4: The plot of the numerical approximation error in L2 norm for the 2D Darcy's equation 1, $p = q \in \{1, 2, 3, 4\}$.

h	*Error in L2 norm*			
	$p, q = 1$	$p, q = 2$	$p, q = 3$	$p, q = 4$
$\frac{1}{2}$	1.19146E-01	2.79916E-02	2.37131E-03	5.64413E-04
$\frac{1}{4}$	3.03356E-02	2.32503E-03	3.10754E-04	3.91211E-05
$\frac{1}{8}$	7.64573E-03	2.57176E-04	1.63701E-05	1.01244E-06
$\frac{1}{16}$	1.91582E-03	3.11214E-05	9.72452E-07	3.00292E-08
$\frac{1}{32}$	4.79238E-04	3.85826E-06	5.99884E-08	9.29503E-10
$\frac{1}{64}$	1.19828E-04	4.81286E-07	3.73697E-09	2.90365E-11

Table 5.5: The error of the numerical approximations in L2 norm for the 2D Darcy's equation 1, $p = q \in \{1, 2, 3, 4\}$.

h	*Convergence rates*			
	$p = 1$	$p = 2$	$p = 3$	$p = 4$
$\frac{1}{4}$	1.97365	3.58967	2.93184	3.85073
$\frac{1}{8}$	1.98829	3.17642	4.24664	5.27204
$\frac{1}{16}$	1.99669	3.04678	4.07329	5.07533
$\frac{1}{32}$	1.99915	3.01188	4.01887	5.01376
$\frac{1}{64}$	1.99978	3.00298	4.00474	5.00052

Table 5.6: The numerical approximation convergence rates for the 2D Darcy's equation 1, $p = q \in \{1, 2, 3, 4\}$.

We consider $p = q \in \{1, 2, 3, 4\}$ and asses the quality of numerical approximations through the L2 norm given in (3.18). Table 5.5 shows the error of numerical approximations in L2 norm for various size of element (h) and order of polynomial (p). Those results are depicted in Figure 5.4. We obtain the order of error is $\mathscr{O}(h^{p+1})$ [45]. The convergence rates in Table 5.6 verify the results of the numerical approximations. It is a strong message that the implemented code for IGA is robust.

Chapter 6

IGA for reservoir simulation

In the previous chapter, we have seen how IGA handles the two benchmark problems and the Darcy's equation 1. Those problems are solved seamlessly. Nonetheless, considering the constructions of the permeability tensor of those problems, we have not exploited the reservoir anisotropy yet. In this section, we will allow drastic changing in the permeability tensor. This changing is meant to represent reservoir layers.

6.1 IGA Darcy's equation 2

Let us define a permeability tensor as follows:

$$\lambda(\mathbf{x}) = \begin{pmatrix} \frac{2}{\pi}\arctan\left(\frac{x-0.5}{\epsilon}\right) + 2 & 0 \\ 0 & \frac{2}{\pi}\arctan\left(\frac{x-0.5}{\epsilon}\right) + 2 \end{pmatrix} \tag{6.1}$$

Having this construction of permeability tensor in $\Omega = (0,1) \times (0,1)$ and $\epsilon > 0$, we will obtain a jump at $x = 0.5$ in the permeability tensor. The actual steepness of the jump is controlled by the size of the parameter ϵ. The smaller the ϵ, the steeper the jump. How the relation between the parameter ϵ and the change in permeability is depicted on Figure 6.1.

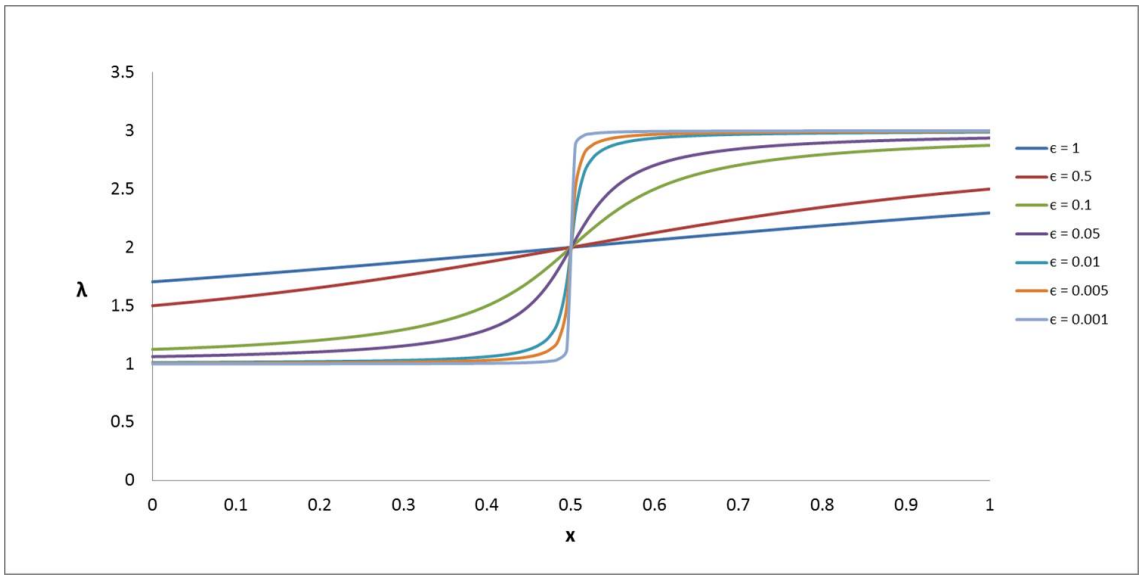

Figure 6.1: Permeability tensor changing towards ϵ on the domain $\Omega = (0,1) \times (0,1)$.

We set the analytical solution of the Darcy's equation 2 as in (5.2) and the permeability tensor as in (6.1). We do reverse calculation to obtain the source function as follows:

$$\tilde{Q}(\mathbf{x}) = 4\pi \sin(\pi x)\sin(\pi y)\Big[\arctan\Big(\frac{x-0.5}{\epsilon}\Big) + \pi\Big] - \frac{2\cos(\pi x)\sin(\pi y)}{\epsilon\Big(1+\big(\frac{x-0.5}{\epsilon}\big)^2\Big)} \tag{6.2}$$

We will observe cases for $\epsilon \in \{1, 0.5, 0.1, 0.05, 0.01, 0.005, 0.001\}$ and $p = q \in \{1, 2, 3, 4\}$. For the purpose of this observation we define a stability criteria. We will stop the computations, if:

$$p\epsilon \geq h \tag{6.3}$$

or the stability of convergence rates is already achieved, whatever comes first. This criteria is meant to avoid premature convergence conclusions and to save computation costs, as we reduce the size of element (h) and increase the order of polynomial (p). Moreover, we also define:

$$h = \frac{1}{2^{i^\star}} \tag{6.4}$$

just for the table of results simplicity.

Table 6.1 - 6.14 show the error of the numerical approximations in L2 norm and the convergence rates, for given ϵ parameter and order of polynomial (p and q). The error of the numerical approximations in L2 norm is depicted in Figure 6.2 - 6.8.

Darcy's equation 2, $\epsilon = 1$

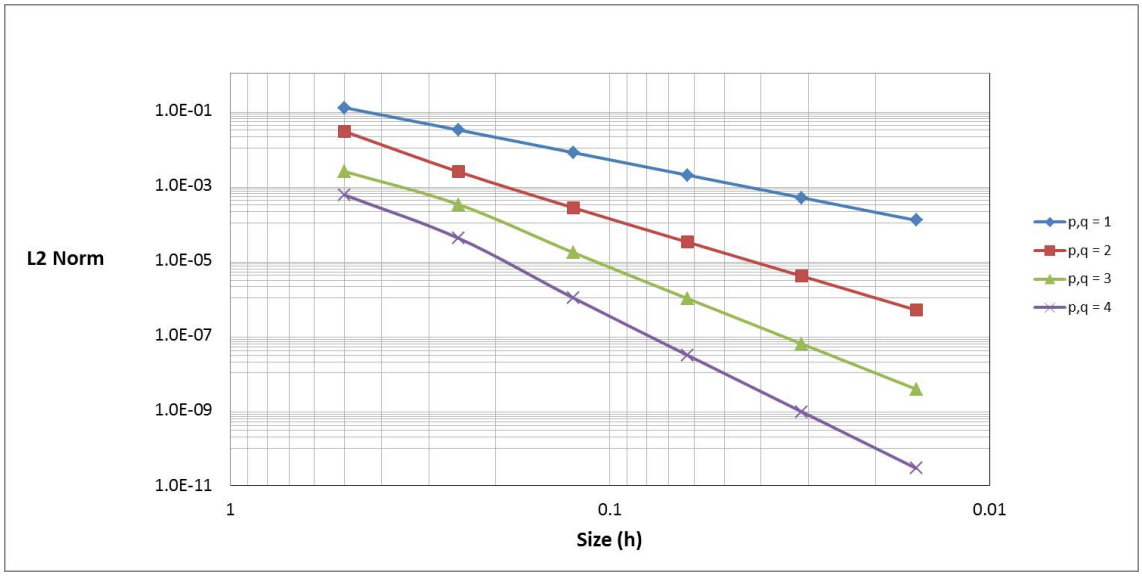

Figure 6.2: The plot of numerical approximation error in L2 norm for the 2D Darcy's equation 2, $\epsilon = 1$.

$i^\star$	*Error in L2 norm*			
	$p, q = 1$	$p, q = 2$	$p, q = 3$	$p, q = 4$
1	1.19146E-01	2.76414E-02	2.36964E-03	5.61259E-04
2	3.01625E-02	2.31361E-03	3.10612E-04	3.90546E-05
3	7.57964E-03	2.56828E-04	1.63692E-05	1.01207E-06
4	1.89761E-03	3.11106E-05	9.72450E-07	3.00272E-08
5	4.74577E-04	3.85792E-06	5.99884E-08	9.29491E-10
6	1.18655E-04	4.81276E-07	3.73697E-09	2.90364E-11

Table 6.1: The numerical approximation error in L2 norm for the 2D Darcy's equation 2, $\epsilon = 1$.

$i^\star$	*Convergence rates*			
	$p,q=1$	$p,q=2$	$p,q=3$	$p,q=4$
2	1.98190	3.57861	2.93148	3.84510
3	1.99255	3.17127	4.24606	5.27011
4	1.99795	3.04532	4.07322	5.07490
5	1.99947	3.01151	4.01887	5.01369
6	1.99987	3.00289	4.00474	5.00051

Table 6.2: The numerical approximation convergence rates for the 2D Darcy's equation 2, $\epsilon = 1$.

Darcy's equation 2, $\epsilon = 0.5$

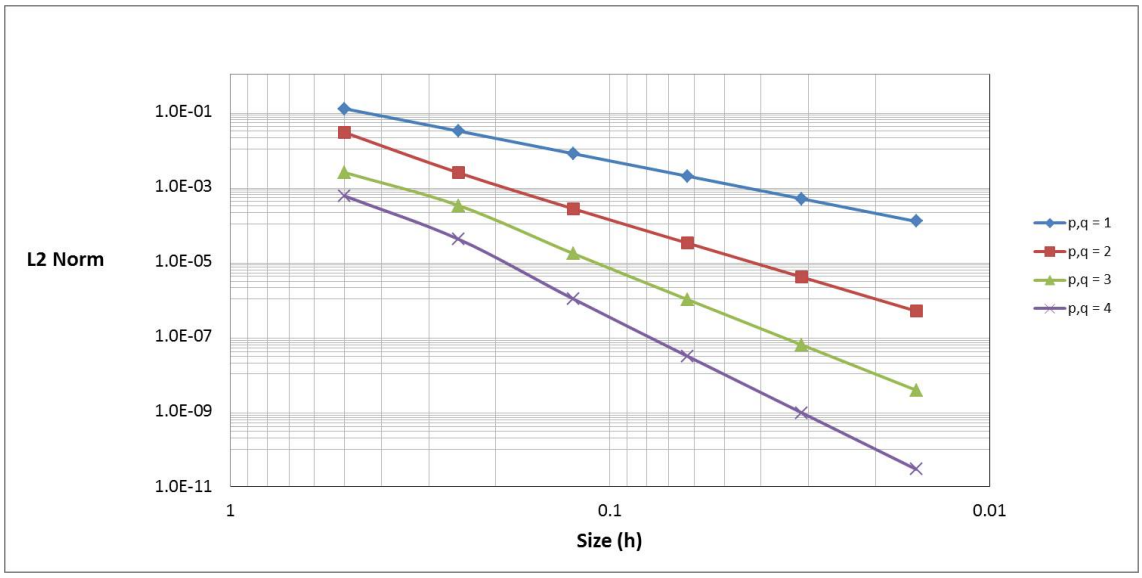

Figure 6.3: The plot of numerical approximation error in L2 norm for the 2D Darcy's equation 2, $\epsilon = 0.5$.

$i^\star$	*Error in L2 norm*			
	$p, q = 1$	$p, q = 2$	$p, q = 3$	$p, q = 4$
1	1.19146E-01	2.80887E-02	2.37267E-03	5.63604E-04
2	2.94068E-02	2.31846E-03	3.11610E-04	3.96580E-05
3	7.34617E-03	2.56841E-04	1.63707E-05	1.01358E-06
4	1.83977E-03	3.11089E-05	9.72458E-07	3.00262E-08
5	4.60062E-04	3.85787E-06	5.99884E-08	9.29483E-10
6	1.15022E-04	4.81274E-07	3.73697E-09	2.90364E-11

Table 6.3: The numerical approximation error in L2 norm for the 2D Darcy's equation 2, $\epsilon = 0.5$.

$i^\star$	*Convergence rates*			
	$p, q = 1$	$p, q = 2$	$p, q = 3$	$p, q = 4$
2	1.98551	3.57938	2.93120	3.84547
3	1.99313	3.17116	4.24606	5.27117
4	1.99808	3.04529	4.07320	5.07482
5	1.99951	3.01150	4.01887	5.01365
6	1.99987	3.00289	4.00474	5.00050

Table 6.4: The numerical approximation convergence rates for the 2D Darcy's equation 2, $\epsilon = 0.5$.

Darcy's equation 2, $\epsilon = 0.1$

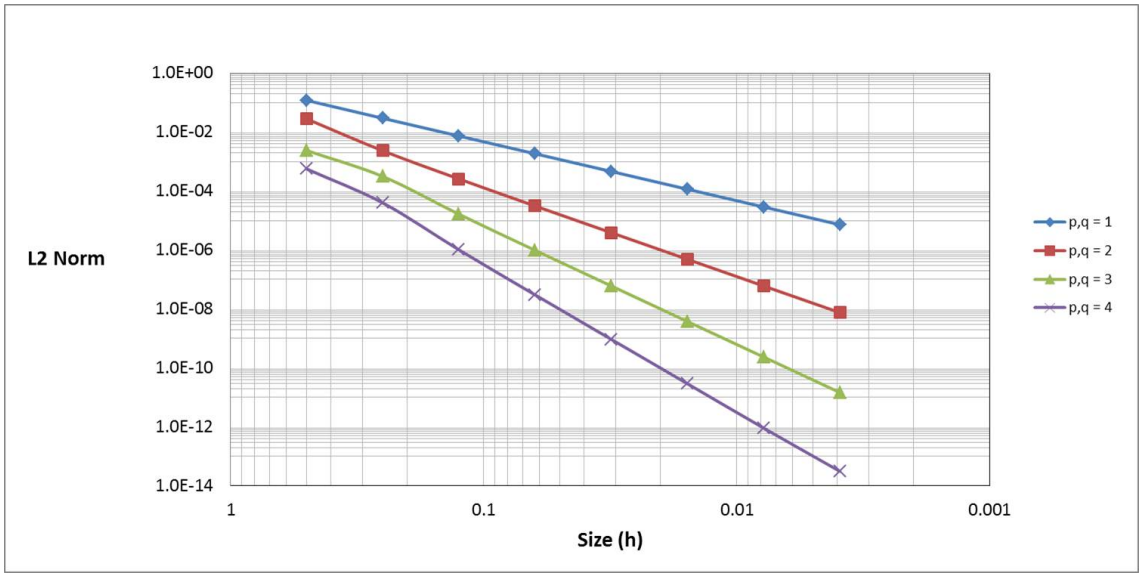

Figure 6.4: The plot of numerical approximation error in L2 norm for the 2D Darcy's equation 2, $\epsilon = 0.1$.

$i^\star$	*Error in L2 norm*			
	$p, q = 1$	$p, q = 2$	$p, q = 3$	$p, q = 4$
1	1.19146E-01	2.80887E-02	2.37267E-03	5.63604E-04
2	2.94068E-02	2.31846E-03	3.11610E-04	3.96580E-05
3	7.34617E-03	2.56841E-04	1.63707E-05	1.01358E-06
4	1.83977E-03	3.11089E-05	9.72458E-07	3.00262E-08
5	4.60062E-04	3.85787E-06	5.99884E-08	9.29483E-10
6	1.15022E-04	4.81274E-07	3.73697E-09	2.90364E-11

Table 6.5: The numerical approximation error in L2 norm for the 2D Darcy's equation 2, $\epsilon = 0.1$.

$i^\star$	*Convergence rates*			
	$p,q=1$	$p,q=2$	$p,q=3$	$p,q=4$
2	2.01851	3.59875	2.92870	3.82900
3	2.00109	3.17422	4.25055	5.29008
4	1.99747	3.04548	4.07334	5.07709
5	1.99963	3.01145	4.01888	5.01365
6	1.99992	3.00287	4.00474	5.00049

Table 6.6: The numerical approximation convergence rates for the 2D Darcy's equation 2, $\epsilon = 0.1$.

Darcy's equation 2, $\epsilon = 0.05$

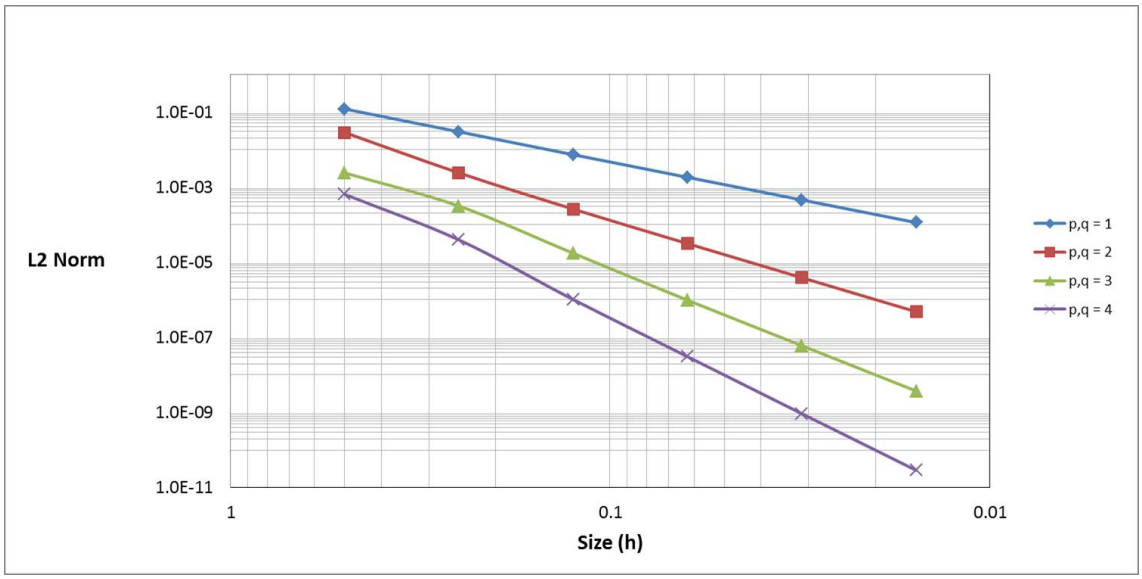

Figure 6.5: The plot numerical approximation error in L2 norm for the 2D Darcy's equation 2, $\epsilon = 0.05$.

$i^\star$	*Error in L2 norm*			
	$p, q = 1$	$p, q = 2$	$p, q = 3$	$p, q = 4$
1	1.19146E-01	2.81618E-02	2.36655E-03	6.37369E-04
2	2.94047E-02	2.37581E-03	3.10636E-04	3.91010E-05
3	7.24233E-03	2.57688E-04	1.72787E-05	1.01394E-06
4	1.81003E-03	3.11612E-05	9.73382E-07	3.05970E-08
5	4.53036E-04	3.85793E-06	5.99921E-08	9.29910E-10
6	1.13270E-04	4.81273E-07	3.73697E-09	2.90365E-11

Table 6.7: The numerical approximation error in L2 norm for the 2D Darcy's equation 2, $\epsilon = 0.05$.

$i^\star$	*Convergence rates*			
	$p, q = 1$	$p, q = 2$	$p, q = 3$	$p, q = 4$
2	2.01861	3.56725	2.92949	4.02685
3	2.02152	3.20472	4.16816	5.26916
4	2.00044	3.04780	4.14984	5.05044
5	1.99832	3.01385	4.02016	5.04016
6	1.99986	3.00290	4.00483	5.00115

Table 6.8: The numerical approximation convergence rates for the 2D Darcy's equation 2, $\epsilon = 0.05$.

For $\epsilon \leq 0.05$, Darcy's equation 2 is solved seamlessly. The numerical approximations converge at the right rate for any polynomial order. Table 6.1 - 6.8 show the error of the numerical approximations in L2 norm and the convergence rates for $\epsilon \leq 0.005$. The error of the numerical approximations in L2 norm is depicted in Figure 6.2 - 6.5. Even though the main objective of this research is not to define the steepness of the drastic changing that IGA can handle. It is a good piece of information for the practical purpose to have an order of magnitude level of anisotropy that IGA can handle.

Darcy's equation 2, $\epsilon = 0.01$

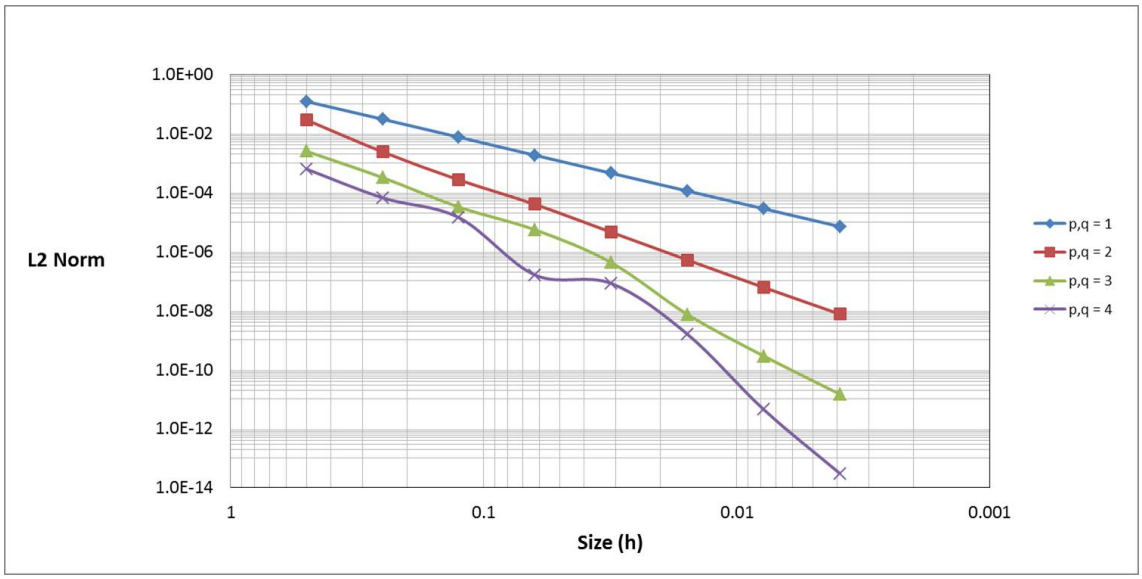

Figure 6.6: The plot of numerical approximation error in L2 norm for the 2D Darcy's equation 2, $\epsilon = 0.01$.

$i^\star$	*Error in L2 norm*			
	$p, q = 1$	$p, q = 2$	$p, q = 3$	$p, q = 4$
1	1.19146E-01	2.82197E-02	2.45353E-03	6.12762E-04
2	2.99488E-02	2.33621E-03	3.15420E-04	6.50551E-05
3	7.38610E-03	2.63458E-04	3.17050E-05	1.39300E-05
4	1.80164E-03	3.90483E-05	5.36104E-06	1.58427E-07
5	4.44350E-04	4.44249E-06	4.16389E-07	8.22373E-08
6	1.10997E-04	5.11089E-07	7.28119E-09	1.56094E-09
7	2.77677E-05	6.02485E-08	2.87173E-10	4.43430E-12
8	6.94253E-06	7.51524E-09	1.45835E-11	3.01189E-14

Table 6.9: The numerical approximation error in L2 norm for the 2D Darcy's equation 2, $\epsilon = 0.01$

$i^\star$	*Convergence rates*			
	$p, q = 1$	$p, q = 2$	$p, q = 3$	$p, q = 4$
2	1.99216	3.59446	2.95951	3.23559
3	2.01961	3.14853	3.31449	2.22347
4	2.03550	2.75424	2.56413	6.45823
5	2.01954	3.13582	3.68651	0.94595
6	2.00118	3.11972	5.83761	5.71931
7	1.99904	3.08458	4.66418	8.45949
8	1.99987	3.00303	4.29951	7.20189

Table 6.10: The numerical approximation convergence rates for the 2D Darcy's equation 2, $\epsilon = 0.01$.

Darcy's equation 2, $\epsilon = 0.005$

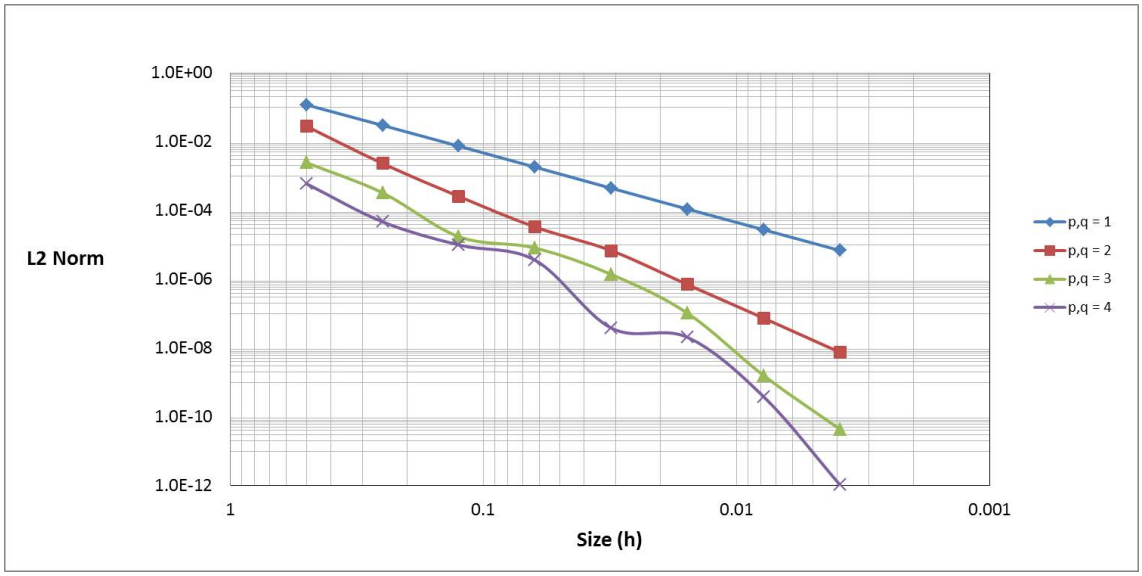

Figure 6.7: The plot of numerical approximation error in L2 norm for the 2D Darcy's equation 2, $\epsilon = 0.005$.

$i^\star$	*Error in L2 norm*			
	$p, q = 1$	$p, q = 2$	$p, q = 3$	$p, q = 4$
1	1.19146E-01	2.82558E-02	2.47282E-03	6.05082E-04
2	3.00641E-02	2.33560E-03	3.26479E-04	4.69107E-05
3	7.47509E-03	2.58133E-04	1.73505E-05	9.97728E-06
4	1.83497E-03	3.32423E-05	8.17861E-06	3.59991E-06
5	4.47852E-04	6.82319E-06	1.39183E-06	3.81845E-08
6	1.10740E-04	7.03588E-07	1.03313E-07	2.06042E-08
7	2.76747E-05	7.42097E-08	1.58522E-09	3.83705E-10

Table 6.11: The numerical approximation error in L2 norm for the 2D Darcy's equation 2, $\epsilon = 0.005$.

$i^\star$	*Convergence rates*			
	$p,q=1$	$p,q=2$	$p,q=3$	$p,q=4$
2	1.98662	3.59668	2.92110	3.68914
3	2.00788	3.17761	4.23394	2.23320
4	2.02633	2.95702	1.08505	1.47069
5	2.03466	2.28450	2.55487	6.55883
6	2.01585	3.27764	3.75189	0.89005
7	2.00054	3.24505	6.02619	5.74680
8	1.99949	3.29342	5.18050	8.51184

Table 6.12: The numerical approximation convergence rates for the 2D Darcy's equation 2, $\epsilon = 0.005$.

Darcy's equation 2, $\epsilon = 0.001$

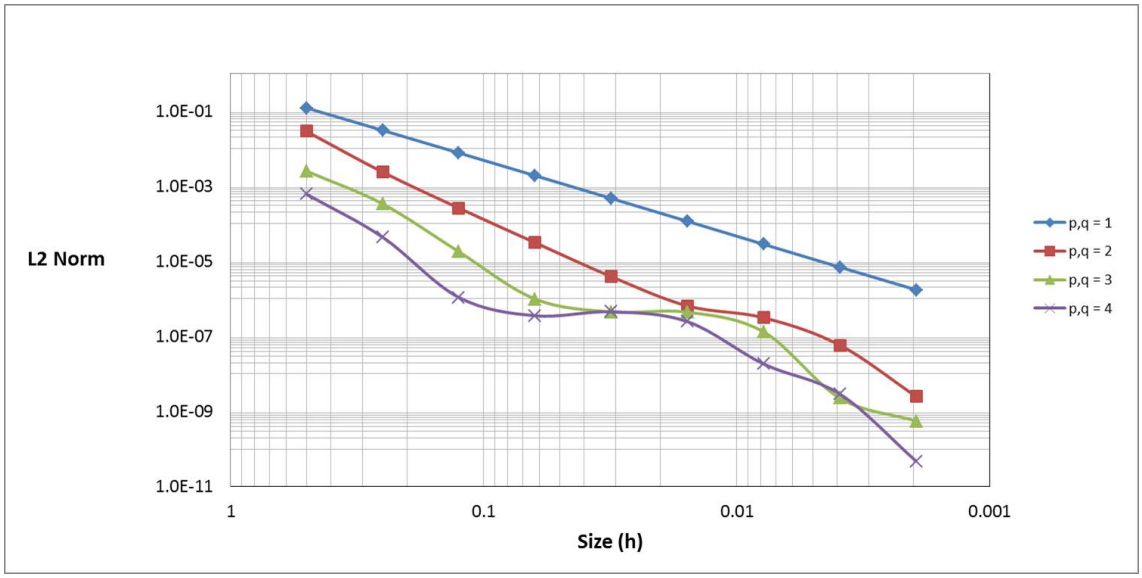

Figure 6.8: The plot of numerical approximation error in L2 norm the 2D Darcy's equation 2, $\epsilon = 0.005$.

$i^\star$	*Error in L2 norm*			
	$p, q = 1$	$p, q = 2$	$p, q = 3$	$p, q = 4$
1	1.19146E-01	2.82884E-02	2.48658E-03	6.05898E-04
2	3.01637E-02	2.33815E-03	3.33218E-04	4.31326E-05
3	7.56327E-03	2.57570E-04	1.77295E-05	1.08113E-06
4	1.88397E-03	3.11366E-05	9.81742E-07	3.53397E-07
5	4.66540E-04	3.87501E-06	4.47077E-07	4.49988E-07
6	1.14673E-04	6.42810E-07	4.40329E-07	2.46020E-07
7	2.80222E-05	3.12895E-07	1.31068E-07	1.83166E-08
8	6.90924E-06	5.80172E-08	2.26624E-09	2.91053E-09
9	1.72619E-06	2.50673E-09	5.59545E-10	4.76789E-11

Table 6.13: The numerical approximation error in L2 norm for the 2D Darcy's equation 2, $\epsilon = 0.001$.

$i^\star$	*Convergence rates*			
	$p, q = 1$	$p, q = 2$	$p, q = 3$	$p, q = 4$
2	1.98185	3.59677	2.89962	3.81222
3	1.99573	3.18233	4.23224	5.31817
4	2.00523	3.04828	4.17466	1.61318
5	2.01370	3.00634	1.13482	-0.34860
6	2.02448	2.59174	0.02194	0.87111
7	2.03288	1.03871	1.74827	3.74755
8	2.01997	2.43113	5.85387	2.65380
9	2.00094	4.53260	2.01797	5.93179

Table 6.14: The numerical approximation convergence rates for the 2D Darcy's equation 2, $\epsilon = 0.001$.

As soon as we decrease the parameter ϵ, $\epsilon < 0.05$, instability occurs on the error in L2 norm and the convergence rates. Table 6.9 - 6.14 show the error of the numerical approximations in L2 norm and the convergence rates. The error of the numerical approximations in L2 norm is depicted in Figure 6.6 - 6.8. The instability even worse for cases $p = q \in \{3, 4\}$.

In IGA, a knot vector is functioned as the domain discretization and the support for basis functions. The higher the order of polynomial of basis functions means the more knots being the support of the basis functions. The $p + 1$ knot spans that is pointed in Section 4.3. For higher order polynomial, in this case $p = q \in \{3, 4\}$, the contributions of the supports that are not parts of the integration of the reference element are unavoidable. Thus the instability occurs. We refer to Figure 6.9 as comparisons of basis functions for different order polynomial.

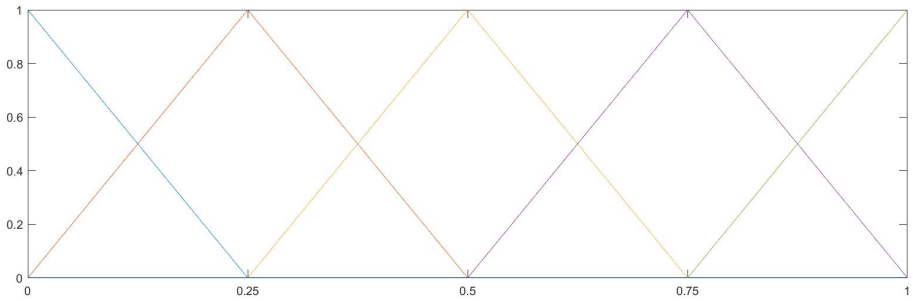

(a) Linear ($p = 1$) basis functions for an open-uniform knot vector, $\Xi = \{0, 0, 0.25, 0.5, 0.75, 1, 1\}$.

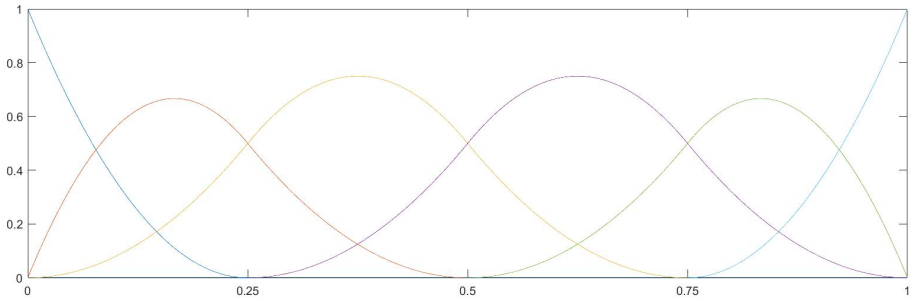

(b) Quadratic ($p = 2$) basis functions for an open-uniform knot vector, $\Xi = \{0, 0, 0, 0.25, 0.5, 0.75, 1, 1, 1\}$.

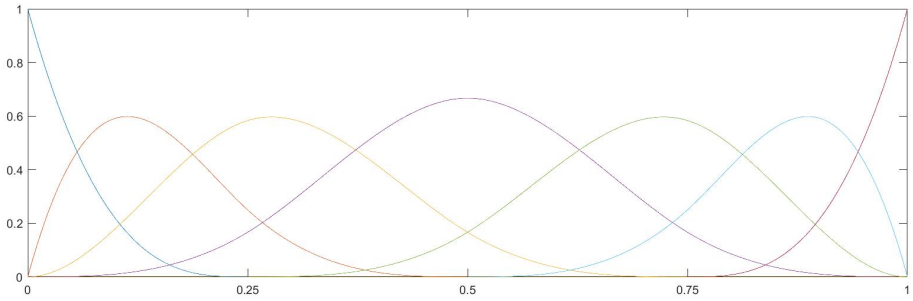

(c) Cubic ($p = 3$) basis functions for an open-uniform knot vector, $\Xi = \{0, 0, 0, 0, 0.25, 0.5, 0.75, 1, 1, 1, 1\}$.

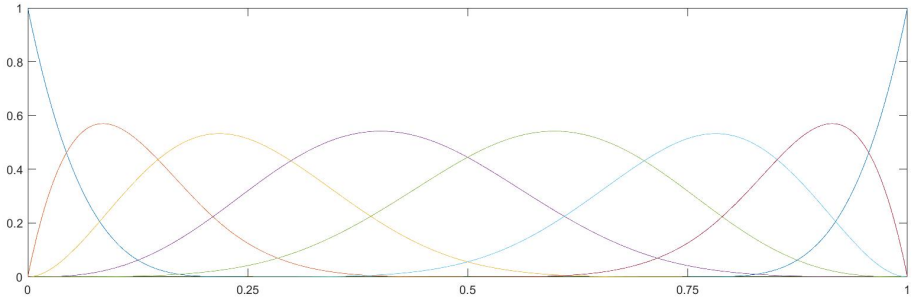

(d) Quartic ($p = 4$) basis functions for an open-uniform knot vector, $\Xi = \{0, 0, 0, 0, 0, 0.25, 0.5, 0.75, 1, 1, 1, 1, 1\}$.

Figure 6.9: Basis functions comparisons for $p = \{1, 2, 3, 4\}$ and $h = 0.25$. From this figure we can see how the basis functions, for $p > 1$, are overlaping an element.

We would like to avoid such instability for the error of the numerical approximations. One proposed approach that is by reducing the continuity of basis functions at $\xi_i = 0.5$. As it has already been pointed in Section 4.3, that the continuity of basis functions at a certain knot can be easily reduced by applying multiplication of the knot itself. However, the number of multiplication can be done at most p, i.e. C^0 continuity at $\xi_i = 0.5$. Suppose we want C^{-1} continuity at $\xi_i = 0.5$ then this single patch assumption no longer holds.

6.2 Basis functions continuity reduction

We will concentrate on the cases $\epsilon \in \{0.01, 0.005, 0.001\}$, in which we know the instability occurs. We increase the multiplicity of the $\xi_i = 0.5$ for at most p, i.e. $m(0.5) \leq p$. We examine the error of the numerical approximations in L2 norm and the convergence rates.

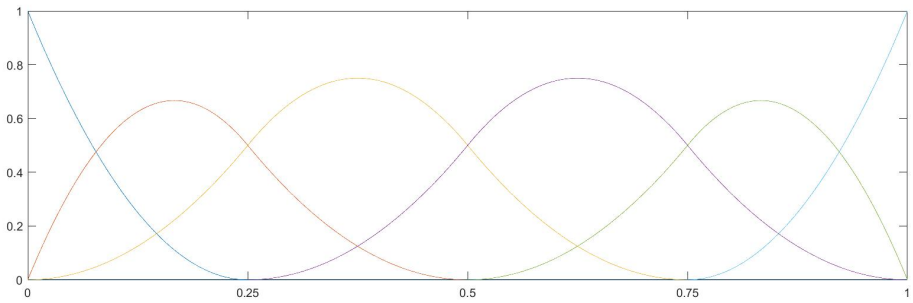

(a) Quadratic ($p = 2$) basis functions for an open, uniform knot vector.

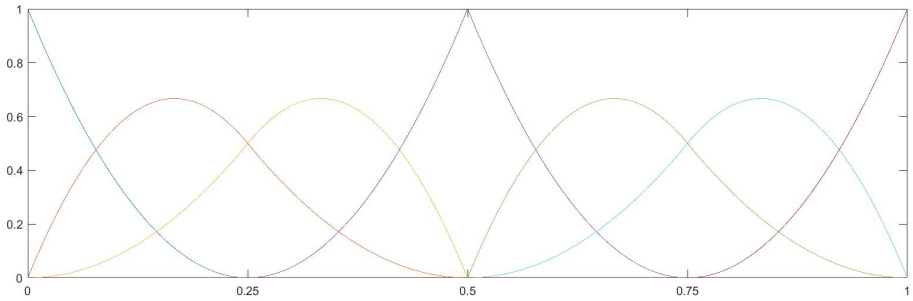

(b) Quadratic ($p = 2$) basis functions for an open, non-uniform knot vector, $m(0.5) = 2$.

Figure 6.10: Basis functions comparisons for uniform and non-uniform knot vector at ξ direction, $p = 2$.

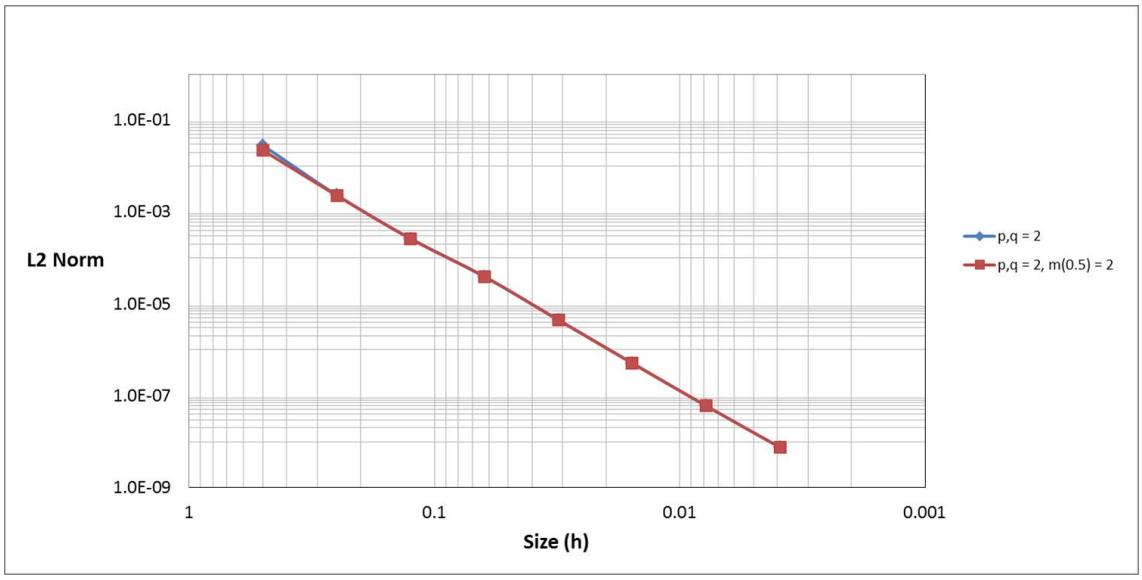

Figure 6.11: The plot of numerical approximation error in L2 norm for the 2D Darcy's equation 2, $p = q = 2$ and $\epsilon = 0.01$.

$i^\star$	*Error in L2 norm*	
	$p, q = 2$	$p, q = 2,\ m(0.5) = 2$
1	2.82197E-02	2.19992E-02
2	2.33621E-03	2.28040E-03
3	2.63458E-04	2.60412E-04
4	3.90483E-05	3.94940E-05
5	4.44249E-06	4.46463E-06
6	5.11089E-07	5.11412E-07
7	6.02485E-08	6.02495E-08
8	7.51524E-09	7.51524E-09

Table 6.15: The numerical approximation error in L2 norm for the 2D Darcy's equation 2, $p = q = 2$ and $\epsilon = 0.01$.

$i^\star$	*Convergence rates*	
	$p, q = 2$	$p, q = 2$, $m(0.5) = 2$
2	3.59446	3.27009
3	3.14853	3.13042
4	2.75424	2.72109
5	3.13582	3.14502
6	3.11972	3.12598
7	3.08458	3.08546
8	3.00303	3.00306

Table 6.16: The numerical approximation convergence rates for the 2D Darcy's equation 2, $p = q = 2$ and $\epsilon = 0.01$.

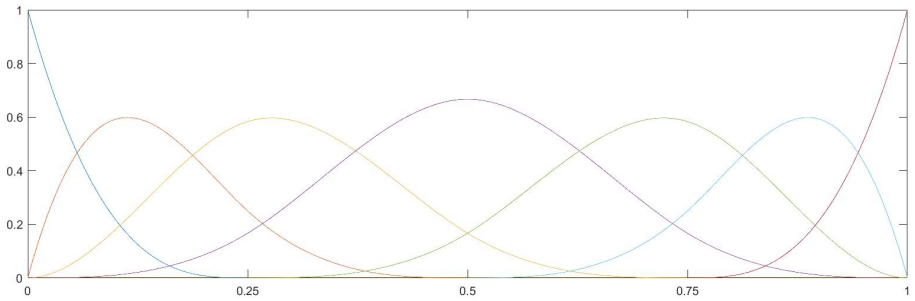

(a) Cubic ($p = 3$) basis functions for an open, uniform knot vector.

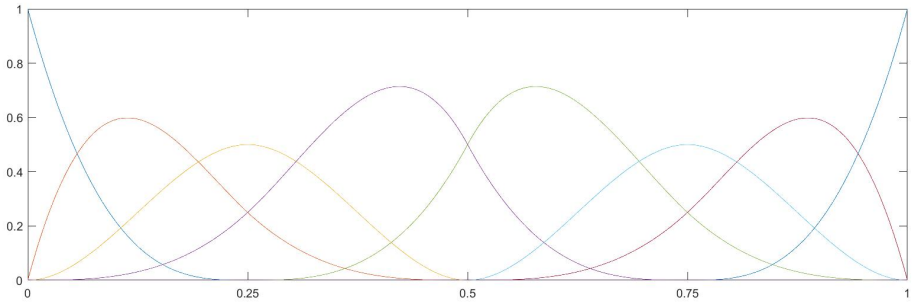

(b) Cubic ($p = 3$) basis functions for an open, non-uniform knot vector, $m(0.5) = 2$.

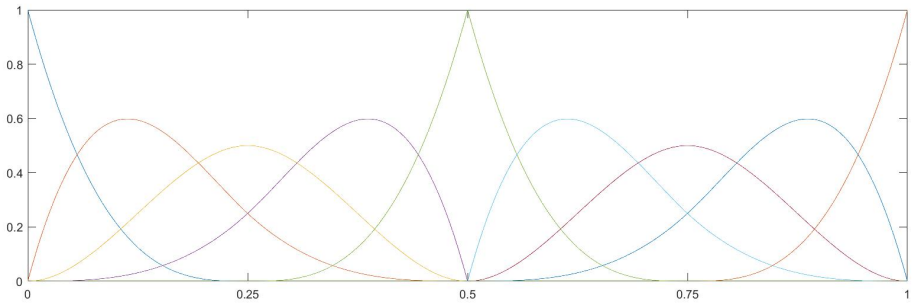

(c) Cubic ($p = 3$) basis functions for an open, non-uniform knot vector, $m(0.5) = 3$.

Figure 6.12: Basis functions comparisons for uniform and non-uniform knot vector at ξ direction, $p = 3$.

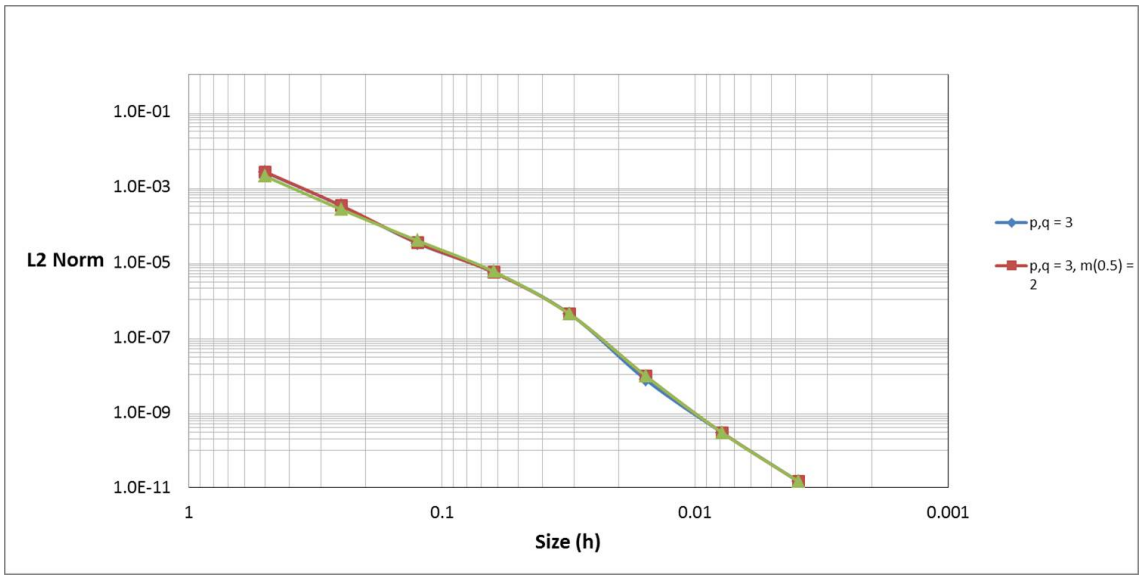

Figure 6.13: The plot of numerical approximation error in L2 norm for the 2D Darcy's equation 2, $p = q = 3$ and $\epsilon = 0.01$.

$i^\star$	*Error in L2 norm*		
	$p, q = 3$	$p, q = 3,\ m(0.5) = 2$	$p, q = 2,\ m(0.5) = 3$
1	2.45353E-03	2.51735E-03	1.93361E-03
2	3.15420E-04	3.19584E-04	2.51258E-04
3	3.17050E-05	3.24606E-05	3.72895E-05
4	5.36104E-06	5.33261E-06	5.63403E-06
5	4.16389E-07	4.10422E-07	4.09310E-07
6	7.28119E-09	9.18565E-09	9.17800E-09
7	2.87173E-10	2.87729E-10	2.86669E-10
8	1.45835E-11	1.45878E-11	1.45665E-11

Table 6.17: The numerical approximation error in L2 norm for the 2D Darcy's equation 2, $p = q = 3$ and $\epsilon = 0.01$.

$i^\star$	*Convergence rates*		
	$p, q = 3$	$p, q = 3$, $m(0.5) = 2$	$p, q = 2$, $m(0.5) = 3$
2	2.95951	2.97764	2.94406
3	3.31449	3.29943	2.75233
4	2.56413	2.60578	2.72653
5	3.68651	3.69966	3.78290
6	5.83761	5.48158	5.47887
7	4.66418	4.99660	5.00072
8	4.29951	4.30188	4.29866

Table 6.18: The numerical approximation convergence rates for the 2D Darcy's equation 2, $p = q = 3$ and $\epsilon = 0.01$.

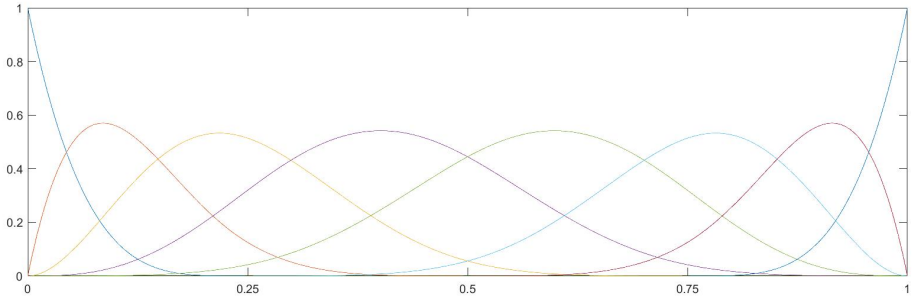

(a) Quartic ($p = 4$) basis functions for an open, uniform knot vector.

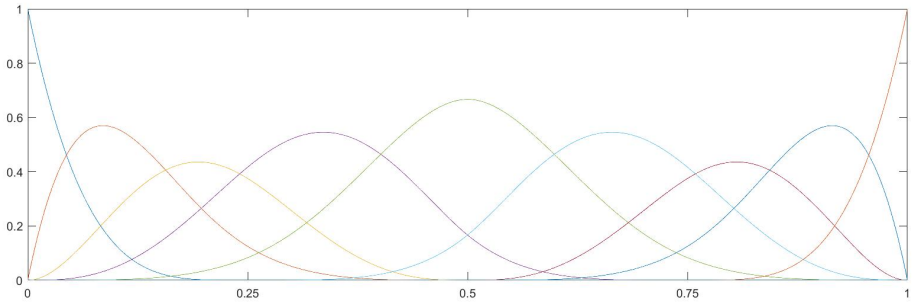

(b) Quartic ($p = 4$) basis functions for an open, non-uniform knot vector, $m(0.5) = 2$.

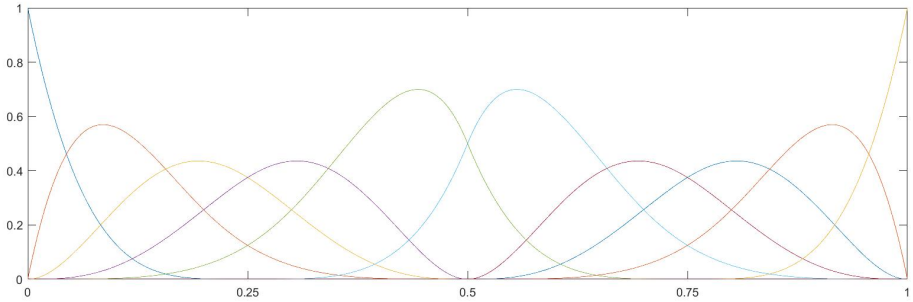

(c) Quartic ($p = 4$) basis functions for an open, non-uniform knot vector, $m(0.5) = 3$.

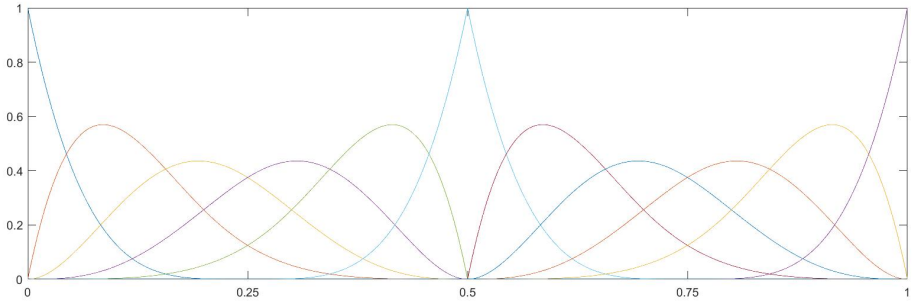

(d) Quartic ($p = 4$) basis functions for an open, non-uniform knot vector, $m(0.5) = 4$.

Figure 6.14: Basis functions comparisons for uniform and non-uniform knot vector at ξ direction, $p = 4$.

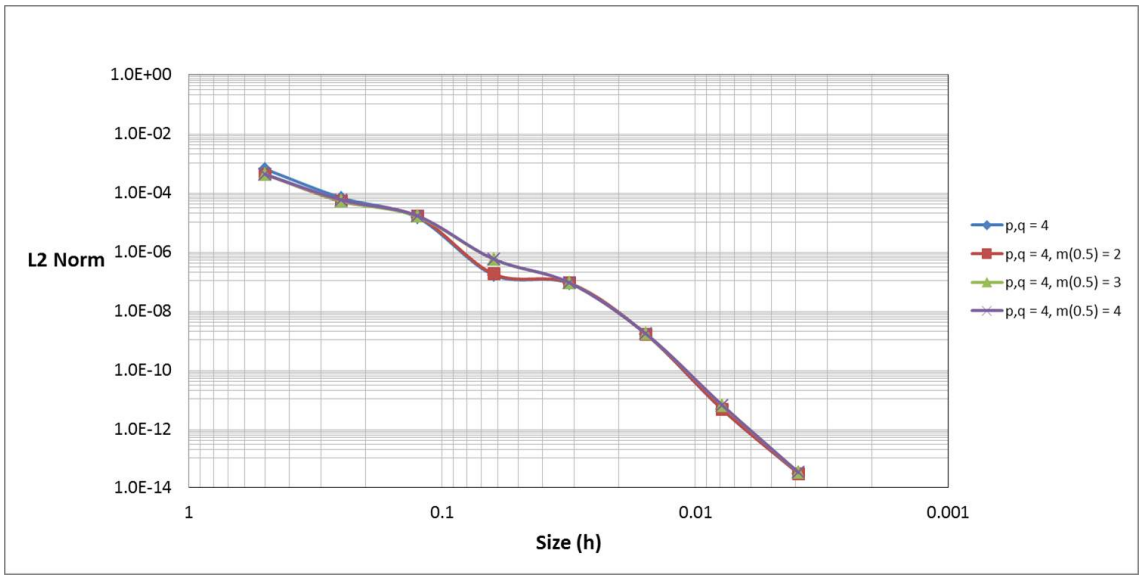

Figure 6.15: The plot of numerical approximation error in L2 norm for the 2D Darcy's equation 2, $p = q = 4$ and $\epsilon = 0.01$.

$i^\star$	*Error in L2 norm*			
	$p, q = 4$	$p, q = 4,\ m(0.5) = 2$	$p, q = 4,\ m(0.5) = 3$	$p, q = 4,\ m(0.5) = 4$
1	6.12762E-04	4.09554E-04	4.09560E-04	4.05254E-04
2	6.50551E-05	4.94855E-05	5.10914E-05	5.53194E-05
3	1.39300E-05	1.52454E-05	1.51766E-05	1.59582E-05
4	1.58427E-07	1.72266E-07	5.36352E-07	5.48274E-07
5	8.22373E-08	8.44578E-08	8.49742E-08	8.53216E-08
6	1.56094E-09	1.57795E-09	1.59513E-09	1.59607E-09
7	4.43430E-12	4.44746E-12	6.13845E-12	6.15893E-12
8	3.01189E-14	2.99834E-14	3.22150E-14	3.24415E-14

Table 6.19: The numerical approximation error in L2 norm for the 2D Darcy's equation 2, $p = q = 4$ and $\epsilon = 0.01$.

$i^\star$	*Convergence rates*			
	$p,q=4$	$p,q=4,\ m(0.5)=2$	$p,q=4,\ m(0.5)=3$	$p,q=4,\ m(0.5)=4$
2	3.23559	3.04898	3.00292	2.87297
3	2.22347	1.69863	1.75123	1.79349
4	6.45823	6.46759	4.82252	4.86326
5	0.94595	1.02834	2.65808	2.68391
6	5.71931	5.74211	5.73528	5.74032
7	8.45949	8.47085	8.02158	8.01763
8	7.20189	7.21267	7.57400	7.56870

Table 6.20: The numerical approximation convergence rates for the 2D Darcy's equation 2, $p=q=4$ and $\epsilon=0.01$.

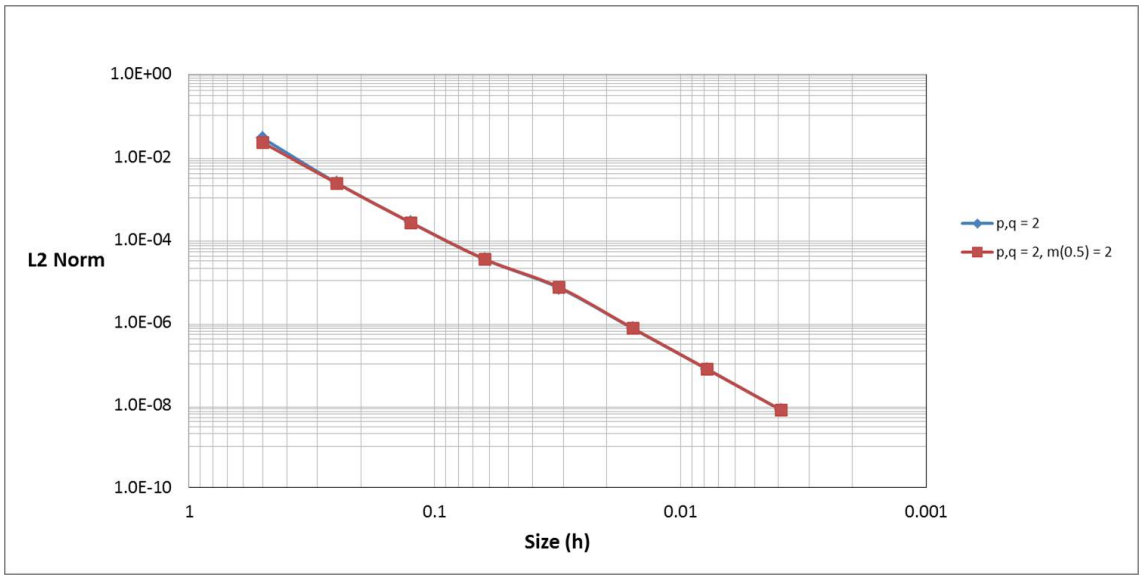

Figure 6.16: The numerical approximation error in L2 norm for the 2D Darcy's equation 2, $p=q=2$ and $\epsilon=0.005$.

$i^\star$	*Error in L2 norm*	
	$p, q = 2$	$p, q = 2$, $m(0.5) = 2$
1	2.82558E-02	2.20042E-02
2	2.33560E-03	2.28209E-03
3	2.58133E-04	2.56415E-04
4	3.32423E-05	3.33327E-05
5	6.82319E-06	7.07860E-06
6	7.03588E-07	7.14101E-07
7	7.42097E-08	7.42902E-08
8	7.56907E-09	7.56930E-09

Table 6.21: The numerical approximation error in L2 norm for the 2D Darcy's equation 2, $p = q = 2$ and $\epsilon = 0.005$.

$i^\star$	*Convergence rates*	
	$p, q = 2$	$p, q = 2$, $m(0.5) = 2$
2	3.59668	3.26935
3	3.17761	3.15380
4	2.95702	2.94347
5	2.28450	2.23540
6	3.27764	3.30926
7	3.24505	3.26488
8	3.29342	3.29494

Table 6.22: The numerical approximation convergence rates for the 2D Darcy's equation 2, $p = q = 2$ and $\epsilon = 0.005$.

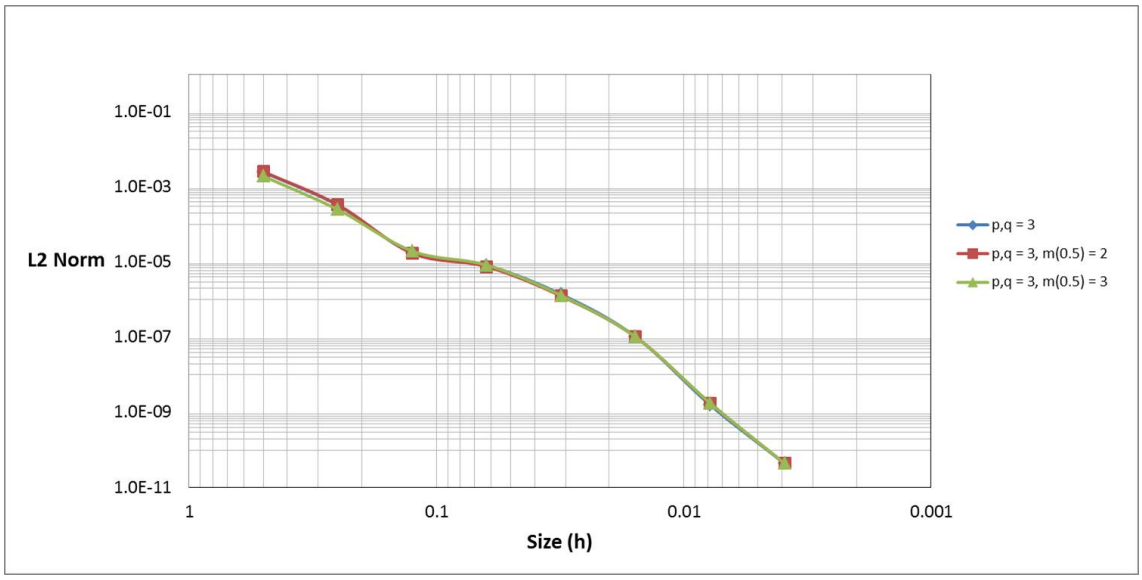

Figure 6.17: The plot of numerical approximation error in L2 norm for the 2D Darcy's equation 2, $p = q = 3$ and $\epsilon = 0.005$.

$i^\star$	*Error in L2 norm*		
	$p, q = 3$	$p, q = 3,\ m(0.5) = 2$	$p, q = 3,\ m(0.5) = 3$
1	2.47282E-03	2.54894E-03	1.93403E-03
2	3.26479E-04	3.35686E-04	2.50518E-04
3	1.73505E-05	1.73215E-05	1.96104E-05
4	8.17861E-06	7.58029E-06	8.32925E-06
5	1.39183E-06	1.25196E-06	1.30131E-06
6	1.03313E-07	1.01855E-07	1.01846E-07
7	1.58522E-09	1.75882E-09	1.76538E-09
8	4.37124E-11	4.38610E-11	4.38234E-11

Table 6.23: The numerical approximation error in L2 norm for the 2D Darcy's equation 2, $p = q = 3$ and $\epsilon = 0.005$.

$i^\star$	*Convergence rates*		
	$p,q=3$	$p,q=3,\ m(0.5)=2$	$p,q=3,\ m(0.5)=3$
2	2.92110	2.92471	2.94862
3	4.23394	4.27648	3.67522
4	1.08505	1.19224	1.23536
5	2.55487	2.59806	2.67822
6	3.75189	3.61960	3.67550
7	6.02619	5.85577	5.85027
8	5.18050	5.32553	5.33213

Table 6.24: The numerical approximation convergence rates for the 2D Darcy's equation 2, $p=q=3$ and $\epsilon=0.005$.

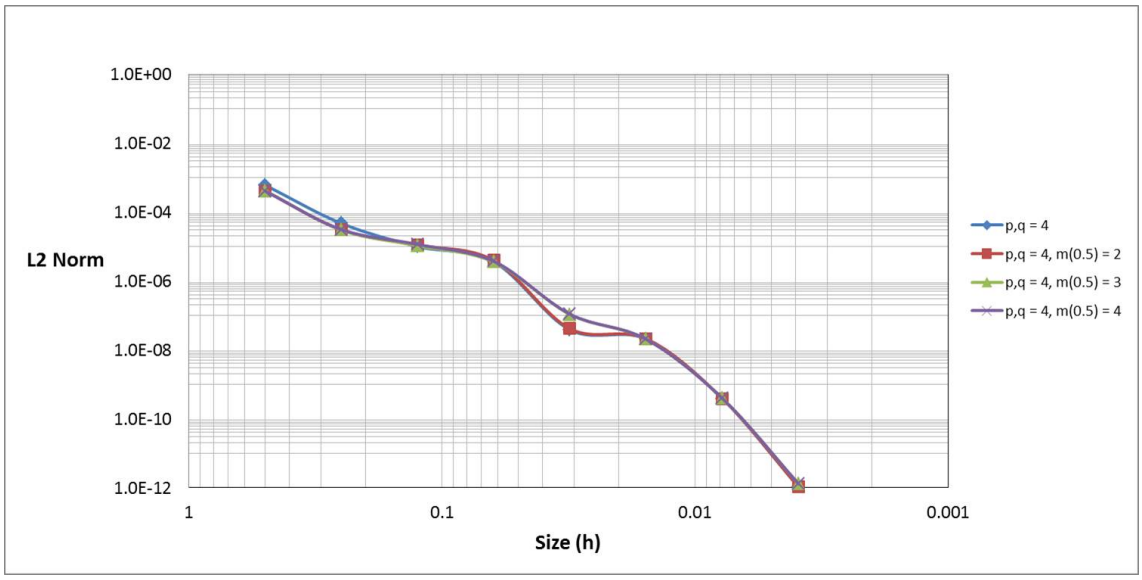

Figure 6.18: The plot of numerical approximation error in L2 norm for the 2D Darcy's equation 2, $p=q=4$ and $\epsilon=0.005$.

$i^\star$	*Error in L2 norm*			
	$p, q = 4$	$p, q = 4$, $m(0.5) = 2$	$p, q = 4$, $m(0.5) = 3$	$p, q = 4$, $m(0.5) = 4$
1	6.05082E-04	4.11145E-04	4.11547E-04	4.03598E-04
2	4.69107E-05	3.02026E-05	3.02194E-05	3.11293E-05
3	9.97728E-06	1.11228E-05	1.04755E-05	1.15208E-05
4	3.59991E-06	3.93009E-06	3.56696E-06	3.73610E-06
5	3.81845E-08	4.11196E-08	1.07309E-07	1.08618E-07
6	2.06042E-08	2.10921E-08	2.03091E-08	2.03572E-08
7	3.83705E-10	3.87130E-10	3.90012E-10	3.90173E-10
8	1.05118E-12	1.05296E-12	1.28896E-12	1.29081E-12

Table 6.25: The numerical approximation error in L2 norm for the 2D Darcy's equation 2, $p = q = 4$ and $\epsilon = 0.005$.

$i^\star$	*Convergence rates*			
	$p, q = 4$	$p, q = 4$, $m(0.5) = 2$	$p, q = 4$, $m(0.5) = 3$	$p, q = 4$, $m(0.5) = 4$
2	3.68914	3.76690	3.76751	3.69657
3	2.23320	1.44115	1.52846	1.43403
4	1.47069	1.50089	1.55425	1.62464
5	6.55883	6.57859	5.05485	5.10420
6	0.89005	0.96312	2.40157	2.41565
7	5.74680	5.76774	5.70246	5.70528
8	8.51184	8.52222	8.24117	8.23969

Table 6.26: The numerical approximation convergence rates for the 2D Darcy's equation 2, $p = q = 4$ and $\epsilon = 0.005$.

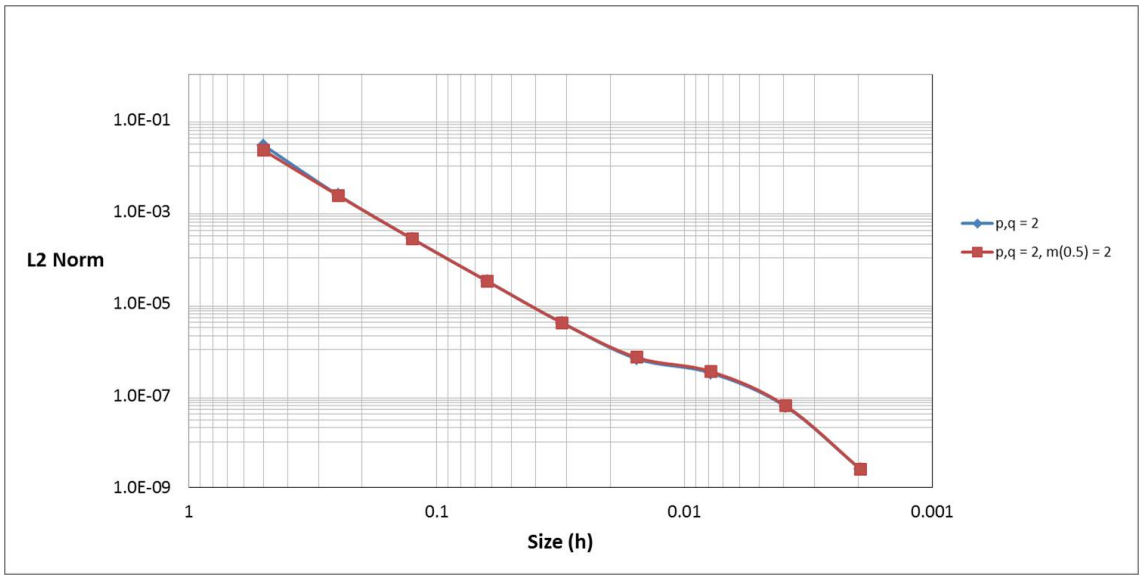

Figure 6.19: The numerical approximation error in L2 norm for the 2D Darcy's equation 2, $p = q = 2$ and $\epsilon = 0.001$.

$i^\star$	*Error in L2 norm*	
	$p, q = 2$	$p, q = 2,\ m(0.5) = 2$
1	2.82884E-02	2.20094E-02
2	2.33815E-03	2.28308E-03
3	2.57570E-04	2.56460E-04
4	3.11366E-05	3.11026E-05
5	3.87501E-06	3.87284E-06
6	6.42810E-07	6.82538E-07
7	3.12895E-07	3.36174E-07
8	5.80172E-08	6.00230E-08
9	2.50673E-09	2.50462E-09

Table 6.27: The numerical approximation error in L2 norm for the 2D Darcy's equation 2, $p = q = 2$ and $\epsilon = 0.001$.

$i^\star$	*Convergence rates*	
	$p, q = 2$	$p, q = 2,\ m(0.5) = 2$
2	3.59677	3.26907
3	3.18233	3.15418
4	3.04828	3.04363
5	3.00634	3.00557
6	2.59174	2.50441
7	1.03871	1.02170
8	2.43113	2.48562
9	4.53260	4.58285

Table 6.28: The numerical approximation convergence rates for the 2D Darcy's equation 2, $p = q = 2$ and $\epsilon = 0.001$.

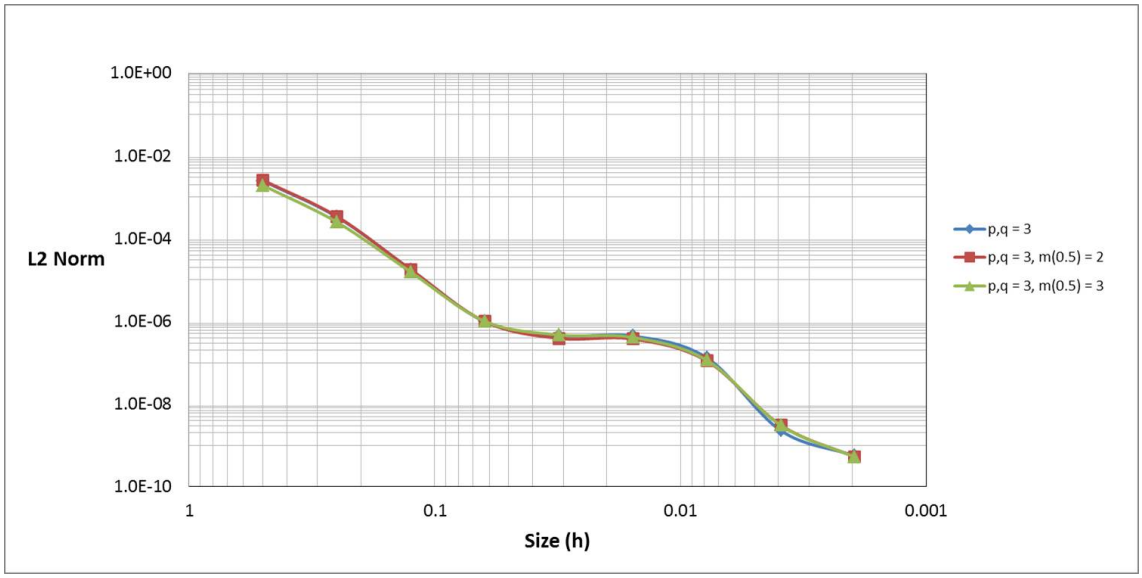

Figure 6.20: The plot of numerical approximation error in L2 norm for the 2D Darcy's equation 2, $p = q = 3$ and $\epsilon = 0.001$.

$i^\star$	*Error in L2 norm*		
	$p, q = 3$	$p, q = 3,\ m(0.5) = 2$	$p, q = 3,\ m(0.5) = 3$
1	2.48658E-03	2.56996E-03	1.93251E-03
2	3.33218E-04	3.44203E-04	2.50644E-04
3	1.77295E-05	1.77412E-05	1.54423E-05
4	9.81742E-07	9.79997E-07	9.93264E-07
5	4.47077E-07	3.86974E-07	4.69117E-07
6	4.40329E-07	3.73254E-07	4.06967E-07
7	1.31068E-07	1.09680E-07	1.13978E-07
8	2.26624E-09	3.07081E-09	3.03674E-09
9	5.59545E-10	5.20292E-10	5.20739E-10

Table 6.29: The numerical approximation error in L2 norm for the 2D Darcy's equation 2, $p = q = 3$ and $\epsilon = 0.001$

$i^\star$	*Convergence rates*		
	$p, q = 3$	$p, q = 3,\ m(0.5) = 2$	$p, q = 3,\ m(0.5) = 3$
2	2.89962	2.90041	2.94676
3	4.23224	4.27808	4.02068
4	4.17466	4.17818	3.95857
5	1.13482	1.34054	1.08223
6	0.02194	0.05208	0.20504
7	1.74827	1.76686	1.83616
8	5.85387	5.15854	5.23009
9	2.01797	2.56123	2.54389

Table 6.30: The numerical approximation convergence rates for the 2D Darcy's equation 2, $p = q = 3$ and $\epsilon = 0.001$.

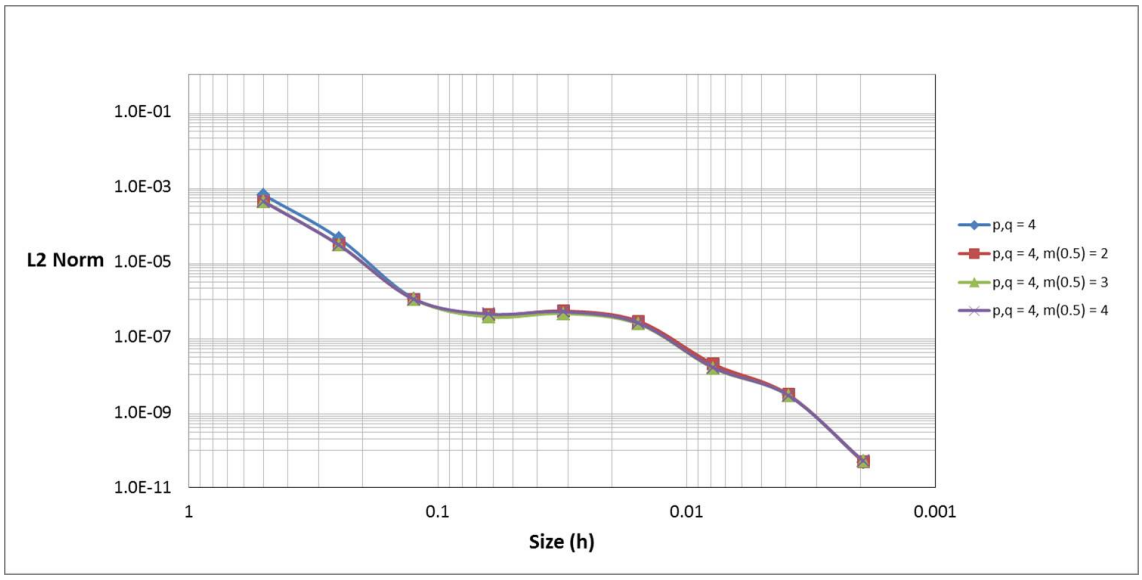

Figure 6.21: The plot of numerical approximation error in L2 norm for the 2D Darcy's equation 2, $p = q = 4$ and $\epsilon = 0.001$.

$i^\star$	*Error in L2 norm*			
	$p, q = 4$	$p, q = 4,\ m(0.5) = 2$	$p, q = 4,\ m(0.5) = 3$	$p, q = 4,\ m(0.5) = 4$
1	6.05898E-04	4.12174E-04	4.12702E-04	4.03646E-04
2	4.31326E-05	2.87111E-05	2.87181E-05	2.86865E-05
3	1.08113E-06	1.03261E-06	1.02820E-06	1.03276E-06
4	3.53397E-07	4.01596E-07	3.49852E-07	4.15734E-07
5	4.49988E-07	5.02626E-07	4.27771E-07	4.77721E-07
6	2.46020E-07	2.67943E-07	2.25724E-07	2.38000E-07
7	1.83166E-08	1.93227E-08	1.50645E-08	1.55781E-08
8	2.91053E-09	2.99523E-09	2.84278E-09	2.84595E-09
9	4.76789E-11	4.81910E-11	5.03528E-11	5.04176E-11

Table 6.31: The numerical approximation error in L2 norm for the 2D Darcy's equation 2, $p = q = 4$ and $\epsilon = 0.001$.

$i^\star$	*Convergence rates*			
	$p, q = 4$	$p, q = 4$, $m(0.5) = 2$	$p, q = 4$, $m(0.5) = 3$	$p, q = 4$, $m(0.5) = 4$
2	3.81222	3.84357	3.84507	3.81465
3	5.31817	4.79724	4.80377	4.79580
4	1.61318	1.36248	1.55530	1.31277
5	-0.34860	-0.32374	-0.29009	-0.20051
6	0.87111	0.90756	0.92228	1.00521
7	3.74755	3.79356	3.90534	3.93337
8	2.65380	2.68956	2.40578	2.45254
9	5.93179	5.95776	5.81909	5.81884

Table 6.32: The numerical approximation convergence rates for the 2D Darcy's equation 2, $p = q = 4$ and $\epsilon = 0.001$.

Table 6.15 - 6.32 show the error of the numerical approximations in L2 norm and the convergence rates for $\epsilon \in \{0.01, 0.005, 0.001\}$ and order of polynomial $p = q \in \{2, 3, 4\}$. Indeed, we do not consider $p = q = 1$ as the continuity of basis functions is already C^0. The plots of the numerical approximations in L2 norm for all cases are depicted in Figure 6.11 - 6.21.

We can see that there are improvements to the error of the numerical approximations in L2 norm and the convergence rates. We can find the error is decreasing in all cases, especially for the early computations (bigger size of h). However, as the size of the element is getting smaller the difference is insignificant. In other words, the error reduction due the size of the element is more fruitful than reducing the continuity of basis functions.

It is important to note that by increasing multiplication of a certain knot in the knot vector does not only mean reducing the continuity of the basis functions, we are also introducing new degrees of freedom into the computations. Therefore, it is a trade-off to bear in mind when we decide which strategy of discretization we are going to pick.

We can conclude that the reduction of the basis functions is one good approach, but still, this method is not sufficient to solve the instability of the numerical approximations error and the convergence rates. Another approach we could go for is the application of DG method in IGA. Consequently, we should also consider the multi-patch applications.

Chapter 7

Multi-patch Discontinuous Galerkin IGA

In the previous chapter, we have already mentioned the motivation why we would like to consider DG application in this thesis. This chapter is devoted to DG application in IGA. Furthermore, we should remember the consequences of this option, which is we should also consider the multi-patch applications. We will refer all previous techniques of IGA as Continous Galerkin (CG) IGA method.

7.1 DG-IGA

In Chapter 4, we have already mentioned that IGA space is local to patches rather than elements, in comparison with FEA. Therefore, the DG application in IGA is a patch to patch relation instead of an element to element. This fact is important to remember, since every time we mention about partitions in the domain, we are referring to patches that consist of elements.

Oden et al. in [42] have already shown impressive work for the application of DG in FEM for Diffusion equation. We are referring to their works for derivations of weak formulation in DG with some adjustments for IGA environment.

Families of regular partitions

Let $P = \{P_h(\Omega)\}_{h>0}$ be a family of regular partitions of $\Omega \subset \mathbb{R}^d$ into $N = N(P_h)$ subdomains Ω_e, such that for $P_h \in P$,

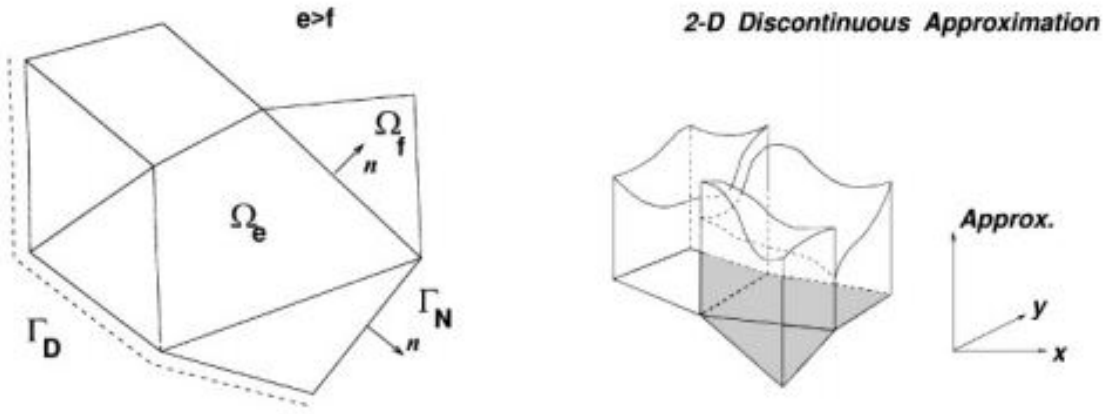

Figure 7.1: Subdomains and boundaries after discretization [42].

$$\bar{\Omega} = \bigcup_{e=1}^{N(P_h)} \bar{\Omega}_e, \text{ and } \Omega_e \cap \Omega_f = \emptyset \text{ for } e \neq f \tag{7.1}$$

Let us define the *interpatch* boundary by

$$\Gamma_{int} = \bigcup_{\Omega_f . \Omega_e \in P_h} (\partial\Omega_f \cap \partial\Omega_e) \tag{7.2}$$

On Γ_{int}, we define $\mathbf{n} = \mathbf{n}_e$ on $\partial\Omega_e \cap \partial\Omega_f \subset \Gamma_{int}$ for indices e, f such that $e > f$.

Broken spaces

We define the so-called broken spaces on the partition $P_h(\Omega)$ as follows:

$$H^m(P_h) = \{v \in L^2(\Omega) : v|_{\Omega_e} \in H^m(\Omega_e) \in P_h(\Omega)\} \tag{7.3}$$

if $v \in H^m(\Omega_e)$, the extension of v to the boundary $\partial\Omega_e$, indicated by the trace operation $\gamma_0 v$, is such that $\gamma_0 v \in H^{m-\frac{1}{2}}(\partial\Omega_e)$, $m > \frac{3}{2}$, which will be written $\nabla v \cdot n|_{\partial\Omega_e}$, is interpreted as generalized flux at the patch boundary $\partial\Omega_e$.

With this notation, for $v|_{\Omega_e} \in H^{\frac{3}{2}+\beta}(\Omega_e)$ and $v|_{\Omega_f} \in H^{\frac{3}{2}+\beta}(\Omega_f)$, we introduce the *jump* operator $[\cdot]$ defined on $\Gamma_{ef} = \bar{\Omega_e} \cap \bar{\Omega_f} \neq \emptyset$ as

$$[\gamma_0 v] = (\gamma_0 v)|_{\partial\Omega_e \cap \partial\Gamma_{ef}} - (\gamma_0 v)|_{\partial\Omega_f \cap \partial\Gamma_{ef}}, \ e > f \tag{7.4}$$

and the *average* operator $\langle\cdot\rangle$ for the normal flux is defined for $(\lambda\nabla v) \cdot n \in L^2(\Gamma_{ef})$ as

$$\big\langle (\lambda\nabla v) \cdot n \big\rangle = \frac{1}{2}\Big(\big((\lambda\nabla v) \cdot n\big)|_{\partial\Omega_e \cap \partial\Gamma_{ef}} + \big((\lambda\nabla v) \cdot n\big)|_{\partial\Omega_f \cap \partial\Gamma_{ef}} \Big), \ e > f \tag{7.5}$$

Note that n represents the outward normal from the element with higher index.

7.2 Weak formulation

Now, let us derive the DG weak formulation for Darcy's equation. Indeed, it is better to recall Darcy's equation in (2.19), that is:

$$\begin{aligned} -\nabla \cdot (\lambda \nabla \Phi) &= \tilde{Q} && \text{in } \Omega \\ \Phi &= \Phi_D && \text{on } \Gamma^D \\ \lambda \nabla \Phi \cdot n &= F_N && \text{on } \Gamma^N \end{aligned}$$

The weak formulation of (2.19) that forms the basis of DG method is defined on a broken space $V(P_h)$, P_h being a member of a family of regular partitions of Ω. The weak formulation of (2.19) reads:

$$\text{find } \Phi \in S \text{ such that for all } v \in V,\ a_{\pm}(\Phi, v) = f_{\pm}(v) \tag{7.6}$$

where:

$$\begin{aligned} a_{\pm}(\Phi, v) &= \sum_{\Omega_e \in P_h} \int_{\Omega_e} \lambda \nabla \Phi \cdot \nabla v \; d\Omega_e + \int_{\Gamma_D} \left(\pm (\lambda \nabla v) \cdot n \; \Phi - v (\lambda \nabla \Phi) \cdot n \right) d\mathbf{s} \\ &\quad + \int_{\Gamma_{int}} \left(\pm \langle (\lambda \nabla v) \cdot n \rangle \; [\Phi] - \langle (\lambda \nabla \Phi) \cdot n \rangle [v] \right) d\mathbf{s} \qquad (7.7) \\ f_{\pm}(v) &= \sum_{\Omega_e \in P_h} \int_{\Omega} \tilde{Q} \; v \; d\Omega \pm \int_{\Gamma_D} (\lambda \nabla v) \cdot n \; \Phi_D \; d\mathbf{s} + \int_{\Gamma_N} F_N \; v \; d\mathbf{s} \qquad (7.8) \end{aligned}$$

Interior penalty formulations

We choose the *minus* option for the weak formulation. This option guarantees the symmetry of the bilinear form of the resulting variational formulation [12, 47]. Furthermore, we impose interior penalty formulations of Wheeler [53] and Arnold [6]. These formulations are actually the same with the method of Nitsche [40, 42]. Thus the final weak formulation reads:

$$\text{find } \Phi \in S \text{ such that for all } v \in V,\ a(\Phi, v) = f(v) \tag{7.9}$$

where:

$$\begin{aligned} a(\Phi, v) &= \sum_{\Omega_e \in P_h} \int_{\Omega_e} \lambda \nabla \Phi \cdot \nabla v \; d\Omega_e - \int_{\Gamma_D} \left((\lambda \nabla v) \cdot n \; \Phi - v (\lambda \nabla \Phi) \cdot n \right) d\mathbf{s} \\ &\quad + \int_{\Gamma_D} \sigma \; v \; \Phi \; d\mathbf{s} - \int_{\Gamma_{int}} \left(\langle (\lambda \nabla v) \cdot n \rangle \; [\Phi] - \langle (\lambda \nabla \Phi) \cdot n \rangle [v] \right) d\mathbf{s} \\ &\quad + \int_{\Gamma_{int}} \sigma [v][\Phi] d\mathbf{s} \qquad (7.10) \\ f(v) &= \sum_{\Omega_e \in P_h} \int_{\Omega} \tilde{Q} \; v \; d\Omega - \int_{\Gamma_D} (\lambda \nabla v) \cdot n \; \Phi_D \; d\mathbf{s} + \int_{\Gamma_D} \sigma \; v \; \Phi_D \; d\mathbf{s} \\ &\quad + \int_{\Gamma_N} F_N \; v \; d\mathbf{s} \qquad (7.11) \end{aligned}$$

It should be noted that this additional terms are meant to avoid the problem of indefinite system [42]. Here σ is the penalty function, that is defined as:

$$\sigma = \frac{K}{h} \tag{7.12}$$

The parameter K is critical. It is problem dependent and has to be chosen carefully, otherwise the rate of convergence is not optimal [42]. We define K as follows [33]:

$$K = (p + d)(p + 1)k \tag{7.13}$$

The constant k takes the role to be the unknown that we should define. To have a clear understanding the effect of σ, or k in this research, let us reconsider Darcy's equation 1.

7.3 DG-IGA Darcy's equation 1

We define two patches, $\Omega_{1,2} = (0, 5) \times (0, 1)$.We consider $p = q \in \{1, 2, 3, 4\}$ and $k \in \{2.5, 5, 7.5, 10, 15\}$. Furthermore, as comparisons, we also consider the single patch CG method for the Darcy's equation 1, that we have already obtained in Section 5.3.

Table 7.1 - 7.16 show the error of the numerical approximations in L2 norm and the convergence rates for $p = q \in \{1, 2, 3, 4\}$ and $k \in \{1, 2.5, 5, 7.5, 10, 15\}$. The error of the numerical approximations in L2 norm is depicted in Figure 7.2 - 7.5.

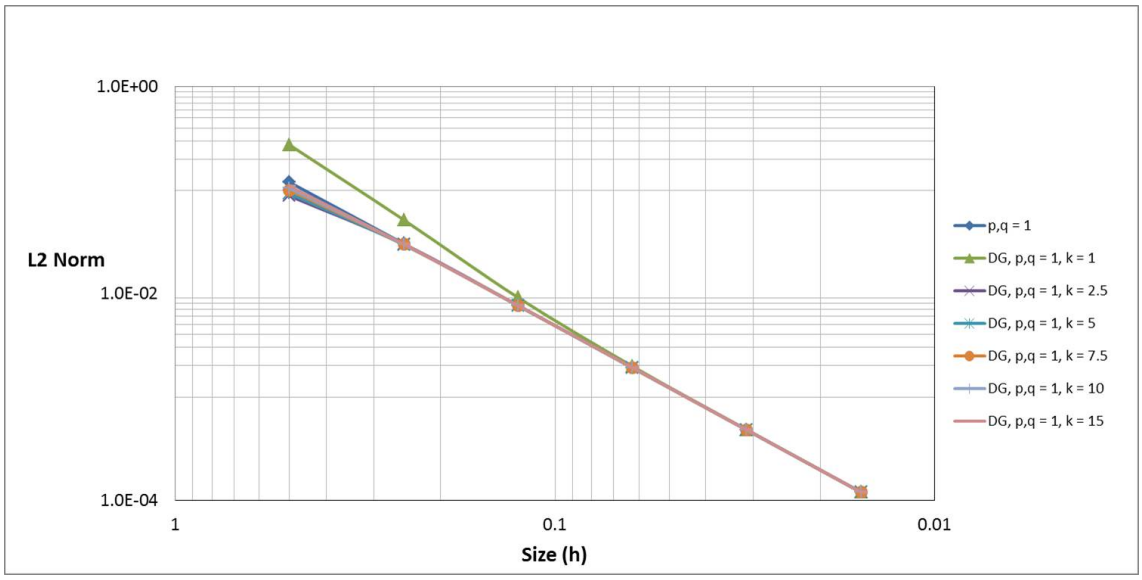

Figure 7.2: The plot of numerical approximation error in L2 norm for the 2D Darcy's equation 1, $p = q = 1$ and $k \in \{1, 2.5, 5, 7.5, 10, 15\}$.

$i^\star$	*Error in L2 norm*			
	$p, q = 1$	$p, q = 1,\ k = 1$	$p, q = 1,\ k = 2.5$	$p, q = 1,\ k = 5$
1	1.19146E-01	2.74199E-01	8.79218E-02	9.30395E-02
2	3.03356E-02	5.15830E-02	3.00132E-02	2.96850E-02
3	7.64573E-03	9.14064E-03	7.66208E-03	7.63492E-03
4	1.91582E-03	1.98090E-03	1.91783E-03	1.91610E-03
5	4.79238E-04	4.81849E-04	4.79393E-04	4.79286E-04
6	1.19828E-04	1.19941E-04	1.19838E-04	1.19831E-04

Table 7.1: The numerical approximation error in L2 norm for the 2D Darcy's equation 1, $p = q = 1$ and $k \in \{1, 2.5, 5\}$.

$i^\star$	*Convergence rates*			
	$p, q = 1$	$p, q = 1,\ k = 1$	$p, q = 1,\ k = 2.5$	$p, q = 1,\ k = 5$
2	1.97365	2.41026	1.55062	1.64811
3	1.98829	2.49653	1.96979	1.95905
4	1.99669	2.20614	1.99826	1.99444
5	1.99915	2.03950	2.00019	1.99921
6	1.99978	2.00626	2.00012	1.99989

Table 7.2: The numerical approximation convergence rates for the 2D Darcy's equation 1, $p = q = 1$ and $k \in \{1, 2.5, 5\}$.

$i^\star$	*Error in L2 norm*		
	$p, q = 1,\ k = 7.5$	$p, q = 1,\ k = 10$	$p, q = 1,\ k = 15$
1	1.00280E-01	1.04547E-01	1.09149E-01
2	2.98293E-02	2.99325E-02	3.00528E-02
3	7.63581E-03	7.63742E-03	7.63967E-03
4	1.91590E-03	1.91585E-03	1.91581E-03
5	4.79266E-04	4.79257E-04	4.79250E-04
6	1.19830E-04	1.19829E-04	1.19829E-04

Table 7.3: The numerical approximation error in L2 norm for the 2D Darcy's equation 1, $p = q = 1$ and $k \in \{7.5, 10, 15\}$.

$i^\star$	*Convergence rates*		
	$p, q = 1,\ k = 7.5$	$p, q = 1,\ k = 10$	$p, q = 1,\ k = 15$
2	1.74923	1.80437	1.86073
3	1.96588	1.97056	1.97592
4	1.99476	1.99510	1.99556
5	1.99912	1.99911	1.99910
6	1.99984	1.99982	1.99980

Table 7.4: The numerical approximation convergence rates for the 2D Darcy's equation 1, $p = q = 1$ and $k \in \{7.5, 10, 15\}$.

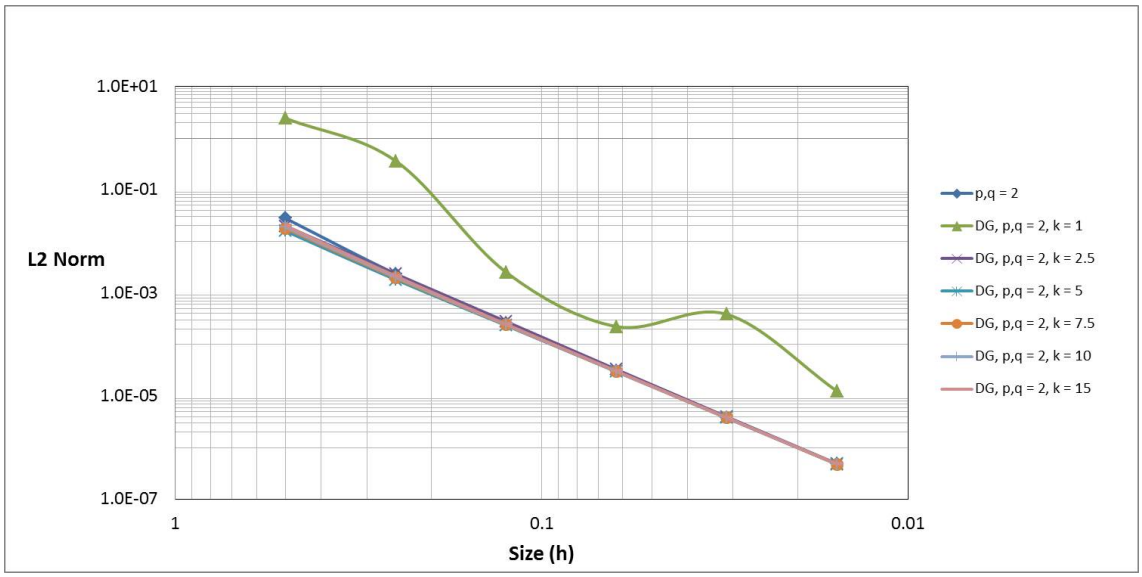

Figure 7.3: The plot of numerical approximation error in L2 norm for the 2D Darcy's equation 1, $p = q = 2$ and $k \in \{1, 2.5, 5, 7.5, 10, 15\}$.

$i^\star$	*Error in L2 norm*			
	$p, q = 2$	$p, q = 2,\ k = 1$	$p, q = 2,\ k = 2.5$	$p, q = 2,\ k = 5$
1	2.79916E-02	2.43203E+00	1.98556E-02	1.58824E-02
2	2.32503E-03	3.62268E-01	2.32882E-03	1.81197E-03
3	2.57176E-04	2.52399E-03	2.79512E-04	2.34134E-04
4	3.11214E-05	2.23246E-04	3.28789E-05	2.97894E-05
5	3.85826E-06	3.86387E-04	3.97468E-06	3.77688E-06
6	4.81286E-07	1.25017E-05	4.88697E-07	4.76242E-07

Table 7.5: The numerical approximation error in L2 norm for the Darcy's equation 1, $p = q = 2$ and $k \in \{1, 2.5, 5\}$.

$i^\star$	*Convergence rates*			
	$p, q = 2$	$p, q = 2,\ k = 1$	$p, q = 2,\ k = 2.5$	$p, q = 2,\ k = 5$
2	3.58967	2.74703	3.09187	3.13180
3	3.17642	7.16521	3.05862	2.95215
4	3.04678	3.49900	3.08768	2.97446
5	3.01188	-0.79141	3.04825	2.97953
6	3.00298	4.94985	3.02383	2.98743

Table 7.6: The numerical approximation convergence rates for the 2D Darcy's equation 1, $p = q = 2$ and $k \in \{1, 2.5, 5\}$.

$i^\star$	*Error in L2 norm*		
	$p, q = 2,\ k = 7.5$	$p, q = 2,\ k = 10$	$p, q = 2,\ k = 15$
1	1.78782E-02	1.89835E-02	2.01039E-02
2	1.94832E-03	2.03159E-03	2.11883E-03
3	2.39198E-04	2.43031E-04	2.47364E-04
4	3.00627E-05	3.02846E-05	3.05412E-05
5	3.79323E-06	3.80675E-06	3.82252E-06
6	4.77248E-07	4.78085E-07	4.79063E-07

Table 7.7: The numerical approximation error in L2 norm for the 2D Darcy's equation 1, $p = q = 2$ and $k \in \{7.5, 10, 15\}$.

$i^\star$	*Convergence rates*		
	$p, q = 1,\ k = 7.5$	$p, q = 1,\ k = 10$	$p, q = 1,\ k = 15$
2	3.19790	3.22406	3.24614
3	3.02595	3.06340	3.09856
4	2.99216	3.00448	3.01781
5	2.98648	2.99195	2.99816
6	2.99062	2.99322	2.99624

Table 7.8: The numerical approximation convergence rates for the 2D Darcy's equation 1, $p = q = 2$ and $k \in \{7.5, 10, 15\}$.

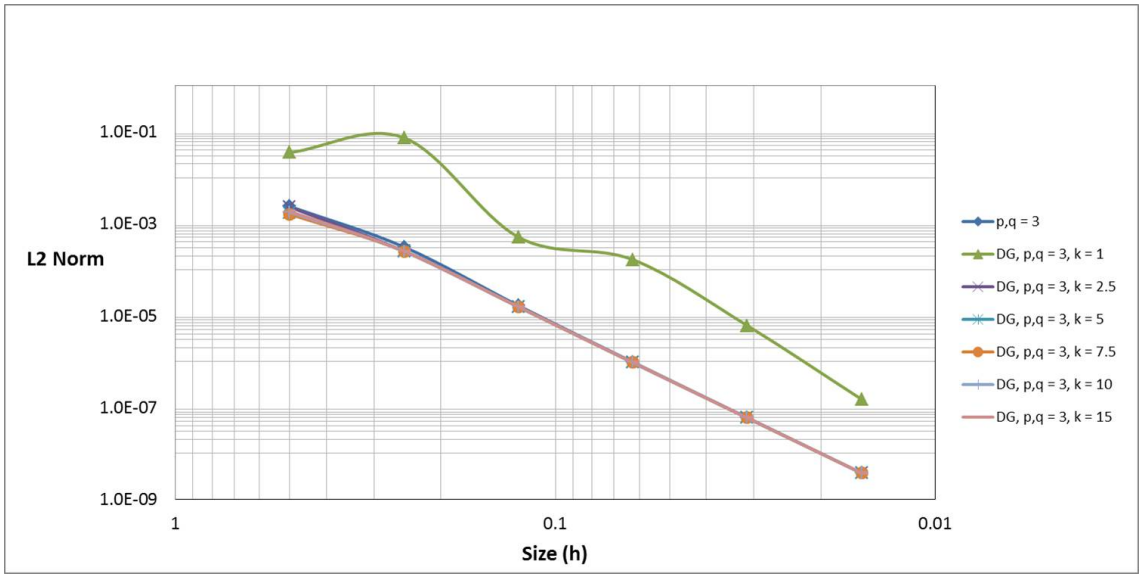

Figure 7.4: The plot of numerical approximation error in L2 norm for the 2D Darcy's equation 1, $p = q = 3$ and $k \in \{1, 2.5, 5, 7.5, 10, 15\}$.

$i^\star$	*Error in L2 norm*			
	$p, q = 3$	$p, q = 3,\ k = 1$	$p, q = 3,\ k = 2.5$	$p, q = 3,\ k = 5$
1	2.37131E-03	3.52930E-02	2.29317E-03	1.71415E-03
2	3.10754E-04	7.40078E-02	2.52456E-04	2.50842E-04
3	1.63701E-05	5.07929E-04	1.54436E-05	1.54433E-05
4	9.72452E-07	1.64628E-04	9.47413E-07	9.47469E-07
5	5.99884E-08	6.05736E-06	5.92255E-08	5.92260E-08
6	3.73697E-09	1.50059E-07	3.71331E-09	3.71331E-09

Table 7.9: The numerical approximation error in L2 norm for the 2D Darcy's equation 1, $p = q = 3$ and $k \in \{1, 2.5, 5\}$.

$i^\star$	*Convergence rates*			
	$p, q = 3$	$p, q = 3,\ k = 1$	$p, q = 3,\ k = 2.5$	$p, q = 3,\ k = 5$
2	2.93184	-1.06830	3.18324	2.77264
3	4.24664	7.18691	4.03095	4.02173
4	4.07329	1.62542	4.02687	4.02676
5	4.01887	4.76438	3.99970	3.99978
6	4.00474	5.33509	3.99544	3.99545

Table 7.10: The numerical approximation convergence rates for the 2D Darcy's equation 1, $p = q = 3$ and $k \in \{1, 2.5, 5\}$.

$i^\star$	*Error in L2 norm*		
	$p, q = 3,\ k = 7.5$	$p, q = 3,\ k = 10$	$p, q = 3,\ k = 15$
1	1.60234E-03	1.76979E-03	1.84872E-03
2	2.50992E-04	2.50904E-04	2.50950E-04
3	1.54433E-05	1.54433E-05	1.54433E-05
4	9.47460E-07	9.47473E-07	9.47476E-07
5	5.92259E-08	5.92260E-08	5.92261E-08
6	3.71331E-09	3.71331E-09	3.71331E-09

Table 7.11: The numerical approximation error in L2 norm for the 2D Darcy's equation 1, $p = q = 3$ and $k \in \{7.5, 10, 15\}$.

$i^\star$	*Convergence rates*		
	$p, q = 3,\ k = 7.5$	$p, q = 3,\ k = 10$	$p, q = 3,\ k = 15$
2	2.67447	2.81837	2.88105
3	4.02259	4.02208	4.02235
4	4.02677	4.02675	4.02675
5	3.99976	3.99978	3.99978
6	3.99545	3.99545	3.99546

Table 7.12: The numerical approximation convergence rates for the 2D Darcy's equation 1, $p = q = 3$ and $k \in \{7.5, 10, 15\}$.

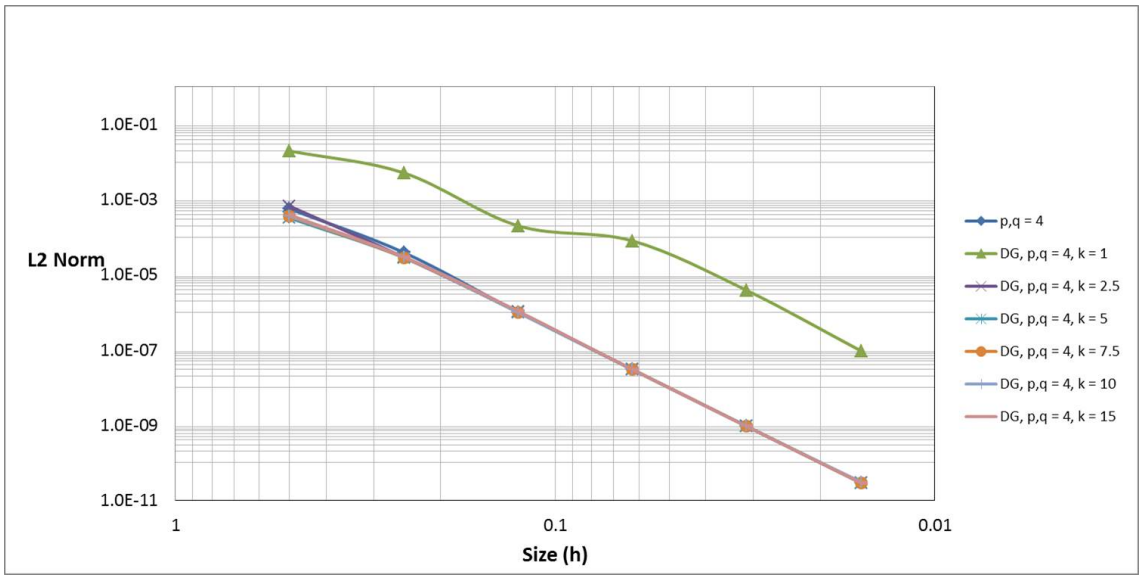

Figure 7.5: The plot of numerical approximation error in L2 norm for the 2D Darcy's equation 1, $p = q = 4$ and $k \in \{1, 2.5, 5, 7.5, 10, 15\}$.

$i^\star$	*Error in L2 norm*			
	$p, q = 4$	$p, q = 4,\ k = 1$	$p, q = 4,\ k = 2.5$	$p, q = 4,\ k = 5$
1	5.64413E-04	1.96904E-02	6.74065E-04	3.23863E-04
2	3.91211E-05	5.14024E-03	2.94480E-05	2.86915E-05
3	1.01244E-06	2.01517E-04	1.01993E-06	1.00447E-06
4	3.00292E-08	7.99947E-05	3.03011E-08	3.00921E-08
5	9.29503E-10	3.84221E-06	9.33853E-10	9.30708E-10
6	2.90365E-11	9.43835E-08	2.91047E-11	2.90560E-11

Table 7.13: The numerical approximation in L2 norm for the 2D Darcy's equation 1, $p = q = 4$ and $k \in \{1, 2.5, 5\}$.

$i^\star$	*Convergence rates*			
	$p, q = 4$	$p, q = 4,\ k = 1$	$p, q = 4,\ k = 2.5$	$p, q = 4,\ k = 5$
2	3.85073	1.93758	4.51665	3.49669
3	5.27204	4.67286	4.85163	4.83612
4	5.07533	1.33293	5.07296	5.06091
5	5.01376	4.37990	5.02003	5.01491
6	5.00052	5.34726	5.00387	5.00142

Table 7.14: The numerical approximation convergence rates for the 2D Darcy's equation 1, $p = q = 4$ and $k \in \{1, 2.5, 5\}$.

$i^\star$	*Error in L2 norm*		
	$p, q = 4,\ k = 7.5$	$p, q = 4,\ k = 10$	$p, q = 4,\ k = 15$
1	3.55131E-04	3.70479E-04	3.93016E-04
2	2.88164E-05	2.96865E-05	2.97509E-05
3	1.00334E-06	1.00173E-06	1.07774E-06
4	3.00569E-08	3.00424E-08	3.00296E-08
5	9.30178E-10	9.29959E-10	9.29765E-10
6	2.90937E-11	3.09010E-11	2.90437E-11

Table 7.15: The numerical approximation error in L2 norm for the Darcy's equation 1, $p = q = 4$ and $k \in \{7.5, 10, 15\}$.

$i^\star$	*Convergence rates*		
	$p, q = 4,\ k = 7.5$	$p, q = 4,\ k = 10$	$p, q = 4,\ k = 15$
2	3.62339	3.64151	3.72358
3	4.84401	4.88924	4.78685
4	5.06097	5.05935	5.16548
5	5.01405	5.01369	5.01338
6	4.99873	4.91144	5.00057

Table 7.16: The numerical approximation convergence rates for the 2D Darcy's equation 1, $p = q = 4$ and $k \in \{7.5, 10, 15\}$.

We immediately realize that $k = 1$ is not the best option for all cases. Perhaps, if we try to be fair, for the case $p = q = 1$ the error is converging slower compared to the others (Figure 7.2). But, for the rest of the cases, the convergence rates are not at maximum speed.

As it has been pointed previously, this study is meant to show how the constant k plays its role in the error of the numerical approximations. Furthermore, from this evaluation also, we can have an idea of the order of magnitude of k for Darcy's equation. Which we can conclude that $k = [2.5, 15]$. This result is important as we will use to reconsider our main problem, the Darcy's equation 2.

7.4 DG-IGA Darcy's equation 2

We a new tool in our hand we are going to reconsider Darcy's equation 2 with permeability tensor that is given on (6.1). We will only consider the critical cases which $\epsilon \in \{0.01, 0.005, 0.001\}$ and $p = q \in \{1, 2, 3, 4\}$. We will evaluate the numerical approximation error and the convergence rates. We will also consider the previous results of the CG method as comparisons.

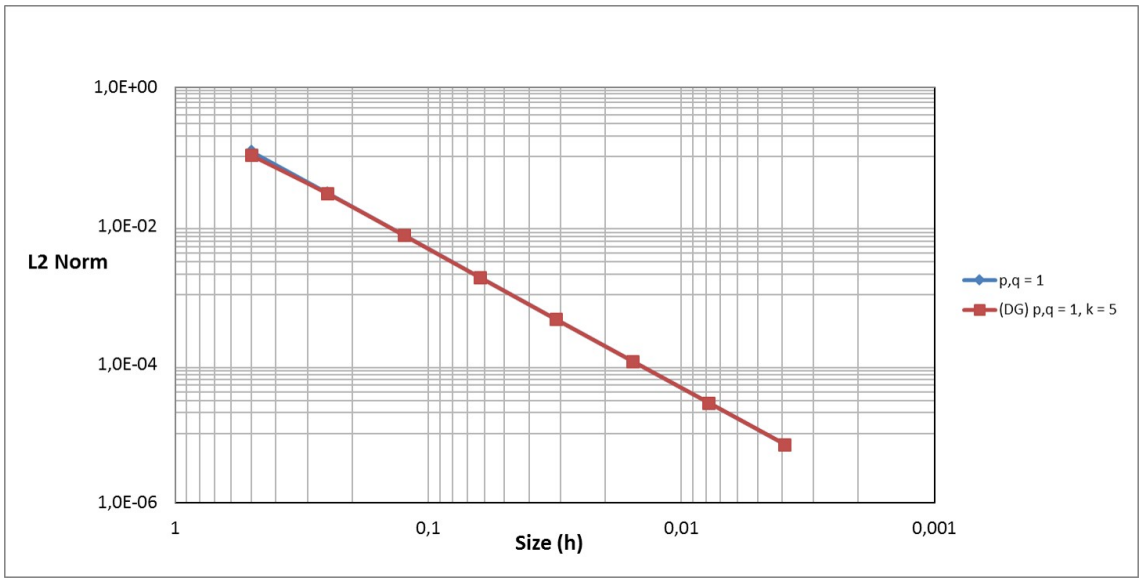

Figure 7.6: The plot of numerical approximation error in L2 norm for the 2D Darcy's equation 2, $p = q = 1$ and $\epsilon = 0.01$. CG and DG method comparisons.

$i^\star$	*Error in L2 norm*	
	$p, q = 1$	DG $p, q = 1$
1	1.19146E-01	1.05093E-01
2	2.99488E-02	2.94972E-02
3	7.38610E-03	7.37210E-03
4	1.80164E-03	1.80123E-03
5	4.44350E-04	4.44339E-04
6	1.10997E-04	1.10996E-04
7	2.77677E-05	2.77677E-05
8	6.94253E-06	6.94253E-06

Table 7.17: The numerical approximation error in L2 norm for the 2D Darcy's equation 2, $p = q = 1$ and $\epsilon = 0.01$. CG and DG method comparisons.

$i^\star$	*Convergence rates*	
	$p, q = 1$	DG $p, q = 1$
2	1.99216	1.83302
3	2.01961	2.00043
4	2.03550	2.03309
5	2.01954	2.01925
6	2.00118	2.00115
7	1.99904	1.99903
8	1.99987	1.99987

Table 7.18: The numerical approximation convergence rates for the 2D Darcy's equation 2, $p = q = 1$ and $\epsilon = 0.01$. CG and DG method comparisons.

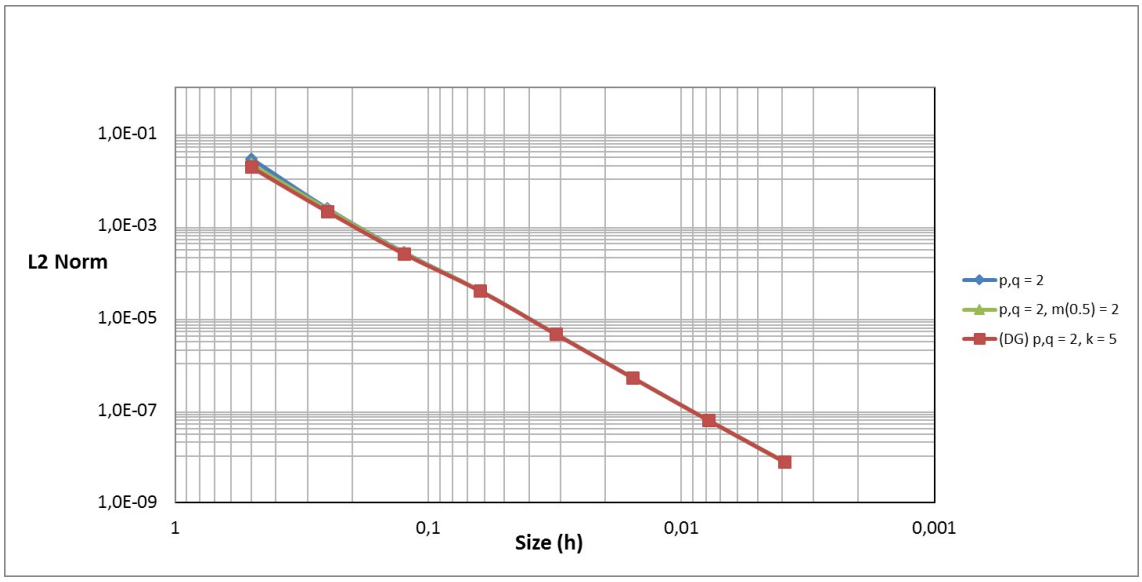

Figure 7.7: The plot of numerical approximation error in L2 norm for the 2D Darcy's equation 2, $p = q = 2$ and $\epsilon = 0.01$. CG, CG with basis functions continuity reduction, and DG method comparisons.

$i^\star$	*Error in L2 norm*		
	$p, q = 2$	$p, q = 2$, $m(0.5) = 2$	DG $p, q = 2$
1	2.82197E-02	2.19992E-02	1.88133E-02
2	2.33621E-03	2.28040E-03	2.02598E-03
3	2.63458E-04	2.60412E-04	2.47647E-04
4	3.90483E-05	3.94940E-05	3.89227E-05
5	4.44249E-06	4.46463E-06	4.42292E-06
6	5.11089E-07	5.11412E-07	5.08538E-07
7	6.02485E-08	6.02495E-08	6.00594E-08
8	7.51524E-09	7.51524E-09	7.50341E-09

Table 7.19: The numerical approximation error in L2 norm for the 2D Darcy's equation 2, $p = q = 2$ and $\epsilon = 0.01$. CG, CG with basis functions continuity reduction, and DG method comparisons.

$i^\star$	*Convergence rates*		
	$p, q = 2$	$p, q = 2$, $m(0.5) = 2$	DG $p, q = 2$
2	3.59446	3.27009	3.21506
3	3.14853	3.13042	3.03226
4	2.75424	2.72109	2.66960
5	3.13582	3.14502	3.13754
6	3.11972	3.12598	3.12057
7	3.08458	3.08546	3.08189
8	3.00303	3.00306	3.00077

Table 7.20: The numerical approximation convergence rates for the 2D Darcy's equation 2, $p = q = 2$ and $\epsilon = 0.01$. CG, CG with basis functions continuity reduction, and DG method comparisons.

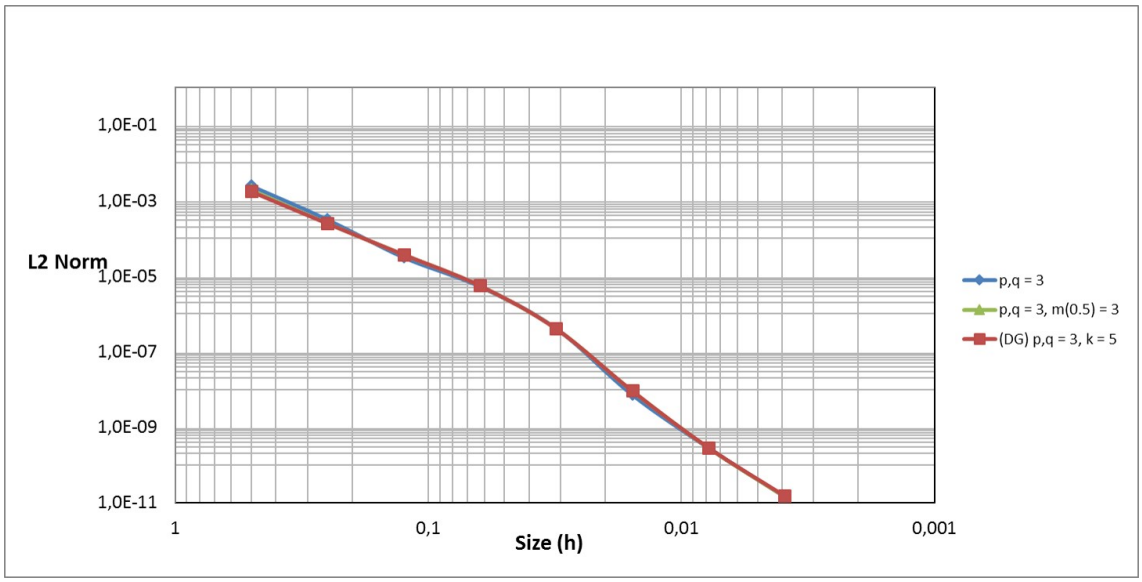

Figure 7.8: The plot of numerical approximation error in L2 norm for the 2D Darcy's equation 2, $p = q = 3$ and $\epsilon = 0.01$. CG, CG with basis functions continuity reduction, and DG method comparisons.

$i^\star$	*Error in L2 norm*		
	$p, q = 3$	$p, q = 3,\ m(0.5) = 3$	DG $p, q = 3$
1	2.45353E-03	1.93361E-03	1.77151E-03
2	3.15420E-04	2.51258E-04	2.51292E-04
3	3.17050E-05	3.72895E-05	3.75038E-05
4	5.36104E-06	5.63403E-06	5.64237E-06
5	4.16389E-07	4.09310E-07	4.09217E-07
6	7.28119E-09	9.17800E-09	9.19712E-09
7	2.87173E-10	2.86669E-10	2.86864E-10
8	1.45835E-11	1.45665E-11	1.51656E-11

Table 7.21: The numerical approximation error in L2 norm for the 2D Darcy's equation 2, $p = q = 3$. CG, CG with basis functions continuity reduction, and DG method comparisons.

$i^\star$	*Convergence rates*		
	$p, q = 3$	$p, q = 3$, $m(0.5) = 3$	DG $p, q = 3$
2	2.95951	2.94406	2.81754
3	3.31449	2.75233	2.74426
4	2.56413	2.72653	2.73266
5	3.68651	3.78290	3.78536
6	5.83761	5.47887	5.47554
7	4.66418	5.00072	5.00274
8	4.29951	4.29866	4.24149

Table 7.22: The numerical approximation convergence rates for the 2D Darcy's equation 2, $p = q = 3$ and $\epsilon = 0.01$. CG, CG with basis functions continuity reduction, and DG method comparisons.

$i^\star$	*Error in L2 norm*		
	$p, q = 4$	$p, q = 4$, $m(0.5) = 4$	DG $p, q = 4$
1	6.12762E-04	4.05254E-04	3.67200E-04
2	6.50551E-05	5.53194E-05	5.58827E-05
3	1.39300E-05	1.59582E-05	1.60131E-05
4	1.58427E-07	5.48274E-07	5.47959E-07
5	8.22373E-08	8.53216E-08	8.53994E-08
6	1.56094E-09	1.59607E-09	1.59616E-09
7	4.43430E-12	6.15893E-12	5.97674E-12

Table 7.23: The numerical approximation error in L2 norm for the 2D Darcy's equation 2, $p = q = 3$ and $\epsilon = 0.01$. CG, CG with basis functions continuity reduction, and DG method comparisons.

$i^\star$	*Convergence rates*		
	$p,q=4$	$p,q=4,\ m(0.5)=4$	DG $p,q=4$
2	3.23559	2.87297	2.71609
3	2.22347	1.79349	1.80315
4	6.45823	4.86326	4.86904
5	0.94595	2.68391	2.68177
6	5.71931	5.74032	5.74155
7	8.45949	8.01763	8.06103

Table 7.24: The numerical approximation convergence rates for the 2D Darcy's equation 2, $p = q = 3$ and $\epsilon = 0.01$. CG, CG with basis functions continuity reduction, and DG method comparisons.

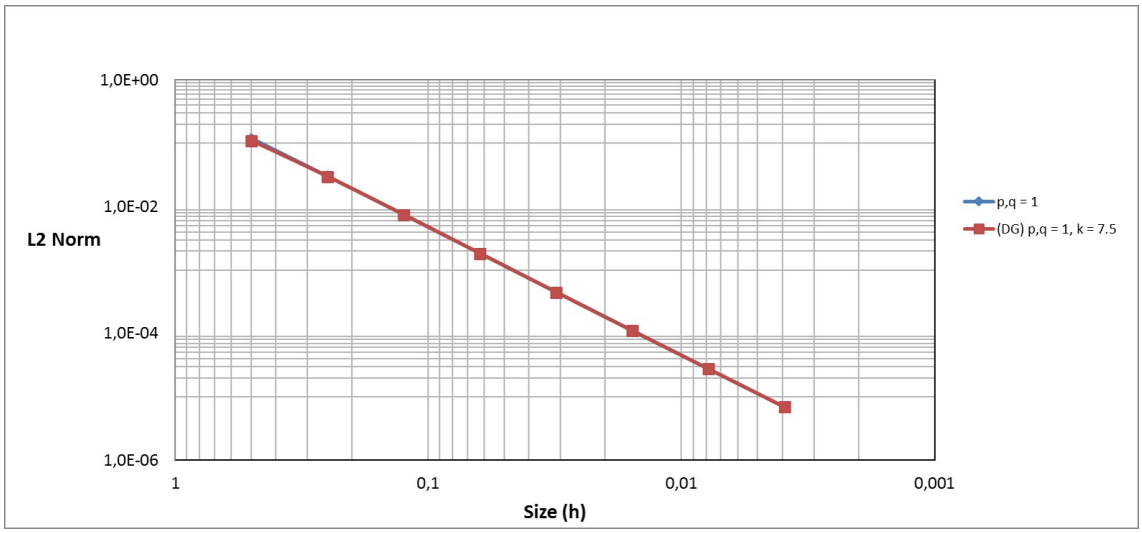

Figure 7.9: The plot of numerical approximation error in L2 norm for the 2D Darcy's equation 2, $p = q = 1$ and $\epsilon = 0.005$. CG and DG method comparisons.

$i^\star$	*Error in L2 norm*	
	$p, q = 1$	DG $p, q = 1$
1	1.19146E-01	1.09452E-01
2	3.00641E-02	2.97454E-02
3	7.47509E-03	7.46500E-03
4	1.83497E-03	1.83463E-03
5	4.47852E-04	4.47835E-04
6	1.10740E-04	1.10740E-04
7	2.76747E-05	2.76747E-05
8	6.92111E-06	6.92110E-06

Table 7.25: The numerical approximation error in L2 norm for the 2D Darcy's equation 2, $p = q = 1$ and $\epsilon = 0.005$. CG and DG method comparisons.

$i^\star$	*Convergence rates*	
	$p, q = 1$	DG $p, q = 1$
2	1.98662	1.87956
3	2.00788	1.99445
4	2.02633	2.02465
5	2.03466	2.03445
6	2.01585	2.01579
7	2.00054	2.00054
8	1.99949	1.99949

Table 7.26: The numerical approximation convergence rates for the 2D Darcy's equation 2, $p = q = 1$ and $\epsilon = 0.01$. CG and DG method comparisons.

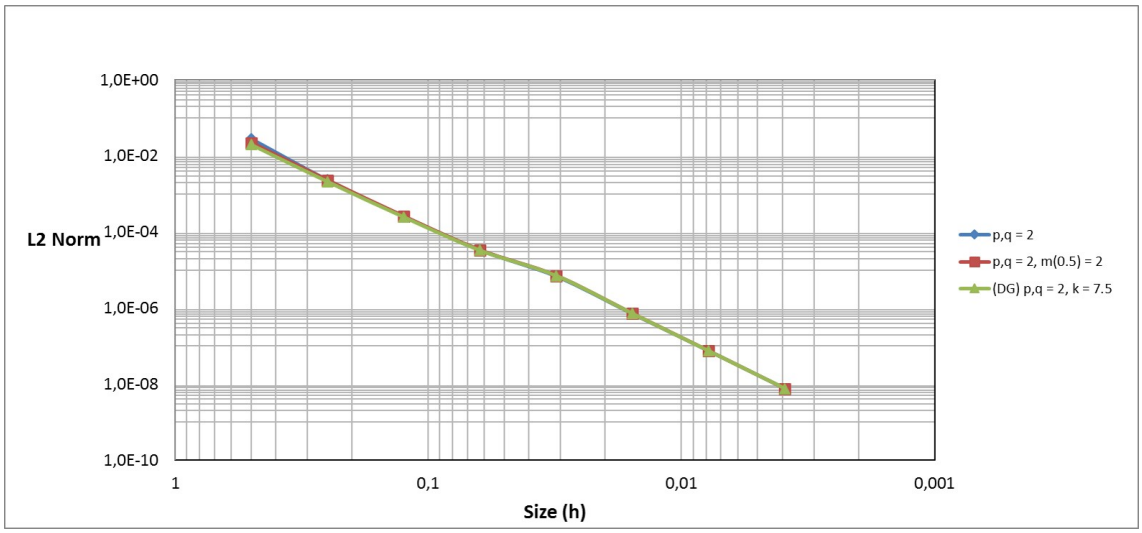

Figure 7.10: The plot of numerical approximation error in L2 norm for the 2D Darcy's equation 2, $p = q = 2$ and $\epsilon = 0.005$. CG, CG with basis functions continuity reduction, and DG method comparisons.

$i^\star$	*Error in L2 norm*		
	$p, q = 2$	$p, q = 2$, $m(0.5) = 2$	DG $p, q = 2$
1	2.82558E-02	2.20042E-02	1.98636E-02
2	2.33560E-03	2.28209E-03	2.10924E-03
3	2.58133E-04	2.56415E-04	2.47185E-04
4	3.32423E-05	3.33327E-05	3.28545E-05
5	6.82319E-06	7.07860E-06	7.06690E-06
6	7.03588E-07	7.14101E-07	7.12704E-07
7	7.42097E-08	7.42902E-08	7.41780E-08
8	7.56907E-09	7.56930E-09	7.56093E-09

Table 7.27: The numerical approximation error in L2 norm for the 2D Darcy's equation 2, $p = q = 2$ and $\epsilon = 0.005$. CG, CG with basis functions continuity reduction, and DG method comparisons.

$i^\star$	*Convergence rates*		
	$p, q = 2$	$p, q = 2$, $m(0.5) = 2$	DG $p, q = 2$
2	3.59668	3.26935	3.23533
3	3.17761	3.15380	3.09306
4	2.95702	2.94347	2.91143
5	2.28450	2.23540	2.21694
6	3.27764	3.30926	3.30970
7	3.24505	3.26488	3.26424
8	3.29342	3.29494	3.29436

Table 7.28: The numerical approximation convergence rates for the 2D Darcy's equation 2, $p = q = 2$ and $\epsilon = 0.005$. CG, CG with basis functions continuity reduction, and DG method comparisons.

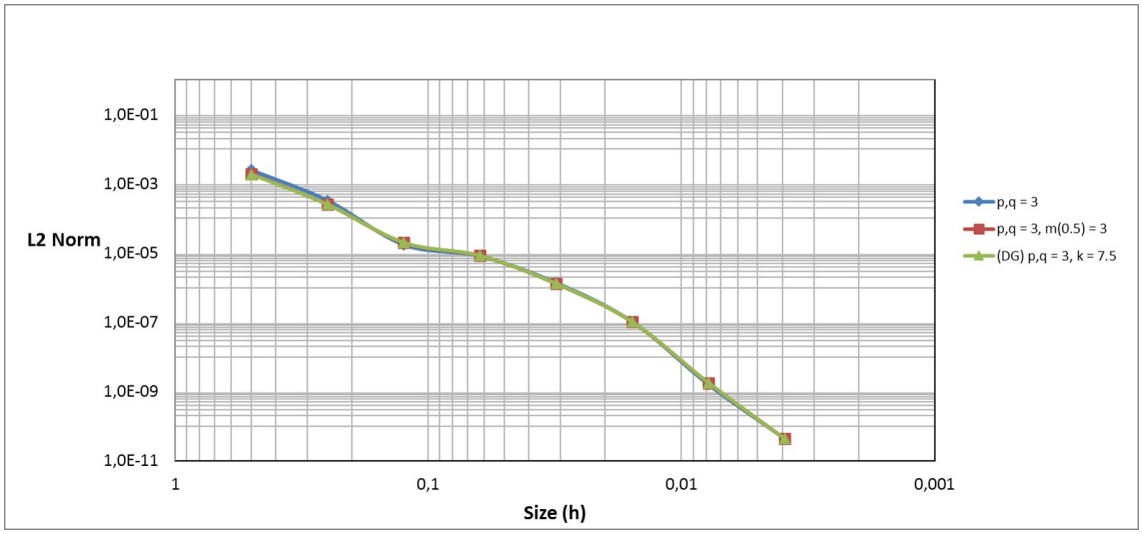

Figure 7.11: The plot of numerical approximation error in L2 norm for the 2D Darcy's equation 2, $p = q = 3$ and $\epsilon = 0.005$. CG, CG with basis functions continuity reduction, and DG method comparisons.

$i^\star$	*Error in L2 norm*		
	$p, q = 3$	$p, q = 3$, $m(0.5) = 3$	DG $p, q = 3$
1	2.47282E-03	1.93403E-03	1.82895E-03
2	3.26479E-04	2.50518E-04	2.50400E-04
3	1.73505E-05	1.96104E-05	1.97599E-05
4	8.17861E-06	8.32925E-06	8.35358E-06
5	1.39183E-06	1.30131E-06	1.30196E-06
6	1.03313E-07	1.01846E-07	1.01827E-07
7	1.58522E-09	1.76538E-09	1.76715E-09
8	4.37124E-11	4.38234E-11	4.32992E-11

Table 7.29: The numerical approximation error in L2 norm for the 2D Darcy's equation 2, $p = q = 3$ and $\epsilon = 0.005$. CG, CG with basis functions continuity reduction, and DG method comparisons.

$i^\star$	*Convergence rates*		
	$p, q = 3$	$p, q = 3$, $m(0.5) = 3$	DG $p, q = 3$
2	2.92110	2.94862	2.86871
3	4.23394	3.67522	3.66359
4	1.08505	1.23536	1.24211
5	2.55487	2.67822	2.68171
6	3.75189	3.67550	3.67649
7	6.02619	5.85027	5.84855
8	5.18050	5.33213	5.35094

Table 7.30: The numerical approximation convergence rates for the 2D Darcy's equation 2, $p = q = 3$ and $\epsilon = 0.005$. CG, CG with basis functions continuity reduction, and DG method comparisons.

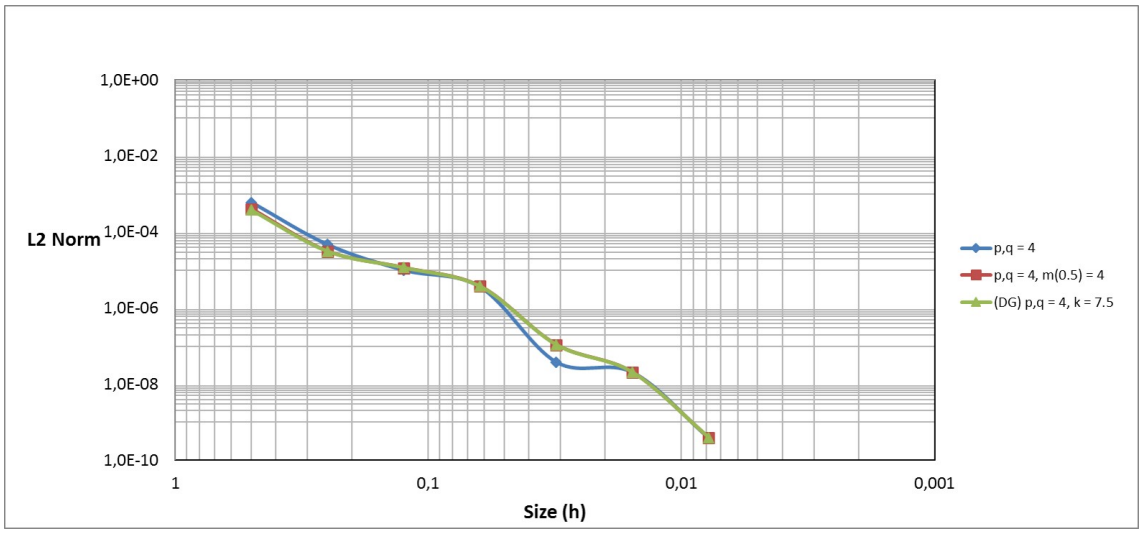

Figure 7.12: The plot of numerical approximation error in L2 norm for the 2D Darcy's equation 2, $p = q = 4$ and $\epsilon = 0.005$. CG, CG with basis functions continuity reduction, and DG method comparisons.

$i^\star$	*Error in L2 norm*		
	$p, q = 4$	$p, q = 4$, $m(0.5) = 4$	DG $p, q = 4$
1	6.05082E-04	4.03598E-04	3.78674E-04
2	4.69107E-05	3.11293E-05	3.12980E-05
3	9.97728E-06	1.15208E-05	1.16081E-05
4	3.59991E-06	3.73610E-06	3.74111E-06
5	3.81845E-08	1.08618E-07	1.08582E-07
6	2.06042E-08	2.03572E-08	2.03610E-08
7	3.83705E-10	3.90173E-10	3.89942E-10
8	1.05118E-12	1.29081E-12	5.32072E-12

Table 7.31: The numerical approximation error in L2 norm for the 2D Darcy's equation 2, $p = q = 4$ and $\epsilon = 0.005$. CG, CG with basis functions continuity reduction, and DG method comparisons.

$i^\star$	*Convergence rates*		
	$p, q = 4$	$p, q = 4$, $m(0.5) = 4$	DG $p, q = 4$
2	3.68914	3.69657	3.59681
3	2.23320	1.43403	1.43094
4	1.47069	1.62464	1.63359
5	6.55883	5.10420	5.10661
6	0.89005	2.41565	2.41490
7	5.74680	5.70528	5.70641

Table 7.32: The numerical approximation convergence rates for the 2D Darcy's equation 2, $p = q = 4$ and $\epsilon = 0.005$. CG, CG with basis functions continuity reduction, and DG method comparisons.

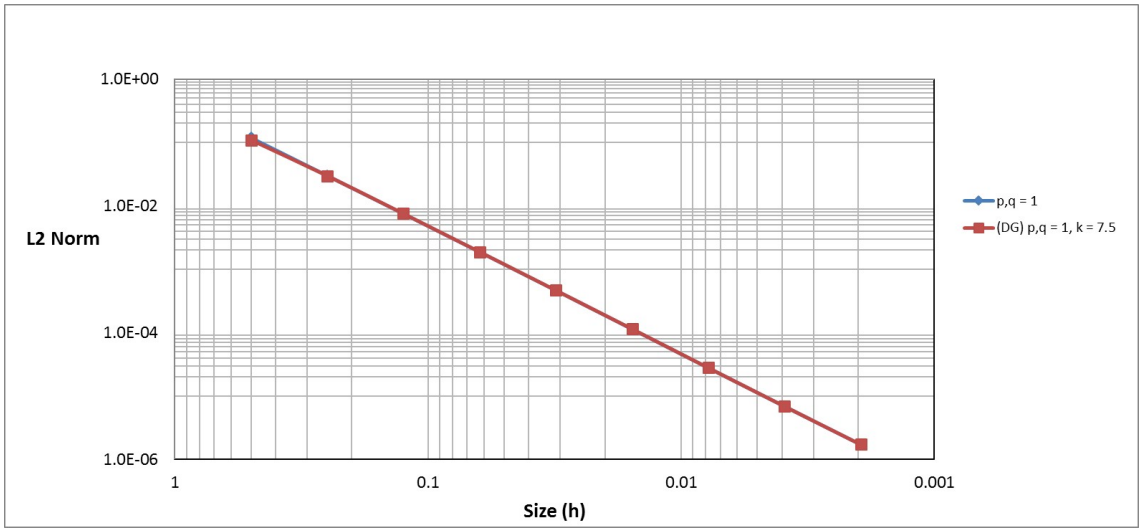

Figure 7.13: The plot of numerical approximation error in L2 norm for the 2D Darcy's equation 2, $p = q = 1$ and $\epsilon = 0.001$. CG and DG method comparisons.

$i^\star$	*Error in L2 norm*	
	$p, q = 1$	DG $p, q = 1$
1	1.19146E-01	1.09446E-01
2	3.01637E-02	2.98439E-02
3	7.56327E-03	7.55300E-03
4	1.88397E-03	1.88362E-03
5	4.66540E-04	4.66511E-04
6	1.14673E-04	1.14665E-04
7	2.80222E-05	2.80206E-05
8	6.90924E-06	6.90920E-06
9	1.72619E-06	1.72619E-06

Table 7.33: The numerical approximation error in L2 norm for the 2D Darcy's equation 2, $p = q = 1$ and $\epsilon = 0.001$. CG and DG method comparisons.

$i^\star$	*Convergence rates*	
	$p, q = 1$	DG $p, q = 1$
2	1.98185	1.87471
3	1.99573	1.98231
4	2.00523	2.00354
5	2.01370	2.01352
6	2.02448	2.02449
7	2.03288	2.03287
8	2.01997	2.01990
9	2.00094	2.00093

Table 7.34: The numerical approximation convergence rates for the 2D Darcy's equation 2, $p = q = 1$ and $\epsilon = 0.001$. CG and DG method comparisons.

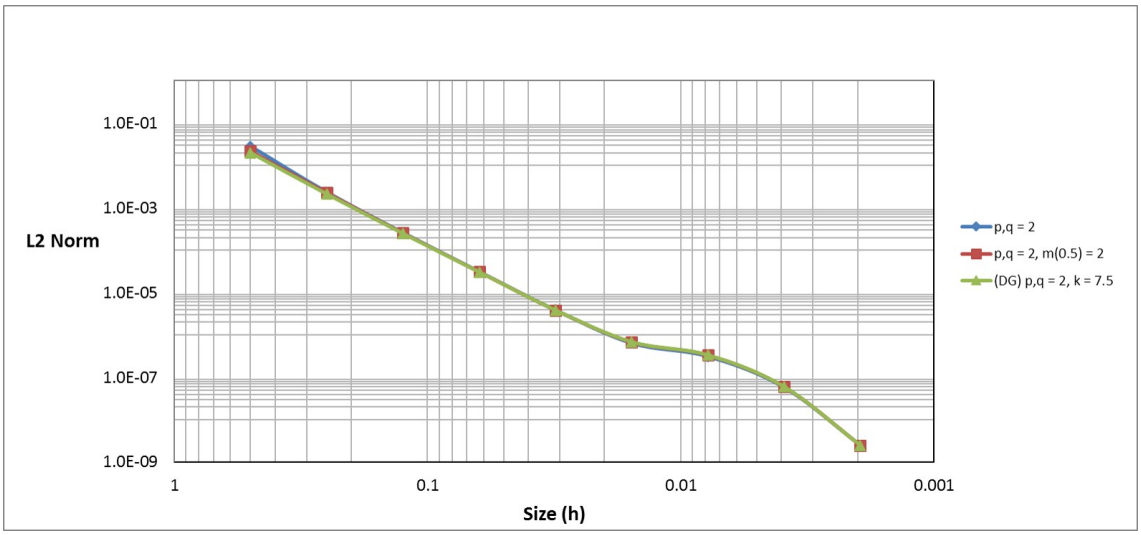

Figure 7.14: The plot of numerical approximation error in L2 norm for the 2D Darcy's equation 2, $p = q = 2$ and $\epsilon = 0.001$. CG, CG with basis functions continuity reduction, and DG method comparisons.

$i^\star$	*Error in L2 norm*		
	$p, q = 2$	$p, q = 2,\ m(0.5) = 2$	DG $p, q = 2$
1	2.82884E-02	2.20094E-02	1.98668E-02
2	2.33815E-03	2.28308E-03	2.11045E-03
3	2.57570E-04	2.56460E-04	2.47215E-04
4	3.11366E-05	3.11026E-05	3.05405E-05
5	3.87501E-06	3.87284E-06	3.84055E-06
6	6.42810E-07	6.82538E-07	6.85284E-07
7	3.12895E-07	3.36174E-07	3.36683E-07
8	5.80172E-08	6.00230E-08	6.00260E-08
9	2.50673E-09	2.50462E-09	2.50449E-09

Table 7.35: The numerical approximation error in L2 norm for the 2D Darcy's equation 2, $p = q = 2$ and $\epsilon = 0.001$. CG, CG with basis functions continuity reduction, and DG method comparisons.

$i^\star$	*Convergence rates*		
	$p, q = 2$	$p, q = 2$, $m(0.5) = 2$	DG $p, q = 2$
2	3.59677	3.26907	3.23474
3	3.18233	3.15418	3.09371
4	3.04828	3.04363	3.01697
5	3.00634	3.00557	2.99134
6	2.59174	2.50441	2.48654
7	1.03871	1.02170	1.02531
8	2.43113	2.48562	2.48773
9	4.53260	4.58285	4.58300

Table 7.36: The numerical approximation convergence rates for the 2D Darcy's equation 2, $p = q = 2$ and $\epsilon = 0.001$. CG, CG with basis functions continuity reduction, and DG method comparisons.

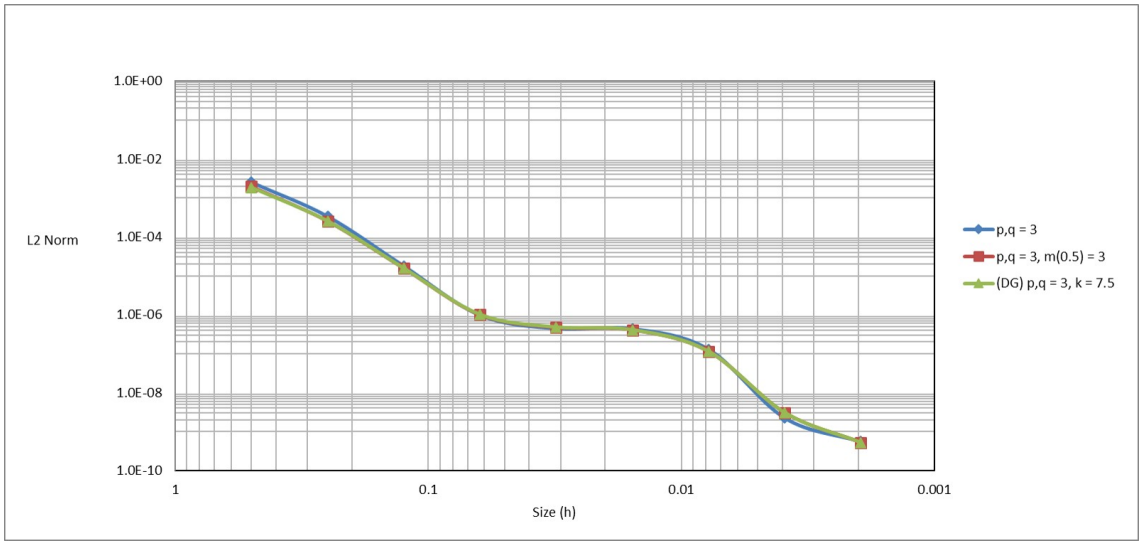

Figure 7.15: The plot of numerical approximation error in L2 norm for the 2D Darcy's equation 2, $p = q = 3$ and $\epsilon = 0.001$. CG, CG with basis functions continuity reduction, and DG method comparisons.

$i^\star$	*Error in L2 norm*		
	$p, q = 3$	$p, q = 3$, $m(0.5) = 3$	DG $p, q = 3$
1	2.48658E-03	1.93251E-03	1.82767E-03
2	3.33218E-04	2.50644E-04	2.50654E-04
3	1.77295E-05	1.54423E-05	1.54401E-05
4	9.81742E-07	9.93264E-07	1.00536E-06
5	4.47077E-07	4.69117E-07	4.78746E-07
6	4.40329E-07	4.06967E-07	4.08107E-07
7	1.31068E-07	1.13978E-07	1.14036E-07
8	2.26624E-09	3.03674E-09	3.03620E-09
9	5.59545E-10	5.20739E-10	5.20932E-10

Table 7.37: The numerical approximation error in L2 norm for the 2D Darcy's equation 2, $p = q = 3$ and $\epsilon = 0.001$. CG, CG with basis functions continuity reduction, and DG method comparisons.

$i^\star$	*Convergence rates*		
	$p, q = 3$	$p, q = 3$, $m(0.5) = 3$	DG $p, q = 3$
2	2.89962	2.94676	2.86624
3	4.23224	4.02068	4.02094
4	4.17466	3.95857	3.94090
5	1.13482	1.08223	1.07038
6	0.02194	0.20504	0.23031
7	1.74827	1.83616	1.83946
8	5.85387	5.23009	5.23108
9	2.01797	2.54389	2.54310

Table 7.38: The numerical approximation convergence rates for the 2D Darcy's equation 2, $p = q = 2$ and $\epsilon = 0.001$. CG, CG with basis functions continuity reduction, and DG method comparisons.

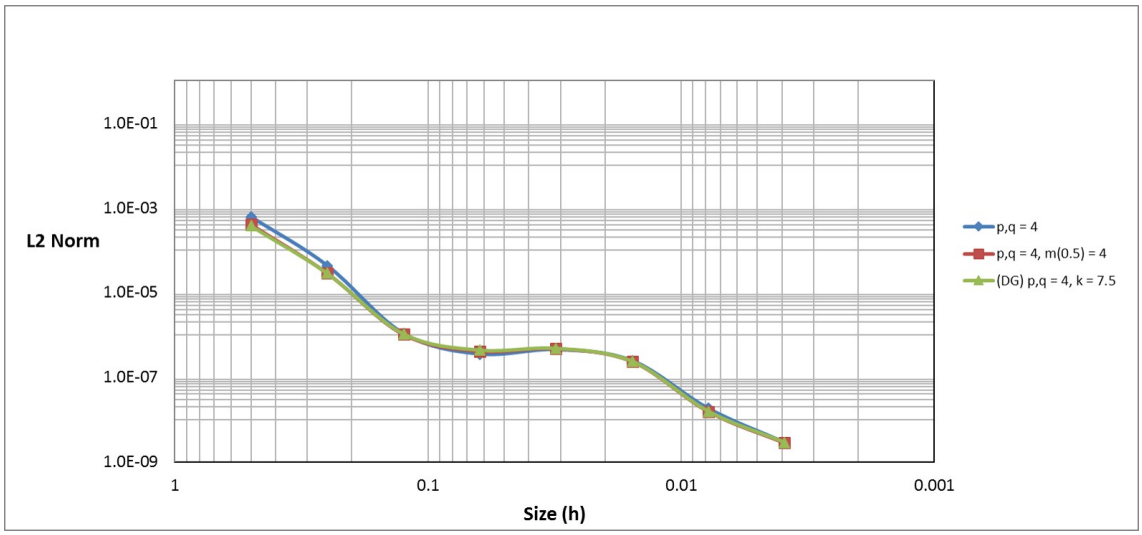

Figure 7.16: The plot of numerical approximation error in L2 norm for the 2D Darcy's equation 2, $p = q = 4$ and $\epsilon = 0.001$. CG, CG with basis functions continuity reduction, and DG method comparisons.

$i^\star$	*Error in L2 norm*		
	$p, q = 4$	$p, q = 4$, $m(0.5) = 4$	DG $p, q = 4$
1	6.05898E-04	4.03646E-04	3.78709E-04
2	4.31326E-05	2.86865E-05	2.86543E-05
3	1.08113E-06	1.03276E-06	1.05542E-06
4	3.53397E-07	4.15734E-07	4.35375E-07
5	4.49988E-07	4.77721E-07	4.81161E-07
6	2.46020E-07	2.38000E-07	2.38165E-07
7	1.83166E-08	1.55781E-08	1.55781E-08
8	2.91053E-09	2.84595E-09	2.86562E-09

Table 7.39: The numerical approximation error in L2 norm for the 2D Darcy's equation 2, $p = q = 3$ and $\epsilon = 0.001$. CG, CG with basis functions continuity reduction, and DG method comparisons.

$i^\star$	*Convergence rates*		
	$p, q = 4$	$p, q = 4$, $m(0.5) = 4$	DG $p, q = 4$
2	3.81222	3.81465	3.72427
3	5.31817	4.79580	4.76286
4	1.61318	1.31277	1.27749
5	-0.34860	-0.20051	-0.14426
6	0.87111	1.00521	1.01456
7	3.74755	3.93337	3.93437
8	2.65380	2.45254	2.44260

Table 7.40: The numerical approximation convergence rates for the 2D Darcy's equation 2, $p = q = 4$ and $\epsilon = 0.001$. CG, CG with basis functions continuity reduction, and DG method comparisons.

Table 7.17 - 7.40 show the error of the numerical approximations in L2 norm and the convergence rates for $p = q \in \{1, 2, 3, 4\}$ and $\epsilon \in \{0.01, 0.005, 0.001\}$. The error of the numerical approximations in L2 norm is depicted in Figure 7.6 - 7.16. We reconsider the CG method with and without continuity basis functions reduction as comparisons.

We can immediately realize that DG method improves the error of the numerical approximations and the convergence rates, in comparison with those of the CG methods. However, those improvements are insignificant as the size of the element is getting smaller. The instability of the convergence rates also occurs for $p = q \in \{3, 4\}$, even though the DG approach is already implemented.

Intuitively speaking, we expect to have better results as we allow discontinuity on the basis functions and an interpatch feature right on the critical position, that is $\xi_i = 0.5$. However, the results show insignificant improvements. The remaining questions are whether it is IGA (CG and IGA) limitation, or could it be a wrong implementation of IGA in the C++ library. A self-checking of the theoretical and the practical aspect of the code will only eliminate the second possibility. And we also already did a validation test for Darcy's equation 1, and the results are as expected.

To avoid the doubt on the results of DG-IGA, we will consider the origin method, which is FEA. Furthermore, to minimize mistakes at the implementation level, we are using deal.II FEA library without extensive modifications.

Chapter 8

Discontinuous Galerkin FEM

This chapter is meant to give comparisons between the DG-IGA with the DG-FEM. We have to admit that IGA is a relatively new method of discretization, and in comparison with FEM, this method is far younger. Therefore, a comparison with FEM is considered essential to evaluate the IGA performance to be specific for Darcy's equation 2 with $\epsilon \in \{0.01, 0.005, 0.001\}$. For the purpose of this evaluation, we are using an open source finite element library that is **deal.II**. The implementation of the deal.II is derived due to the necessity of a robust FEM code, and from the practical point of view, it will be a fair comparison as this library is developed by different and reliable developers. Indeed, we will do some tests. We will reconsider the 2D benchmark problem (Poisson's equation), and the Darcy's equation 2 for $\epsilon = 1$. We have seen in those two cases; the numerical approximations converge at maximum rates. Therefore, intuitively, we would expect more or less the same results.

We will not review the theoretical part of DG-FEM, since in the previous chapter we have seen the technical part of DG-IGA, and it is sufficient to be used for DG-FEM with some adjustments.

8.1 DG-FEM test cases

We are evaluating the numerical approximations of the DG-FEM for the 2D benchmark problem and the Darcy's equation 2 for $\epsilon = 1$. The L2 norm and the convergence rates of the numerical approximations are depicted in Figure 8.1 - 8.2 and Table 8.1 - 8.4.

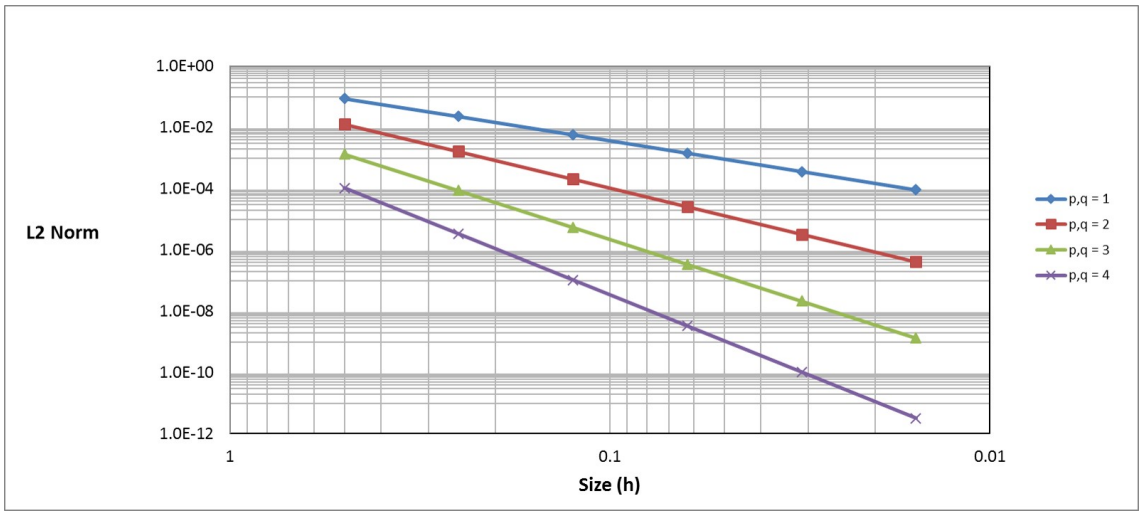

Figure 8.1: The plot of DG-FEM numerical approximation error in L2 norm for the 2D benchmark problem.

$i^\star$	*Error in L2 norm*			
	$p, q = 1$	$p, q = 2$	$p, q = 3$	$p, q = 4$
1	8.91406E-02	1.30197E-02	1.35213E-03	1.07053E-04
2	2.32382E-02	1.66564E-03	8.74019E-05	3.37805E-06
3	5.86801E-03	2.09411E-04	5.51081E-06	1.05762E-07
4	1.47063E-03	2.62142E-05	3.45191E-07	3.30647E-09
5	3.67884E-04	3.27795E-06	2.15865E-08	1.03338E-10
6	9.19853E-05	4.09781E-07	1.34934E-09	3.22940E-12

Table 8.1: The DG-FEM numerical approximation error in L2 norm for the 2D benchmark problem.

$i^\star$	*Convergence rates*			
	$p,q=1$	$p,q=2$	$p,q=3$	$p,q=4$
2	1.93958	2.96655	3.95143	4.98599
3	1.98556	2.99167	3.98733	4.99730
4	1.99644	2.99792	3.99680	4.99939
5	1.99911	2.99948	3.99919	4.99985
6	1.99978	2.99987	3.99980	4.99996

Table 8.2: The DG-FEM numerical approximation convergence rates for the 2D benchmark problem.

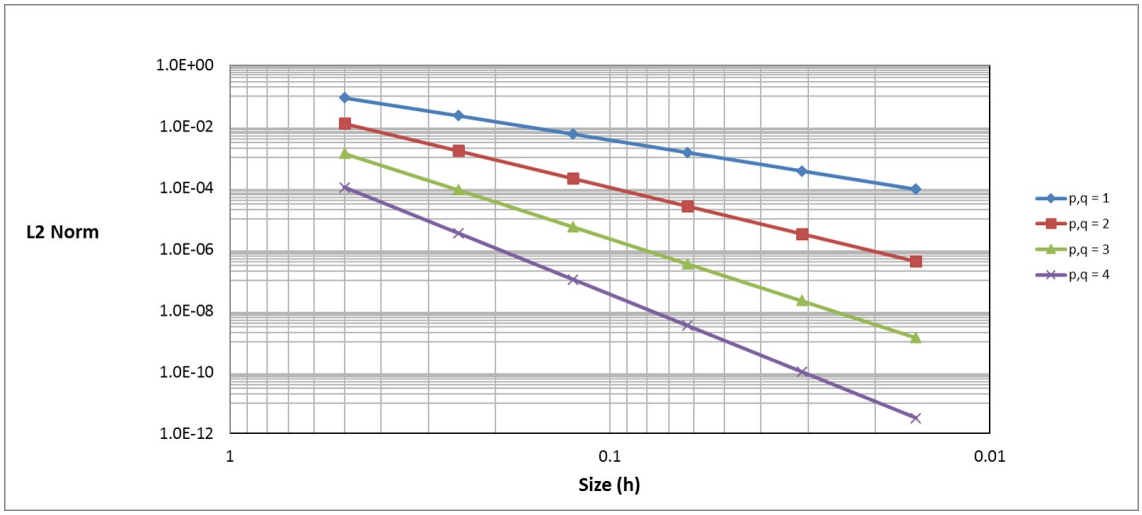

Figure 8.2: The plot of DG-FEM numerical approximation error in L2 norm for the 2D Darcy's equation 2, $\epsilon = 1$.

$i^\star$	*Error in L2 norm*			
	$p, q = 1$	$p, q = 2$	$p, q = 3$	$p, q = 4$
1	8.91899E-02	1.30193E-02	1.35235E-03	1.07046E-04
2	2.32412E-02	1.66563E-03	8.74041E-05	3.37807E-06
3	5.86820E-03	2.09411E-04	5.51084E-06	1.05762E-07
4	1.47064E-03	2.62142E-05	3.45192E-07	3.30647E-09
5	3.67885E-04	3.27795E-06	2.15865E-08	1.03338E-10
6	9.19853E-05	4.09781E-07	1.34934E-09	3.22941E-12

Table 8.3: The DG-FEM numerical approximation error in L2 norm for the 2D Darcy's equation 2, $\epsilon = 1$.

$i^\star$	*Convergence rates*			
	$p, q = 1$	$p, q = 2$	$p, q = 3$	$p, q = 4$
2	1.93958	2.96655	3.95143	4.98599
3	1.98556	2.99167	3.98733	4.99730
4	1.99644	2.99792	3.99680	4.99939
5	1.99911	2.99948	3.99919	4.99985
6	1.99978	2.99987	3.99980	4.99996

Table 8.4: The DG-FEM numerical approximation convergence rates for the 2D Darcy's equation 2, $\epsilon = 1$.

As it is expected, we find no surprising results of the numerical approximations for both cases. All the numerical approximations converge at their optimum rates which is $\mathcal{O}(h^{p+1})$ [45]. Therefore, it is clear that the deal.II is a robust and reliable tool for this study.

8.2 DG-FEM for Darcy's equation 2

Now, with a reliable tool in our hands we will revisit the Darcy's equation 2. We will only revisit our main concern cases, which are $\epsilon \in \{0.01, 0.005, 0.001\}$. The plots of the numerical approximations error are depicted in Figure 8.1 - 8.2. Furthermore, the numerical approximations error in L2 norm and the convergence rates are shown in Table 8.5 - 8.10.

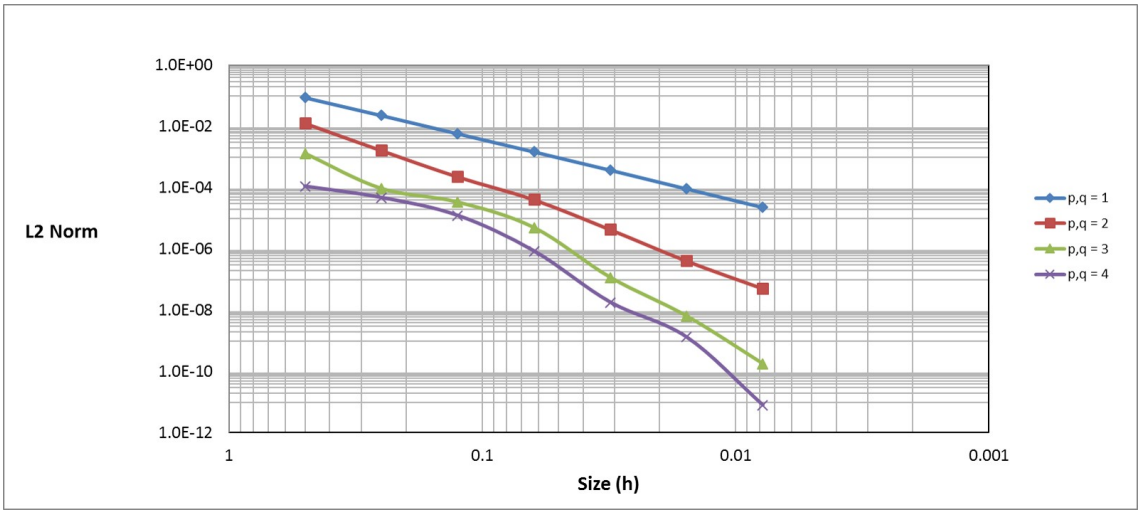

Figure 8.3: The plot of DG-FEM numerical approximation error in L2 norm for the 2D Darcy's equation 2, $\epsilon = 0.01$.

$i^\star$	*Error in L2 norm*			
	$p, q = 1$	$p, q = 2$	$p, q = 3$	$p, q = 4$
1	8.91714E-02	1.30382E-02	1.33341E-03	1.10500E-04
2	2.32751E-02	1.67955E-03	9.54156E-05	4.76209E-05
3	5.91381E-03	2.30958E-04	3.42755E-05	1.23942E-05
4	1.50884E-03	4.12891E-05	5.03373E-06	8.59390E-07
5	3.80541E-04	4.35644E-06	1.18646E-07	1.81915E-08
6	9.31739E-05	4.10658E-07	6.50297E-09	1.32607E-09
7	2.30518E-05	5.12590E-08	1.78526E-10	7.92922E-12

Table 8.5: The DG-FEM numerical approximation error in L2 norm for the 2D benchmark problem, $\epsilon = 0.01$.

$i^\star$	*Convergence rates*			
	$p, q = 1$	$p, q = 2$	$p, q = 3$	$p, q = 4$
2	1.93779	2.95660	3.80475	1.21438
3	1.97663	2.86237	1.47705	1.94193
4	1.97065	2.48380	2.76748	3.85021
5	1.98732	3.24454	5.40689	5.56198
6	2.03005	3.40714	4.18942	3.77804
7	2.01505	3.00206	5.18689	7.38576

Table 8.6: The DG-FEM numerical approximation convergence rates for the 2D Darcy's equation 2, $\epsilon = 0.01$.

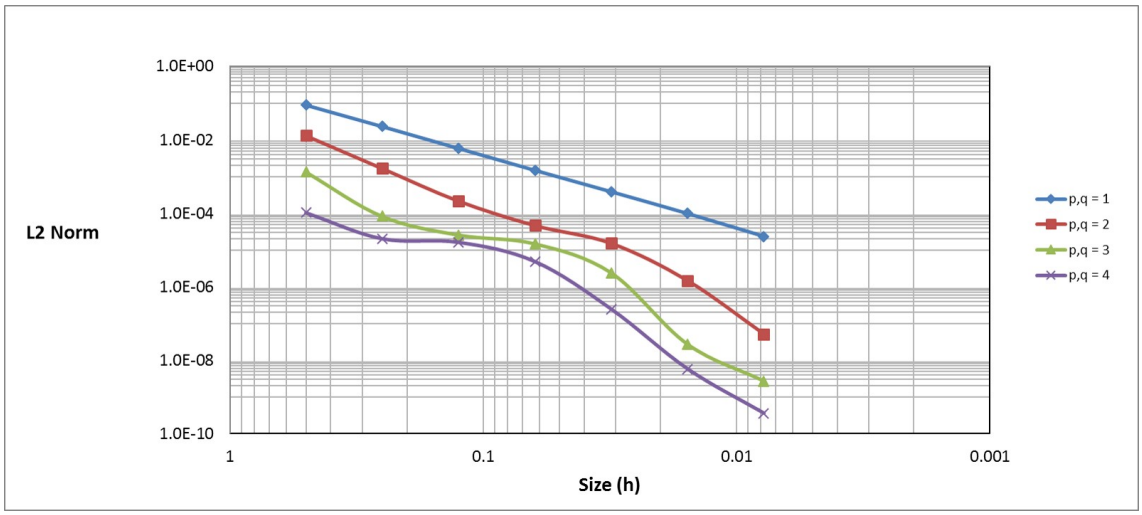

Figure 8.4: The plot of DG-FEM numerical approximation error in L2 norm for the 2D Darcy's equation 2, $\epsilon = 0.005$.

$i^\star$	*Error in L2 norm*			
	$p, q = 1$	$p, q = 2$	$p, q = 3$	$p, q = 4$
1	8.91496E-02	1.30241E-02	1.34751E-03	1.03796E-04
2	2.32480E-02	1.66888E-03	8.29859E-05	2.02952E-05
3	5.88261E-03	2.15431E-04	2.58021E-05	1.62949E-05
4	1.49180E-03	4.66694E-05	1.48517E-05	4.87192E-06
5	3.88184E-04	1.52760E-05	2.38681E-06	2.46634E-07
6	9.92517E-05	1.47605E-06	2.68944E-08	5.78395E-09
7	2.36482E-05	5.19070E-08	2.66873E-09	3.58695E-10

Table 8.7: The DG-FEM numerical approximation error in L2 norm for the 2D benchmark problem, $\epsilon = 0.005$.

$i^\star$	*Convergence rates*			
	$p,q=1$	$p,q=2$	$p,q=3$	$p,q=4$
2	1.93912	2.96423	4.02129	2.35454
3	1.98258	2.95358	1.68538	0.31672
4	1.97940	2.20668	0.79686	1.74186
5	1.94224	1.61121	2.63747	4.30405
6	1.96758	3.37145	6.47163	5.41417
7	2.06936	4.82967	3.33308	4.01123

Table 8.8: The DG-FEM numerical approximation convergence rates for the 2D Darcy's equation 2, $\epsilon = 0.005$.

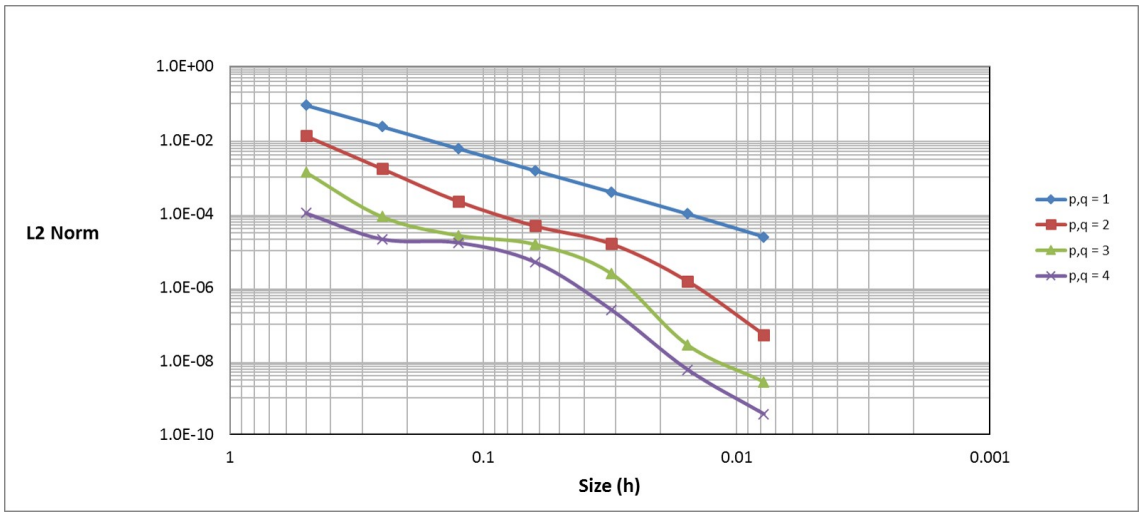

Figure 8.5: The plot of DG-FEM numerical approximation error in L2 norm for the 2D Darcy's equation 2, $\epsilon = 0.005$.

$i^\star$	*Error in L2 norm*			
	$p, q = 1$	$p, q = 2$	$p, q = 3$	$p, q = 4$
1	8.91415E-02	1.30199E-02	1.35199E-03	1.06926E-04
2	2.32387E-02	1.66575E-03	8.71178E-05	3.35705E-06
3	5.86866E-03	2.09525E-04	5.21072E-06	1.42918E-06
4	1.47180E-03	2.65763E-05	2.88417E-06	2.36895E-06
5	3.70104E-04	7.13864E-06	4.26496E-06	2.70403E-06
6	9.62652E-05	7.53398E-06	3.48542E-06	1.39887E-06
7	2.98278E-05	4.33729E-06	1.00509E-06	1.66684E-07

Table 8.9: The DG-FEM numerical approximation error in L2 norm for the 2D benchmark problem, $\epsilon = 0.005$.

$i^\star$	*Convergence rates*			
	$p, q = 1$	$p, q = 2$	$p, q = 3$	$p, q = 4$
2	1.93957	2.96647	3.95597	4.99327
3	1.98543	2.99098	4.06341	1.23201
4	1.99545	2.97891	0.85333	-0.72906
5	1.99158	1.89642	-0.56438	-0.19086
6	1.94284	-0.07776	0.29120	0.95085
7	1.69036	0.79662	1.79401	3.06907

Table 8.10: The DG-FEM numerical approximation convergence rates for the 2D Darcy's equation 2, $\epsilon = 0.005$.

From the numerical approximations error and the convergence rates. It is clear that for $p = q \in \{1, 2\}$ the numerical approximations error converges at optimum rate, but is not the case for $p = q \in \{3, 4\}$. It is a clear message that the instability of the numerical approximation error and the convergence rates also occur even for DG-FEM. Therefore, we have already, more or less, answered the questions raised in the previous chapter.

8.3 IGA and DG-FEM comparisons

Even though IGA and FEA come from the same root, IGA and FEA is not comparable. We can consider CG applications, for instance. FEA is using C^0 continuity for its basis functions across its elements. It is not the case for IGA. IGA is using C^{p-1} continuity for its basis functions. At the DG level even there is a huge difference. What it is so-called an element in FEA is equal to a patch in IGA sense. Without repeating the theoretical part, we understand that a patch comprises elements. Therefore, DG-IGA and DG-FEA are not equivalent.

All arguments above are valid at theoretical aspect, but when it comes to the practical issue, it would be a question which method serves the best. The best in the sense of small numerical approximations error and reasonable computation costs. One good comparison we might perform is to compare the number of DOF and the numerical approximations error.

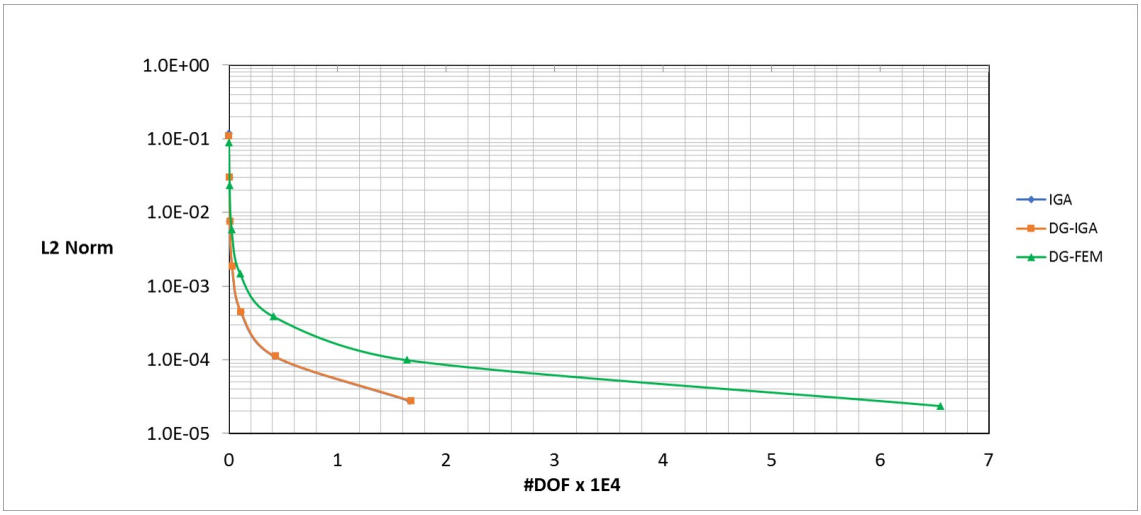

Figure 8.6: IGA, DG-IGA, and DG-FEM numerical approximation error in L2 norm for the 2D Darcy's equation 2. $\epsilon = 0.005$ and $p = q = 1$.

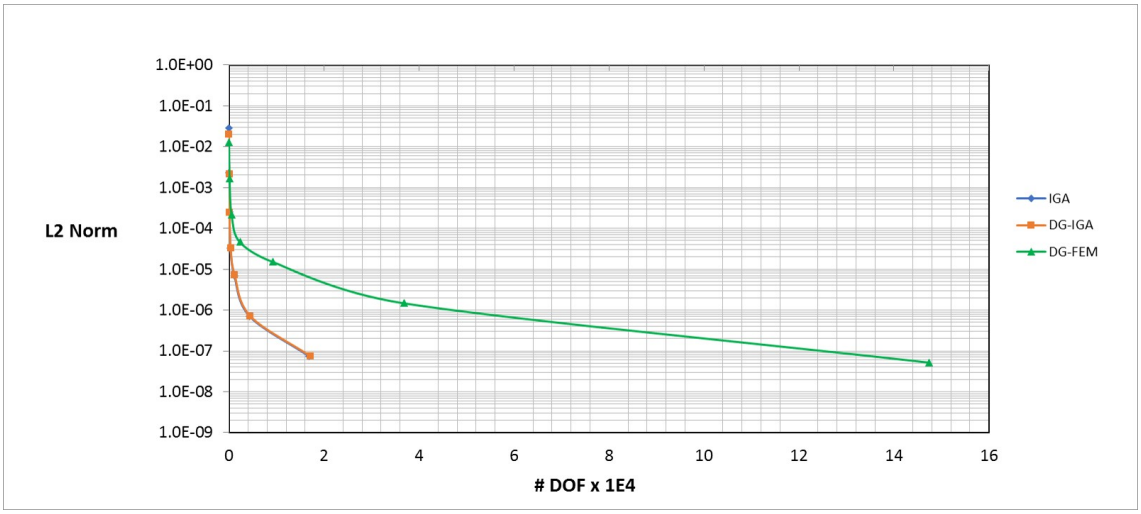

Figure 8.7: IGA, DG-IGA, and DG-FEM numerical approximation error in L2 norm for the 2D Darcy's equation 2. $\epsilon = 0.005$ and $p = q = 2$.

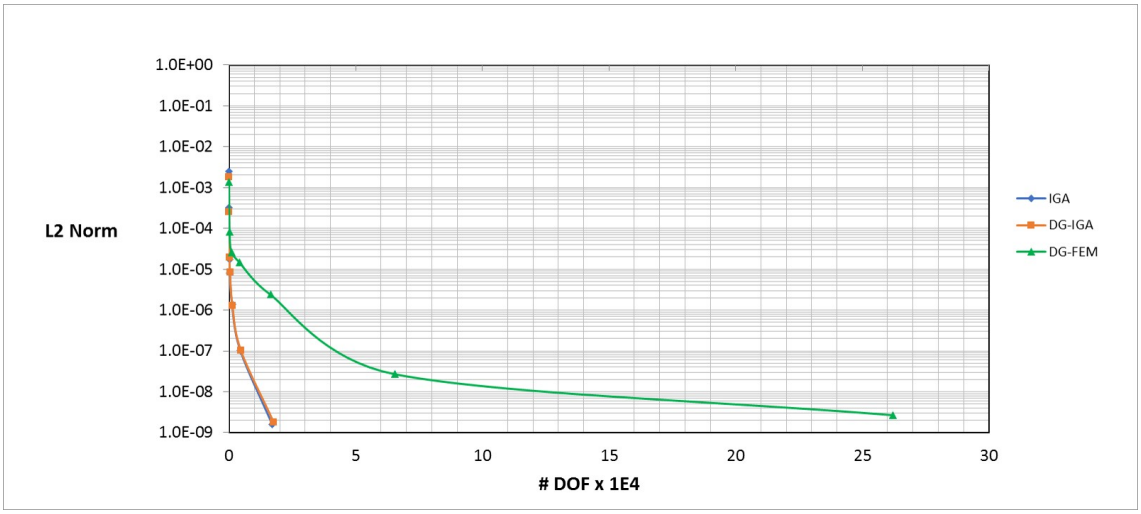

Figure 8.8: IGA, DG-IGA, and DG-FEM numerical approximation error in L2 norm for the 2D Darcy's equation 2. $\epsilon = 0.005$ and $p = q = 3$.

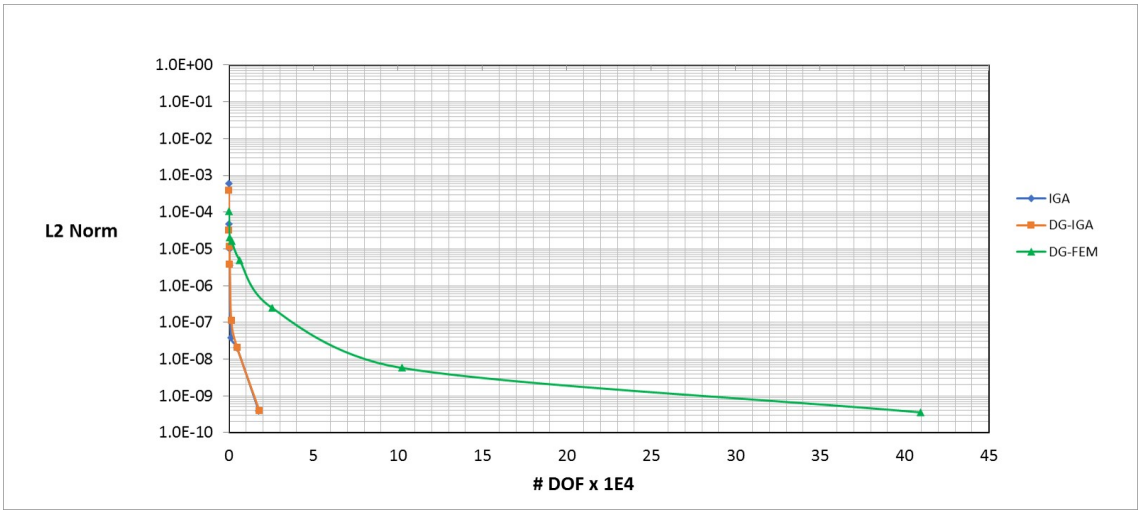

Figure 8.9: IGA, DG-IGA, and DG-FEM numerical approximation error in L2 norm for the 2D Darcy's equation 2. $\epsilon = 0.005$ and $p = q = 4$.

The comparisons of IGA, DG-IGA, and DG-FEA are depicted in Figure 8.6 - 8.7. We might get an impression that DG-FEA is the worst method considering the fact that IGA and DG-IGA will give the same accuracy but with far less number of DOF. However, the main message of those comparisons is to show that a smart choice of discretization technique could give a huge advantage. We can immediately realize the role of the patch in minimizing the computation costs.

Chapter 9

Conclusions

In this thesis, we started with the motivations why we would like to consider IGA as a discretization technique for reservoir simulation. They are due to the necessity of a reliable reservoir simulation as one of the solutions for the present challenge in oil and gas industry, and also due to the fact that FEA-based approach is better than those of FVM-based approach for extensive cases in reservoir simulation [27].

We visited the origin method, which is FEA, to have an introduction of IGA. In this chapter also, we prepare ourselves with the tools that are used to analyze the IGA numerical approximation results. Later, we developed several test cases to see the robustness of the code we developed. And finally, we consider a case in which reservoir anisotropy is exposed.

We can conclude that IGA is a powerful tool. It allows many options in the discretization technique. It offers flexibility for refinements, in this thesis we consider knot insertions and order elevation. It also provides an option to enrich basis functions with reduction of basis functions continuity, and it gives more reasonable computation costs when Discontinuous Galerkin approach is considered, thanks to the multi-patch applications.

Even though in this thesis we figured out that all features in IGA we mentioned before could not give significant improvements for the case in which reservoir anisotropy is exposed, it does not mean that IGA is a poor method. The poor results are also the case for FEA. Furthermore, a strong message is delivered in this thesis, that is a smart choice of discretization technique will save computation costs a lot. And IGA definitely is a better option than FEA.

9.1 Future developments

In this thesis, we restrict ourselves to 2D, incompressible, and single phase Darcy's equation. Indeed, it is far from an ideal reservoir simulation. In the future development, it is expected to examine compressible and multiphase problems. It is important to note that the necessity to compare IGA with FEA was brought due to surprising results of the DG-IGA in handling reservoir anisotropy. It was not planned at the beginning of the project. Therefore, to have a comparison with FEA is strongly

recommended in the future development.

It would be an ideal case to have extensive study such as in [27], which is basically a comparison study of several methods under real reservoir environment. The inclusion of geomechanics effects in the simulation would also be an interesting topic. One of the applications is to avoid sand production due to drastic pressure drawdown in a reservoir.

Bibliography

[1] Autodesk Simulation CFD 2014. Finite element vs finite volume, 2014.

[2] I Aavatsmark and GT Eigestad. Numerical convergence of the mpfa o-method and u-method for general quadrilateral grids. *International journal for numerical methods in fluids*, 51(9-10):939–961, 2006.

[3] Ivar Aavatsmark. An introduction to multipoint flux approximations for quadrilateral grids. *Computational Geosciences*, 6(3-4):405–432, 2002.

[4] Ivar Aavatsmark, Geir T Eigestad, Bjorn-ove Heimsund, Bradley Mallison, Jan M Nordbotten, Erlend Øian, et al. A new finite-volume approach to efficient discretization on challenging grids. *SPE Journal*, 15(03):658–669, 2010.

[5] International Energy Agency. *2015 Key World Energy Statistics*. International Energy Agency, 2015.

[6] Douglas N Arnold. An interior penalty finite element method with discontinuous elements. *SIAM journal on numerical analysis*, 19(4):742–760, 1982.

[7] Khalid Aziz and Antonin Settari. *Petroleum reservoir simulation*. Chapman & Hall, 1979.

[8] BR Baliga and SV Patankar. A new finite-element formulation for convection-diffusion problems. *Numerical Heat Transfer*, 3(4):393–409, 1980.

[9] BR Baliga and SV Patankar. A control volume finite-element method for two-dimensional fluid flow and heat transfer. *Numerical Heat Transfer*, 6(3):245–261, 1983.

[10] Jorge Len; Aguilera Roberto F; Tallett Martin Ban, Jan; Arellano. *2015 World Oil Outlook*. Organization of the Petroleum Exporting Countries, 2015.

[11] W. Bangerth, D. Davydov, T. Heister, L. Heltai, G. Kanschat, M. Kronbichler, M. Maier, B. Turcksin, and D. Wells. The `deal.II` library, version 8.4. *Journal of Numerical Mathematics*, 24, 2016.

[12] Federica Brunero, Luca Franco Pavarino, and Clemens Pechstein. Discontinuous galerkin methods for isogeometric analysis. Master's thesis, 2012.

[13] Irfan Cibaj, Noor Syarifuddin, Untung Ashari, Agung Wiweko, and Khoiril A Maryunani. Stratigraphic interpretation of middle miocene mahakam delta deposits: implications for reservoir distribution and quality. 2007.

[14] K.H. Coats. Reservoir simulation (1987 peh chapter 48). 1987.

[15] J Austin Cottrell, Thomas JR Hughes, and Yuri Bazilevs. *Isogeometric analysis: toward integration of CAD and FEA*. John Wiley & Sons, 2009.

[16] BL Darlow, Richard E Ewing, MF Wheeler, et al. Mixed finite element method for miscible displacement problems in porous media. *Society of Petroleum Engineers Journal*, 24(04):391–398, 1984.

[17] Carl De Boor, Carl De Boor, Etats-Unis Mathématicien, Carl De Boor, and Carl De Boor. *A practical guide to splines*, volume 27. Springer-Verlag New York, 1978.

[18] SR De Groot and P Mazur. Non-equilibrium thermodynamics dover. *New York*, 1984.

[19] Michael G Edwards and Clive F Rogers. Finite volume discretization with imposed flux continuity for the general tensor pressure equation. *Computational Geosciences*, 2(4):259–290, 1998.

[20] RE Ewing, RF Heinemann, et al. Incorporation of mixed finite element methods in compositional simulation for reduction of numerical dispersion. In *SPE Reservoir Simulation Symposium*. Society of Petroleum Engineers, 1983.

[21] Robert Eymard, Thierry Gallouët, and Raphaèle Herbin. Discretization of heterogeneous and anisotropic diffusion problems on general nonconforming meshes sushi: a scheme using stabilization and hybrid interfaces. *IMA Journal of Numerical Analysis*, page drn084, 2009.

[22] Robert Eymard, Cindy Guichard, and Raphaele Herbin. Small-stencil 3d schemes for diffusive flows in porous media. *ESAIM: Mathematical Modelling and Numerical Analysis*, 46(02):265–290, 2012.

[23] Peter A Forsyth et al. A control volume finite element method for local mesh refinement. In *SPE Symposium on Reservoir Simulation*. Society of Petroleum Engineers, 1989.

[24] LS-K Fung, AD Hiebert, Long X Nghiem, et al. Reservoir simulation with a control-volume finite-element method. *SPE Reservoir Engineering*, 7(03):349–357, 1992.

[25] Martin J Gander and Gerhard Wanner. From euler, ritz, and galerkin to modern computing. *Siam Review*, 54(4):627–666, 2012.

[26] Fathi Habashi. The first oil well in the world. *Bull. Hist. Chem*, 25(1):65, 2000.

[27] H Hćgland, I Aavatsmark, Cindy Guichard, Roland Masson, and R Kaufmann. Comparison of a finite element method and a finite volume method for flow on general grids in 3d. In *ECMOR XIII-13th European Conference on the Mathematics of Oil Recovery*, 2012.

[28] Bjørn Ove Heimsund. *Mathematical and numerical methods for reservoir fluid flow simulation*. PhD thesis, 2005.

[29] Thomas JR Hughes, John A Cottrell, and Yuri Bazilevs. Isogeometric analysis: Cad, finite elements, nurbs, exact geometry and mesh refinement. *Computer methods in applied mechanics and engineering*, 194(39):4135–4195, 2005.

[30] Albert Jack. *They Laughed at Galileo: How the Great Inventors Proved Their Critics Wrong*. Skyhorse Publishing, 2015.

[31] AM Jaeschke. Isogeometric analysis for compressible flows with application in turbomachinery. Master's thesis, TU Delft, Delft University of Technology, 2015.

[32] Bert Jüttler, Ulrich Langer, Angelos Mantzaflaris, Stephen E Moore, and Walter Zulehner. Geometry+ simulation modules: Implementing isogeometric analysis. *PAMM*, 14(1):961–962, 2014.

[33] Ulrich Langer, Angelos Mantzaflaris, Stephen E Moore, and Ioannis Toulopoulos. Multipatch discontinuous galerkin isogeometric analysis. In *Isogeometric Analysis and Applications 2014*, pages 1–32. Springer, 2015.

[34] Ulrich Langer and Ioannis Toulopoulos. Analysis of multipatch discontinuous galerkin iga approximations to elliptic boundary value problems. *arXiv preprint arXiv:1408.0182*, 2014.

[35] Eric A Lynd, John T Foster, Quoc P Nguyen, et al. An application of the isogeometric analysis method to reservoir simulation. In *SPE Europec featured at 78th EAGE Conference and Exhibition*. Society of Petroleum Engineers, 2016.

[36] Sébastien François Matringe. *Mixed finite element methods for discretization and streamline tracing*. PhD thesis, Stanford University, 2008.

[37] Matthias Möller. Assembly strategies in isogeometric analysis. 2015.

[38] V.M. Calo N. Collier, L. Dalcin. PetIGA: High-performance isogeometric analysis. *arxiv*, (1305.4452), 2013. http://arxiv.org/abs/1305.4452.

[39] Ardiansyah Negara. *Subsurface Flow Modeling in Single and Dual Continuum Anisotropic Porous Media using the Multipoint Flux Approximation Method*. PhD thesis, 2015.

[40] Joachim Nitsche. Über ein variationsprinzip zur lösung von dirichlet-problemen bei verwendung von teilräumen, die keinen randbedingungen unterworfen sind. In *Abhandlungen aus dem mathematischen Seminar der Universität Hamburg*, volume 36, pages 9–15. Springer, 1971.

[41] Jan Martin Nordbotten and Geir Terje Eigestad. Discretization on quadrilateral grids with improved monotonicity properties. *Journal of computational physics*, 203(2):744–760, 2005.

[42] J Tinsley Oden, Ivo Babuŝka, and Carlos Erik Baumann. A discontinuoushpfinite element method for diffusion problems. *Journal of computational physics*, 146(2):491–519, 1998.

[43] Les Piegl and Wayne Tiller. *The NURBS book*. Springer Science & Business Media, 2012.

[44] HS Price, JC Cavendish, RS Varga, et al. Numerical methods of higher-order accuracy for diffusion-convection equations. *Society of Petroleum Engineers Journal*, 8(03):293–303, 1968.

[45] Alfio Quarteroni and Alberto Valli. *Numerical approximation of partial differential equations*, volume 23. Springer Science & Business Media, 2008.

[46] Stephen Rassenfoss et al. Making unconventional resources less so. *JPT*, 65:p40–44, 2013.

[47] Beatrice Riviere. *Discontinuous Galerkin methods for solving elliptic and parabolic equations: theory and implementation*. Society for Industrial and Applied Mathematics, 2008.

[48] Brad J Rozon et al. A generalized finite volume discretization method for reservoir simulation. In *SPE Symposium on Reservoir Simulation*. Society of Petroleum Engineers, 1989.

[49] A Settari, HS Price, T Dupont, et al. Development and application of variational methods for simulation of miscible displacement in porous media. *Society of Petroleum Engineers Journal*, 17(03):228–246, 1977.

[50] YM Shum et al. Use of the finite-element method in the solution of diffusion-convection equations. *Society of Petroleum Engineers Journal*, 11(02):139–144, 1971.

[51] AF Stephansen. Convergence of the mpfa l-method–strengths and difficulties. In *ECMOR XII-12th European Conference on the Mathematics of Oil Recovery*, 2010.

[52] Jos van Kan, A Segal, and Fred Vermolen. *Numerical methods in scientific computing*. VSSD, 2005.

[53] Mary Fanett Wheeler. An elliptic collocation-finite element method with interior penalties. *SIAM Journal on Numerical Analysis*, 15(1):152–161, 1978.